Edith Cowan University

Research Online

Theses: Doctorates and Masters

Theses

2015

Stand-alone solar-pv hydrogen energy systems incorporating reverse osmosis

Daniel Clarke
Edith Cowan University

Follow this and additional works at: https://ro.ecu.edu.au/theses

 Part of the Power and Energy Commons

Recommended Citation

Clarke, D. (2015). *Stand-alone solar-pv hydrogen energy systems incorporating reverse osmosis*. https://ro.ecu.edu.au/theses/1750

This Thesis is posted at Research Online.
https://ro.ecu.edu.au/theses/1750

Edith Cowan University
Research Online

Theses: Doctorates and Masters | Theses

2015

Stand-alone solar-pv hydrogen energy systems incorporating reverse osmosis

Daniel Clarke
Edith Cowan University

Recommended Citation

Clarke, D. (2015). *Stand-alone solar-pv hydrogen energy systems incorporating reverse osmosis*. Retrieved from http://ro.ecu.edu.au/theses/1750

This Thesis is posted at Research Online.
http://ro.ecu.edu.au/theses/1750

USE OF THESIS

The Use of Thesis statement is not included in this version of the thesis.

Edith Cowan University

Copyright Warning

You may print or download ONE copy of this document for the purpose of your own research or study.

The University does not authorize you to copy, communicate or otherwise make available electronically to any other person any copyright material contained on this site.

You are reminded of the following:

- Copyright owners are entitled to take legal action against persons who infringe their copyright.

- A reproduction of material that is protected by copyright may be a copyright infringement. Where the reproduction of such material is done without attribution of authorship, with false attribution of authorship or the authorship is treated in a derogatory manner, this may be a breach of the author's moral rights contained in Part IX of the Copyright Act 1968 (Cth).

- Courts have the power to impose a wide range of civil and criminal sanctions for infringement of copyright, infringement of moral rights and other offences under the Copyright Act 1968 (Cth). Higher penalties may apply, and higher damages may be awarded, for offences and infringements involving the conversion of material into digital or electronic form.

Stand-Alone Solar-PV Hydrogen Energy Systems Incorporating Reverse Osmosis

By

Daniel P. Clarke

A PhD thesis is presented in fulfilment of the requirements for the Degree of Doctor of Philosophy

School of Engineering
Faculty of Computing, Health and Science
Edith Cowan University

November 2015

© Daniel Clarke 2015

Abstract

The world's increasing energy demand means the rate at which fossil fuels are consumed has increased resulting in greater carbon dioxide emissions. For many small (marginalised) or coastal communities, access to potable water is limited alongside good availability of renewable energy sources (solar or wind). One solution is to utilise small-scale renewably powered stand-alone energy systems to help supply power for everyday utilities and to operate desalination systems serving potable water (drinking) needs reducing diesel generator dependence. In such systems, on-site water production is essential so as to service electrolysis for hydrogen generation for Proton Exchange Membrane (PEM) fuel cells. Whilst small Reverse Osmosis (RO) units may function as a (useful) dump load, it also directly impacts the power management of stand-alone energy systems and affects operational characteristics. However, renewable energy sources are intermittent in nature, thus power generation from renewables may not be adequate to satisfy load demands. Therefore, energy storage and an effective Power Management Strategy (PMS) are vital to ensure system reliability.

This thesis utilises a combination of experiments and modelling to analyse the performance of renewably powered stand-alone energy systems consisting of photovoltaic panels, PEM electrolysers, PEM fuel cells, batteries, metal hydrides and Reverse Osmosis (RO) under various scenarios. Laboratory experiments have been done to resolve time-resolved characteristics for these system components and ascertain their impact on system performance. However, the main objective of the study is to ascertain the differences between applying (simplistic) predictive/optimisation techniques compared to intelligent tools in renewable energy systems. This is achieved through applying intelligent tools such as Neural Networks and Particle Swarm Optimisation for different aspects that govern system design and operation as well as solar irradiance prediction.

Results indicate the importance of device level transients, temporal resolution of available solar irradiance and type of external load profile (static or time-varying) as system performance is affected differently. In this regard, minute resolved simulations are utilised to account for all component transients including predicting the key input to the system, namely available solar resource which can be affected by various climatic conditions such as rainfall. System behaviour is (generally) more accurately predicted utilising Neural Network solar irradiance prediction compared to the ASHRAE clear sky model when benchmarked against measured irradiance data. Allowing Particle Swarm Optimisation (PSO) to further adjust

specific control set-points within the systems PMS results in improvements in system operational characteristics compared to using simplistic rule-based design methods. In such systems, increasing energy storage capacities generally allow for more renewable energy penetration yet only affect the operational characteristics up to a threshold capacity. Additionally, simultaneously optimising system size and PMS to satisfy a multi-objective function, consisting of total Net Present Cost and CO_2 emissions, yielded lower costs and carbon emissions compared to HOMER, a widely adopted sizing software tool. Further development of this thesis will allow further improvements in the development of renewably powered energy systems providing clean, reliable, cost-effective energy. All simulations are performed on a desktop PC having an Intel i3 processor using either MATLAB/Simulink or HOMER.

The declaration page
is not included in this version of the thesis

Acknowledgements

In the name of Allah, the Most Gracious and the Most Merciful, all praises to Allah for the strengths and His blessing in completing this thesis.

First and foremost, I would like to express my gratitude to my supervisors, Dr. Yasir Al-Abdeli and Dr Ganesh Kothapalli, whose expertise, understanding, and patience, have instilled upon me the necessary skills to become a quality researcher. I appreciate their vast knowledge and skills in many areas (i.e. Renewable energy, hydrogen systems as well as intelligent prediction and optimisation techniques), and their countless hours assisting in the writing process of this thesis and the containing journal papers. The role of Dr Magdalena Wajrak and Mr Alexander O'Neil in the preparation and measurement of feedwater samples is also gratefully acknowledged. The role of Miss Nisha Mubarak in the graphical rendering of Figures 1.3 and 3.1 is also gratefully acknowledged.

I also gratefully acknowledge the financial support provided to me by an Australian Postgraduate Award from Edith Cowan University and a top-up scholarship from the National Centre for Excellence in Desalination-Australia (NCEDA) in a project designed to investigate the integration of water desalting into hydrogen (renewable) energy systems. Additionally, I am grateful to Western Power, a Western Australian State Government owned corporation, in facilitating access to data for the simulations undertaken.

Finally, I would also like to thank my family for the support they provided me through my entire life and in particular, I must acknowledge my fiancé and best friend, Nisha, without whose love, encouragement and assistance, I would not have finished this thesis.

List of Journal Publications Stemming from this Candidature

For publishers' permission letter for use of the journal publications below, please refer to Appendix A. Additionally, refer to Appendix B for statement of the contribution of co-authors.

Clarke DP, Al-Abdeli YM, Kothapalli G. The effects of including intricacies in the modelling of a small-scale solar-PV reverse osmosis desalination system. Desalination. 2013; 311:127-36.

Clarke DP, Al-Abdeli YM, Kothapalli G. The impact of renewable energy intermittency on the operational characteristics of a stand-alone hydrogen generation system with on-site water production. International Journal of Hydrogen Energy. 2013; 38:12253-65.

Clarke DP, Al-Abdeli YM, Kothapalli G. The impact of using Particle Swarm Optimisation on the operational characteristics of a stand-alone hydrogen system with on-site water production. International Journal of Hydrogen Energy. 2014; 39:15307-19.

Clarke DP, Al-Abdeli YM, Kothapalli G. Multi-objective optimisation of renewable hybrid energy systems with desalination. Energy. 2015; 88:457-68.

List of Conference Publications Stemming from this Candidature

Clarke DP, Al-Abdeli YM, Kothapalli G. Modelling Small-Scale Stand-Alone (PV) Energy Systems with Reverse Osmosis Integration. 19th International Congress on Modelling and Simulation. Perth, Australia 2011. p. 3031-7.

Clarke DP. Effect of salinity on reverse osmosis for hydrogen production in a small-scale PV energy system. The Thirteenth Postgraduate Electrical Engineering & Computing Symposium (PEECS 2012). Perth, Australia 2012.

Table of Contents

Nomenclature

Symbol	Description
α	Self-discharge rate (%/month)
δ	Declination angle of the sun (degrees)
Φ	Latitude (degrees)
θ_Z	Zenith angle (degrees)
ω	Hour angle (degrees)
ΔT_{pv}	Temperature difference between the cell and back surface (°C)
A	Solar irradiation (W/m^2)
a	Diode quality factor
a_c	Empirical constant
A_{PV}	PV panel area (m^2)
ASHRAE	American Society of Heating, Refrigeration, and Air Conditioning
BAT_{SOC}	Battery's instantaneous State of Charge (%)
b_c	Empirical constant
BOP	Balance of Plant
c_1	Cognitive acceleration constant
c_2	Social acceleration constant
C_B	Battery capacity (Ah)
C_{Bmin}	Minimum battery discharge capacity (Ah)
C_{CO2}	Cost penalty for carbon emissions ($/kg CO_2)
C_H	Maximum hydrogen storage capacity (kg)
C_{H2O}	Minimum water capacity threshold (litres)
$C_{H2O(batt)}$	Minimum threshold water tank level (litres) before battery power is used for water generation
$C_{H2O(PV)}$	Minimum percentage (of maximum desalinated water storage capacity) (%)
C_i	Capital cost ($)
C_{MH}	Minimum hydrogen storage capacity level (litres)
COE	Cost of Energy ($/kWhr)
CP_{CO2}	Monetary cost of CO_2 ($/ton)
CRF	Capacity Recovery Factor
E_g	Energy band gap (eV)
E_i	Annual power consumption per component (kWhr/yr)
E_{IN}	Battery initial charge (Ah)
$E_{load,served}$	Electric load served (kWhr/yr)
ET	Equation of Time
G_{best}	Global best solution from all particles
H_2O_{max}	Maximum water storage capacity (L)
HOMER	Hybrid Optimization of Multiple Energy Resources

I	Operation current (A)
i	Component
IB	Beam Radiation (W/m^2)
I_B	Battery current (A)
I_D	Hourly diffuse radiation (W/m^2)
I_{FC}	Fuel cell operating current (A)
I_G	Hourly global irradiance (W/m^2)
I_{GNOCT}	Nominal Operating Cell Temperature (°C)
I_L	Photocurrent (A)
$I_{L.ref}$	Short circuit current at reference temperature (A)
I_N	Hourly beam radiation (W/m^2)
I_O	Diode reverse saturation current (A)
I_{PV}	Short circuit current (A)
i_R	Interest rate (%)
I_{SC}	Irradiance Constant (1367 W/m^2)
$I_{sc.ref}$	Short circuit current (A)
i_R	Interest rate (%)
K	Constriction Factor
K_I	Polarisation coefficient (C/m^2)
l	Longitude of location (degrees)
LAT	Local Apparent Time
n	nth day of the year (Chapter 2)
n	Electrons per mole of H_2O (Chapter 3)
n	Season (Chapter 4)
N_B	Number of Lead-acid batteries
n_C	Number of electrolyte cells
N_{Elect}	Number of PEM electrolysers
n_F	Faradays efficiency (%)
N_H	Number of Metal Hydride Canisters
n_{H2}	Hydrogen flow rate (mol/s)
NN	Neural Network
NPC	Net Present Cost ($)
N_{RO}	Number of RO units
$O\&M_i$	Operational and Maintenance cost ($/yr)
OECD	The Organisation of Economic Co-operation and Development
O_{EDF}	Duty factor for the electrolyser (litres/start-stop)
O_{ESS}	Number of start/stop cycles for a PEM electrolyser
O_{FC}	Minute resolved hydrogen consumption (litres/minute)
O_{FCSS}	Number of start/stop cycles for a PEM fuel cell
O_H	Total hydrogen generation (litres)

O_{HT}	Target hydrogen yield (litres)
O_W	Total of desalinated water (litres)
P_B	Battery Power (Ah)
P_{best}	Particle Personal Best
PEM	Proton Exchange Membrane
P_{FC}	Fuel Cell Power (W)
P_{IN}	Battery input power supplied (Ah)
PLC	Programmable Logic Controller
PMS	Power Management Strategy
PMU	Power Management Unit
P_0	Output power drawn (W)
P_{PV}	PV Panel Power (W)
P_{RO}	RO Power (W)
PSO	Particle Swarm Optimisation
PV	Photovoltaic
Q_R	Rate of accumulated charge
R_1	Constants
R_2	Constants
R_i	Replacement cost ($)
$R_{i,CO2}$	Carbon emission rate per component (CO_2/kWhr)
R_{proj}	Project lifetime (yrs)
RO	Reverse Osmosis
RQ	Research Question
R_S	Series resistance (Ω)
R_{sh}	Shunt resistance (Ω)
R_T	Internal resistance (Ω)
S_i	Salvage value ($)
SOC_{BAT}	Battery State-Of-Charge (%)
ST	Standard time
STL	Standard meridian for local time zone
t	Time step
T_{Elect}	Minimum duration the PEM electrolyser(s) can operate (minute)
T_A	Ambient temperature (°C)
T_{annual}	Total load demand to be served (kWhr/yr)
TE	Min runtime for electrolyser (minute)
TDS	Total Dissolved Salts
T_{LOL}	Loss of Load (kWhr)
T_{mpv}	Back surface temperature of the PV module (°C)
T_{pv}	PV panel operating temperature (°C)
$T_{pv.ref}$	PV panel reference temperature (°C)

T_{REF}	Reference Temperature (°C)
T_W	Deionised water temperature (°C)
μ_{Isc}	Temperature coefficient of the short circuit current
U_{Load}	Maximum permissible unmet load (%)
U_B	Battery voltage (V)
U_{OC}	Voltage max load (V)
U_{PV}	Open circuit voltage (V)
V_{FC}	Fuel cell voltage (V)
V_i^k	Particle velocity
$V_{oc.ref}$	Short circuit voltage (V)
V_t^k	Plausible position of particle
$W_{load,served}$	Water load served (kWhr/yr)
W_S	Wind speed (m/s)
X	Optimisation decision variable
X_i^k	Position of particle
X_{max}	Upper bound of decision variable
X_{min}	Lower bound of decision variable

List of Figures

List of Tables

Chapter 1. General Introduction

1.1 - World Energy and Water Demands

Continued growth in global energy demand means increased fossil fuel consumption and higher emissions. Society is becoming more environmentally aware of carbon emissions and the need for sustainable energy to replace fossil fuels. Interest internationally and in Australia is directed to the utilisation of renewable sources [1] with the aim of reducing emissions associated with electricity generation via fossil fuels. Figure 1.1, sourced from the Key Energy Statistics 2014 by the International Energy Agency [2], indicates that only 0.1% of total power was generated renewably (via solar, wind, geothermal etc.) in 1973 compared to 1.1% in 2012. Over the same period, there was a corresponding increase in power generation based on fossil-fuels from 6,106Mtoe to 13,371Mtoe (1Mtoe=11,630 GWh).

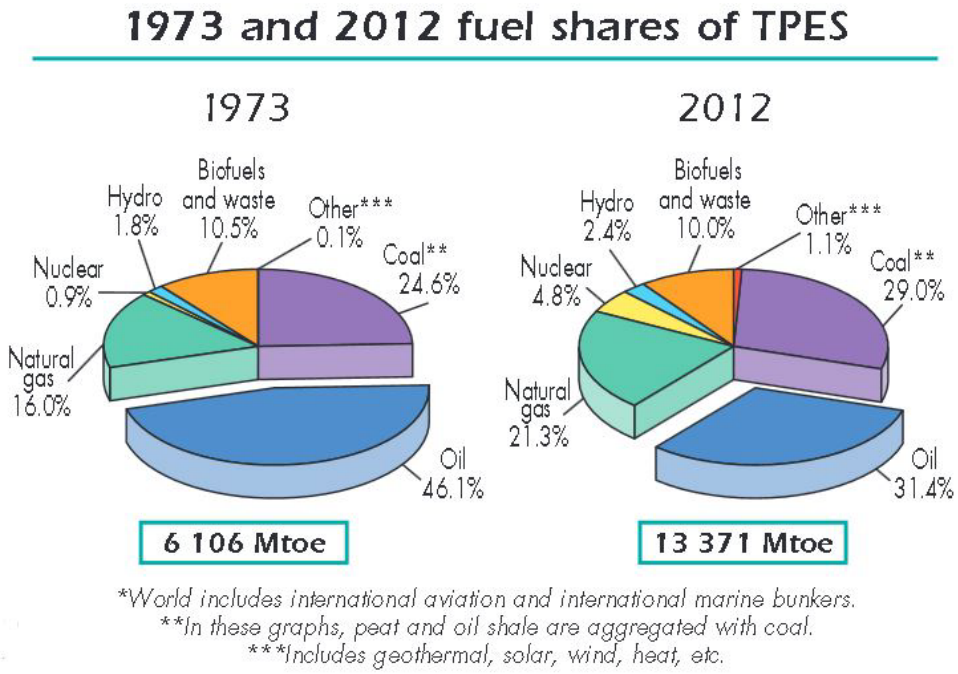

Figure 1.1 - World total primary energy supply Ratios for countries of the Organisation of Economic Co-operation and Development (OECD). Source: [2]

Whilst population growth contributes to a rise in total power consumption, the demand for potable water also increases across four main sectors including agriculture, production of energy, industrial uses and human consumption. The production of crops and livestock is the

most demanding on water reserves accounting for 70% of all water withdrawn [3]. Furthermore, the transport of potable water to remote locations also provides additional costs. In some countries, the supply cost ($/m^3) of potable water can be up to 800% more compared to non-potable water at the same location [4, 5]. This provides an opportunity to utilise on-site desalination systems reducing the cost of potable water generation through effective on-site energy management [5-7].

Desalination has the potential to help meet rising worldwide water demands, but is limited by its cost due to the relatively large specific energy consumption (kWhr/m^3). The energy consumption of desalination also has an environmental impact, in particular the release of carbon dioxide (CO_2) into the atmosphere through the burning of fossil fuels. Additionally, the effects of climate change and demographics can exacerbate widespread problems with access to potable water for many small (marginalised) or coastal communities. In its 2010 report, the National Centre of Excellence in Desalination, an Australian government initiative for the study of water security against the natural variability of rainfall and potential future impacts of climate change reported that "the need is urgent for large-scale production of potable water from alternative water supplies for Australia's metropolitan and rural regions, including affordable and sustainable desalination technologies" [8].

1.2 - The Role of Renewable Energy

The central focus of world energy policy in recent years is aimed at increasing the proportion of energy derived from renewables as seen in Figure 1.1, and thus reducing dependence on fossil energy sources [1, 9]. Renewable energy is generated from naturally occurring resources including sunlight and wind as well as hydroelectric, tidal and geothermal sources. Energy produced through renewable sources provides a "clean" alternative for the production of electricity compared to fossil based fuels. Electricity production through renewable sources is naturally sustainable and can significantly reduce carbon emissions compared to fossil fuels. However, while renewable energy is environmentally friendly, its disadvantages are low energy conversion efficiencies, high set-up cost and intermittent supply when compared to fossil fuels [9].

Figure 1.2 - Western Australian remote power generation. Source: [10]

Figure 1.2 highlights diesel generators as the primary source of energy, alongside natural gas, for remote locations in Western Australia. For rural communities away from hydroelectric sources, solar and wind have the potential to alleviate dependence on diesel in addition to decreasing the carbon footprint. In particular, the attractiveness of solar-PV systems lies in their good reliability and relative ease of installation, particularly for small scale applications. The major advantage of using solar-PV panels is that, once panels are set up their operational cost and reliability are favourable. The main disadvantage of solar-PV panels is their low efficiency energy conversion and dependence on seasonal environmental conditions (e.g.

temperature and cloud cover during daylight hours) affect power output. Conventional solar-PV panel efficiencies are typically between 15-20% [11].

Due to the intermittent nature of both solar and wind, two options exist to provide reliable power supply:

- In conjunction with renewable energy, use fossil fuel generators to make up the deficit; or
- Store excess renewable energy, so that the stand-alone energy system can run when available renewable energy is insufficient.

To ensure minimal dependence on fossil fuels for power generation, localised energy storage and improvements in the overall efficiency of the energy system are needed. While many other forms of energy storage exist (i.e. flywheels, capacitors or hydrogen), batteries are most commonly integrated into stand-alone energy systems [12] but they are not adequate for long term (seasonal) storage due to high parasitic losses and relatively low storage capacities [13]. The potential of hydrogen as an energy carrier provides the ideal opportunity for both seasonal storage and meeting daily power requirements through an energy conversion device (e.g. fuel cell).

1.3 - The Hydrogen Economy

Global awareness about the carbon emissions has generated considerable interest internationally and in Australia in the 'hydrogen economy', whereby hydrogen is considered as an energy carrier which is utilised via a fuel cell for power generation to provide an alternative to fossil fuels. Hydrogen is attracting significant research globally as a possible long term, renewable energy carrier as opposed to fossil fuels. Its advantage is as a clean energy source, when derived from renewable sources, for fuel cell systems. Hydrogen is the most abundant element on Earth and burns readily with oxygen, releasing considerable amounts of energy as heat with only water as a chemical by-product and no carbon-based greenhouse gas emissions.

$$2H_2 + O_2 \rightarrow 2H_2O$$

While fuel cell technology has allowed various stationary and vehicle applications to be possible as listed in section 1.4, there are technical and economic challenges that have limited the uptake of the use of hydrogen as an alternative fuel. These challenges include:

- Large-scale hydrogen production from fossil fuels must currently be used until hydrogen can be obtained economically from renewable sources;
- Infrastructure for hydrogen delivery and filling stations;
- Improved technologies for hydrogen transport and long term storage;
- Fuel cells with improved reliability and lower costs; and
- Addressing public concerns about safety.

Hydrogen is highly flammable with a high energy content by weight (nearly three times that of gasoline), but has a low energy density by volume at a standard temperature and atmospheric pressure. However, hydrogen is a carrier of energy and must be used in combination with devices such as fuel cells to generate useful electricity. Furthermore, hydrogen does not exist in a natural state and must be refined.

Today, hydrogen for use as a feedstock for industrial processes where power generation is not the function, is most commonly produced through steam reforming of natural gas. Although other techniques exist such as partial oxidation, pyrolysis, biomass and water electrolysis [14, 15], the drawback of the generating hydrogen through hydrocarbons is the resulting carbon emissions. In this regard, it is desirable to produce hydrogen from water electrolysis using renewable energy sources rather than fossil fuels because emissions are minimised but is usually more costly because it requires greater energy expenditure than using fossil fuels. Generated hydrogen on-site, is an attractive option for remote communities which cannot be economically supplied via the electrical grid.

1.4 - Stand-Alone Energy Systems

A stand-alone energy system can generally be considered as a power system, not connected to the main electrical grid, which is solely responsible for providing power to meet external load demands. Stand-alone systems are most commonly utilised in remote locations where connecting to the electrical grid is too expensive. Such systems can be easily be deployed and can be custom designed for a variety of applications including:

- Telecommunications: e.g. back-up and UPS systems for mobile phone network infrastructure in remote areas [16]
- Agriculture: e.g. water pumping [5, 17]
- Environmental: e.g. habitat monitoring [18]
- Power generation: e.g. power supply for remote communities [19]
- Marine: e.g. fresh water production and powering ships [20]

However, many of these systems are still largely reliant on fossil fuels with renewable sources increasingly being integrated [21]. Among stand-alone renewable energy systems, various technological options are suitable for different applications using combinations of renewable sources. Commonly, solar and wind are the preferred sources of renewable energy for small scale applications [22]. Additionally, devices such as Reverse Osmosis can be integrated into renewable energy systems to provide water in periods of excess renewable energy (i.e. act as a useful dump load) for electrolysis or drinking requirements.

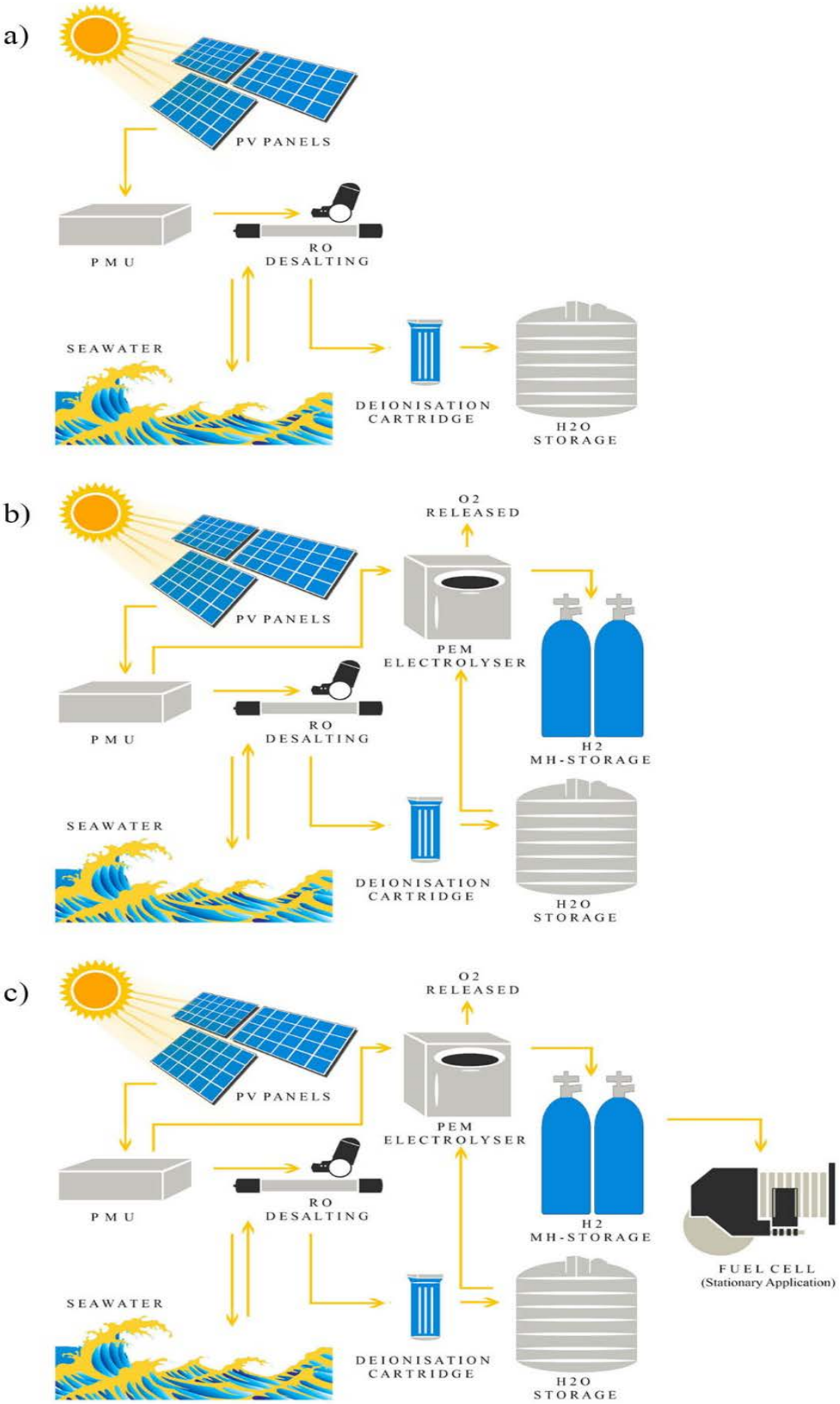

Figure 1.3 - System block diagram for a) Solar desalination system; b) Solar hydrogen generation system with integrated desalination; and c) Solar energy system incorporating desalination.

A typical renewably powered stand-alone power system, with on-site desalination can be separated into three distinct sub-systems is shown in Figure 1.3 which forms the technological focus of this thesis. These systems are:

1. A stand-alone solar-PV desalination system (Figure 1.3a), responsible for providing potable water via renewables through the use of a Reverse Osmosis device;
2. Through the addition of a PEM electrolyser to the architecture of Figure 1.3a, a stand-alone solar hydrogen generation subsystem is formed responsible for producing hydrogen and potable water from on-site desalination; and
3. Finally, integrating a fuel cell into the architecture of 1.3b, a full stand-alone solar-PV hydrogen energy system is created (Figure 1.3c) responsible for generating power and desalinated water.

Whilst each subsystem is able to be operated individually, each subsystem (i.e. hydrogen generation and water production) contributes to a full operating system depicted in Figure 1.3c whereby both electrical and desalinated water demands are met. This full system makes use of all available solar energy either by directly powering system devices or storing excess energy via batteries, as hydrogen or extra water. Therefore, it is critical to break down the entire system (Figure 1.3c) into subsystems (Figures 1.3a and 1.3b) to analyse how each subsystem performs.

The aforementioned systems comprise of a PV array, a Reverse Osmosis (RO) unit, batteries, a Proton Exchange Membrane (PEM) electrolyser and a PEM fuel cell, with the metal hydrides for hydrogen storage. Photovoltaics are the preferable option for the stand-alone energy system because of their high reliability, low maintenance cost (no moving parts) and greater consistency/predictability of solar radiation compared to wind. A PEM fuel cell is essential alongside sufficient reserves of hydrogen to allow reliable power supply in periods where the renewable energy source is insufficient to serve the load. Unlike other fuel cells (e.g. solid-oxide and alkaline fuel cells), a PEM fuel cell can operate at lower temperatures and with higher energy efficiency. Additionally, the incorporation of a RO into the system architecture not only helps provide drinking water but also the water needed for on-site hydrogen generation through electrolysis.

For the electrolysis process, a PEM electrolyser is preferred due to its higher energy efficiency, better lifetime (no degradation associated with switching ON/OFF),

environmentally friendly status (no corrosive electrolyte), and easy maintenance compared to conventional alkaline electrolysers [23-25]. Its main advantage is that it can generate hydrogen and store it at an elevated pressure (i.e. up to 15bar [26]) without the need for a separate compressor which would increase the energy consumption. The intermittency of renewable energy means energy storage is critical for system reliability. The investigated system includes two forms of energy storage, namely Lead-acid batteries and hydrogen. Whilst other battery technologies exist (e.g. Nickel-Cadmium, Lithium Ion etc.), Lead-acid batteries remain the cheaper option as a short term energy storage/buffer device. For long-term energy storage, that accounts for seasonal effects (i.e. winter months), metal hydride canisters can be directly coupled with the PEM electrolyser as well as with hydrogen stored at relatively safe, low temperatures and pressures [27].

1.5 - Research Questions

There is a need to optimise the design (i.e. operational strategy and sizing) of stand-alone renewable energy systems incorporating on-site water generation to meet increasing demands (power and water) and alleviate dependency on fossil fuels. In this regard, this research is multi-disciplinary in that it not only addresses renewable energy conversion, system operation and storage, and water production, but also evaluates artificial intelligence in such systems. The four research questions (RQ's) addressed are:

Research Question 1 (RQ 1): How is the overall performance of solar-PV energy systems affected when accounting for dynamic device transients?

Research Question 2 (RQ 2): Can the incorporation of (intelligent/adaptive) predictive software tools significantly improve the performance of these energy systems, compared to non-predictive (simplistic) energy balancing techniques?

Research Question 3 (RQ 3): Can the use of (intelligent/adaptive) optimisation software tools improve system performance when meeting single and multi-objective functions compared to a more widely adopted technique?

Research Question 4 (RQ 4): How does scalability affect energy systems incorporating desalination, solar-PV and hydrogen fuel cells/storage?

1.6 - Outcomes

From the above research questions the following outcomes were achieved:

- Transients of laboratory scale devices have been experimentally derived and incorporated into the models of the stand-alone energy systems depicted in Figure **1.3** with the impact of temporal resolution on system performance evaluated (Chapter 2);
- Neural Network solar irradiance prediction has been compared against the ASHRAE clear sky model to test their validity and effects on system performance (i.e. component operational characteristics as shown in Figure 1.3b) over two seasons (Chapter 3);
- A new optimisation model (Particle Swarm Optimisation) has been proposed for system sizing and Power Management Strategy and compared to a more well-known sizing program (HOMER). This comparison has been evaluated for specific system objectives such as maximum hydrogen generation, specific amount of hydrogen to be generated only and to minimise loss of load (Chapter 4);
- To document the application of PSO for the sizing and Power Management Strategy of the system depicted in Figure 1.3c, to meet different types of external load demands (i.e. electricity and potable water requirements) with technical and environmental performance evaluated (Chapter 5); and
- The significance of component and external load scale has been analysed to determine its influence on system operational characteristics and the system's ability to meet desired objectives (Chapter 2 to 5).

Although solar irradiance, rainfall, power and water demand profiles used in this research have been sourced in the Western Australian context, the methods used can be adapted for different geological locations.

1.7 - Thesis Structure

In the following section, a general overview of the thesis structure is presented with a summary of methods used, shown in Table 1.1. Whilst full details of each experiment are not supplied, this outline serves to provide a summary of the chapters in this thesis and a linkage to the publications.

Research Methods								
	ASHRAE	**Neural Network**	**Meteorological Data**	**Device Transients**	**PSO**	**HOMER**	**Electric Load**	**Water Load**
Chapter 2	X			X				
Chapter 3	X	X	X	X				
Chapter 4			X	X	X		X	X
Chapter 5			X	X	X	X	X	X

Table 1.1 - Summary of methods used in each chapter.[1]

Chapter 1 provides a general introduction to the global energy situation as well as potable water generation for remote locations. This serves to highlight the need for increased use of renewable energy in power generation, particularly outside of the main electrical grid. The chapter then moves to present the broad research questions and outcomes which the thesis will address.

Chapter 2, published in Desalination, reviews current literature pertaining to stand-alone energy systems incorporating desalination and system component models used in such systems. It then details a methodology used to model a small-scale, stand-alone, solar-PV powered Reverse Osmosis (RO) system (Figure 1.3a), which forms the first subsystem (water generation), investigating the effect of including system component intricacies. It explains dynamic device characteristics and analyses the scale of solar-PV panels, with and without battery storage, in terms of total annual desalinated water produced.

Chapter 3, published in the International Journal of Hydrogen Energy, extends upon Chapter 2 through the inclusion of a PEM electrolyser in the system architecture (Figure 1.3b) forming the second subsystem (hydrogen generation). Based on literature for solar irradiance prediction techniques, a methodology to study renewable energy intermittency on system performance is proposed. The impact on the operational characteristics of a stand-alone, solar-PV hydrogen generation system is analysed using two different solar irradiance prediction techniques for different battery storage capacities. The comparison between the performance of the ASHRAE clear sky model and Neural Network prediction is conducted

[1] Details for ASHRAE and PSO (optimisation algorithm) can be seen in Chapter 3.7 and Appendix F, respectively. HOMER is a well-known sizing tool for energy systems.

for two seasons (Western Australian winter and summer) which provide two levels of solar irradiance intermittency.

Chapter 4 further develops upon the stand-alone hydrogen energy system used in Chapter 3 by examining the impact of renewable energy intermittency and optimisation on the operational characteristics of the full system depicted in Figure 1.3c. Published in the International Journal of Hydrogen Energy, this chapter demonstrates the validity of applying Particle Swarm Optimisation (PSO) on the sizing and Power Management Strategy (PMS) deployed in such systems for a single objective function. The proposed optimisation method additionally identifies the choice of PSO acceleration parameters that yield best results. Three scenarios are developed for the analysis of implementing PSO, and a comparison with a simplistic method is made.

Chapter 5, published in Energy, investigates the techno-economic and environmental feasibility in sizing a stand-alone solar-PV hydrogen energy system (Figure 1.3c) for two external demand profiles (electric and water). In this chapter, the effect of scalability of water storage capacity and electric demand on system performance, when using two optimisation techniques (HOMER and PSO) to minimise Net Present Cost (NPC) and CO_2 emissions, is identified.

Chapter 6 provides a brief overview of the study, including a statement of the problem and the methods involved. The chapter then provides a summary and discussion pertaining to the four research questions developed in Chapter 1. Furthermore, the relevance of the results when designing stand-alone solar-PV energy systems incorporating desalination is discussed.

Chapter 7 concludes the work done in this thesis, together with recommendations of further investigations that can contribute to the development of stand-alone hydrogen energy systems incorporating on-site water production.

1.8 - Chapter References

[1] Doukas H, Patlitzianas KD, Kagiannas AG, Psarras J. Renewable energy sources and rationale use of energy development in the countries of GCC: Myth or reality? Renewable Energy. 2006;31:755-70.

[2] International Energy Agency. Key world energy statistics. Available from, http://www.iea.org/publications/freepublications/publication/KeyWorld2014.pdf; 2014. [accessed 2014].

[3] United Nations World Water Development Programme. Global water resources under increasing pressure from rapidly growing demands and climate change, according to new UN World Water Development Report. Available from, http://www.unesco.org/new/fileadmin/MULTIMEDIA/HQ/SC/pdf/WWDR4%20Background%20Briefing%20Note_ENG.pdf; 2012. [accessed 2014].

[4] Bourouni K, Chaibi M. Solar energy for application to desalination in Tunisia: description of a demonstration project. Renewable Energy in the Middle East: Enhancing Security through Regional Cooperation. 2009:125-49.

[5] Bouguecha S, Hamrouni B, Dhahbi M. Small scale desalination pilots powered by renewable energy sources: case studies. Desalination. 2005;183:151-65.

[6] Mohamed ES, Papadakis G, Mathioulakis E, Belessiotis V. The effect of hydraulic energy recovery in a small sea water reverse osmosis desalination system; experimental and economical evaluation. Desalination. 2005;184:241-6.

[7] Agbossou K, Bilodeau A, Doumbia ML. Development of a control method for a renewable energy system with fuel cell. AFRICON, AFRICON '09 2009. Canada p. 1-5.

[8] National Centre of Excellence in Desalination. Australian Desalination Research Roadmap. Available from, http://desalination.edu.au/wp-content/uploads/2010/02/NCED-Australian-Desalination-Research-Roadmap-2010.pdf; 2011. [accessed 2011].

[9] Azarpour A, Suhaimi S, Zahedi G, Bahadori A. A review on the drawbacks of renewable energy as a promising energy source of the future. Arabian Journal for Science and Engineering. 2013;38:317-28.

[10] Horizon Power. Annual Report 2011/12. Available from, http://www.parliament.wa.gov.au/publications/tabledpapers.nsf/displaypaper/3815375adcf718345f70895648257a86000942a3/$file/5375.pdf; 2012. [accessed 2013].

[11] Imenes AG, Mills DR. Spectral beam splitting technology for increased conversion efficiency in solar concentrating systems: a review. Solar Energy Materials and Solar Cells. 2004;84:19-69.

[12] Hadjipaschalis I, Poullikkas A, Efthimiou V. Overview of current and future energy storage technologies for electric power applications. Renewable and Sustainable Energy Reviews. 2009;13:1513-22.

[13] Dufo-López R, Bernal-Agustín JL, Contreras J. Optimization of control strategies for stand-alone renewable energy systems with hydrogen storage. Renewable Energy. 2007;32:1102-26.

[14] Holladay JD, Hu J, King DL, Wang Y. An overview of hydrogen production technologies. Catalysis Today. 2009;139:244-60.

[15] McLellan B, Shoko E, Dicks AL, Costa JCDd. Hydrogen production and utilisation oppurtunities for Australia. International Journal of Hydrogen Energy. 2005;30:669-79.

[16] Agbossou K, Chahine R, Hamelin J, Laurencelle F, Anouar A, St-Arnaud JM, Bose TK. Renewable energy systems based on hydrogen for remote applications. Journal of Power Sources. 2001;96:168-72.

[17] Banat F, Qiblawey H, Al-Nasser Q. Economic evaluation of a small RO unit powered by PV installed in the village of Hartha, Jordan. Desalination and Water Treatment. 2009;3:169-74.

[18] Mainwaring A, Culler D, Polastre J, Szewczyk R, Anderson J. Wireless sensor networks for habitat monitoring. Proceedings of the 1st ACM international workshop on Wireless sensor networks and applications. Atlanta, Georgia, USA: ACM; 2002. p. 88-97.

[19] Kanase-Patil AB, Saini RP, Sharma MP. Integrated renewable energy systems for off grid rural electrification of remote area. Renewable Energy. 2010;35:1342-9.

[20] Lee K-J, Shin D, Lee J-P, Kim T-J, Kim H-J. Experimental investigation on the hybrid smart green ship. In: Lee J, Lee M, Liu H, Ryu J-H, editors. Intelligent Robotics and Applications: Springer Berlin Heidelberg; 2013. p. 338-44. Available from, http://dx.doi.org/10.1007/978-3-642-40849-6_33

[21] Ghosh PC, Emonts B, Janßen H, Mergel J, Stolten D. Ten years of operational experience with a hydrogen-based renewable energy supply system. Solar Energy. 2003;75:469-78.

[22] Shakya BD, Aye L, Musgrave P. Technical feasibility and financial analysis of hybrid wind–photovoltaic system with hydrogen storage for Cooma. International Journal of Hydrogen Energy. 2005;30:9-20.

[23] Clarke RE, Giddey S, Badwal SPS. Stand-alone PEM water electrolysis system for fail safe operation with a renewable energy source. International Journal of Hydrogen Energy. 2010;35:928-35.

[24] Kolhe M, Atlam O. Empirical electrical modeling for a proton exchange membrane electrolyzer. International Conference on Applied Superconductivity and Electromagnetic Devices (ASEMD) Sydney, Australia 2011. p. 131-4.

[25] Millet P, Mbemba N, Grigoriev SA, Fateev VN, Aukauloo A, Etiévant C. Electrochemical performances of PEM water electrolysis cells and perspectives. International Journal of Hydrogen Energy. 2011;36:4134-42.

[26] Clarke DP, Al-Abdeli YM, Kothapalli G. The impact of renewable energy intermittency on the operational characteristics of a stand-alone hydrogen generation system with on-site water production. International Journal of Hydrogen Energy. 2013;38:12253-65.

[27] Bielmann M, Vogt UF, Zimmermann M, Zuttel A. Seasonal energy storage system based on hydrogen for self sufficient living. Journal of Power Sources. 2011;196:4054-60.

Chapter 2. The Effects of Including Intricacies in the Modelling of a Small- Scale Solar-PV Reverse Osmosis Desalination System

Daniel P. Clarke*, Yasir M. Al-Abdeli and Ganesh Kothapalli

This chapter was published as a full research paper in Desalination. Whilst all efforts were made to retain the original features of this article, minor changes such as the layout, number formats, font size and style were implemented in order to maintain consistency in the formatting style of the thesis.

2.1 - Abstract

With the global demand for freshwater rising alongside the cost of power generation from fossil-based fuels, access to potable water in small (marginalised) or coastal communities can be alleviated using renewable energy sources such as solar or wind. Whilst large-scale renewably powered desalination systems have been the focus of much research, where smaller systems are concerned, there remains ambiguity as to the significance of modelling all system intricacies and the effects of Solar-Photovoltaics (solar-PV) scalability on total water yield.

After detailing the methodology used to model such Reverse Osmosis (RO) systems, this chapter presents the results of simulations used to investigate a small-scale, stand-alone, solar-PV powered (RO) system, with/without battery storage. Results indicate system performance was affected differently when including power characteristics of RO devices and also by the temporal resolution used in simulations. The scale of the renewable energy conversion used (solar-PV) appears to be a factor in some cases. Parameters varied in the simulations include RO (unit) power characteristics, saline water concentration/temperature, PV panel power characteristics as well as the dynamic charging and discharging of batteries and the efficiency of power conditioning used in the renewable energy system. Simulations are done using MATLAB and use laboratory-based data to establish device characteristics.

2.2 - Introduction

The supply of drinkable water is a global concern with many areas throughout the world suffering from increased water shortages [1, 2]. Whilst access to potable water networks and

grid-connected power (for water purification) may be exacerbated for remote communities, this situation can be alleviated through the availability of renewable energy sources (solar or wind). The effect of drought, climate change and population growth means desalination of seawater offers the assurance of contributing to meet increasing water demand. However, due to high energy demands associated with seawater desalination diesel generators remain predominately in use to provide power in remote areas which leads to an increase in fossil fuel consumption and wider emissions [3]. The International Energy Agency [4] estimates that only 0.2% of total power in 1973 was generated renewably compared to 1.1% in 2009, with a corresponding increase in power generation based on fossil-fuels from 3724Mtoe to 5170Mtoe (1Mtoe=11,630 GWh). It is believed that renewably powered stand-alone desalination systems will have an increasingly critical role in the long-term water security of many nations, as well as alleviating reliance on fossil fuels and minimising environmental impact. In this regard, the use of solar-PV [5-10] as well as other renewable energies has been utilised [11-18].

Desalination systems based on solar-PV form the largest renewable energy conversion method used in conjunction with potable water production, with RO being the most common pathway [19, 20]. The attractiveness of solar-PV lies in its good reliability and relative ease of installation particularly for off-grid, small-scale systems. Coupling RO with solar-PV is well aligned with strategic water industry issues, namely “development of simple, low maintenance renewable energy systems that can supplement power supply for small desalination facilities” [21].

Optimally integrating desalination into energy systems necessitates quantifying total renewable energy availability, its conversion efficiency into energy carriers such as electricity and its subsequent utilization or storage. When modelling these systems, the temporal aspects used in simulations will also likely affect the overall predictions of system performance and potable water production. Such simulations can include the modelling of energy system components [11, 22] and desalination processes [23, 24] and is made possible using software tools [25]. Although fairly complex modelling techniques have been applied [11], where small stand-alone renewable powered desalination systems are concerned, more research is also warranted into the energy storage options available for such systems, including the integration of battery-free energy storage (e.g., via hydrogen) during seasonal variability of renewable energy sources [19]. The temporal resolution used in such simulations also

remains a key consideration as it not only impacts the total time needed for data processing but also has the potential to affect the accuracy of the results attained. Limited research has been done to investigate this with many results being based on a nominal time step of 1 hour [9, 11, 16, 24, 26] and simulation lengths of one year [27] as the most commonly implemented. Additionally, whilst the use of simulations based on daily averages can provide an excellent (quick) overview of system performance [10], the use of such relatively lengthy time steps raises the question as to the degree to which such temporal resolution impacts the outcomes and whether smaller time steps are always warranted [28]. The inclusion of different desalination system power characteristics in these simulations can further complicate the predictions and may also be affected by system scalability.

This chapter sheds new light on the interplay between renewably powered desalination system components, RO devices and overall system performance, under different temporal resolutions. The research does this by examining the effects which these factors have on annual predictions of potable water production and renewable energy utilization. This is done using simulations conducted in the MATLAB/Simulink environment.

2.3 - Experimentation

To accurately model device characteristics in the systems simulations, a series of tests were undertaken to resolve the efficiencies and power characteristics of modelled components[2]. Figure 2.1 gives the general layout of the systems tested and modelled while Figure 2.2 depicts the RO unit and data acquisition system. A solar energy system incorporating PV panels (make: Heckert Solar- Germany, model: HS-PL 135) was tested in conjunction with its Power Management Unit (PMU) that is capable of supplying loads of up to 700W. The PMU consists of four components: a Programmable Logic Controller (make: Beckhoff-Germany, model: BC9000) to regulate operational modes; a 12Volt lead acid battery with a minimum depth of discharge at 20% of rated capacity; Converters (DC-DC and DC-AC); and a charge controller (make: SMART Power Systems-Germany, model: SMART MS 300) to limit the charging current of the battery banks to a maximum (solar) charging current of 30A

[2] Refer to Appendix C for error analysis methods.

at 12V and maintain full battery capacity without overcharging.

Parameter	Value	Parameter	Value
ISC (Irradiance constant)	1367 W/m2	Longtiude (location)	115.8°
ID (diffuse radiation)	0.25IB (bean radiation)	Latitude (location)	-31.75°
A (model constant)	1000	B (model constant)	0.18

Table 2.1 gives basic hardware specifications and relevant model parameters for PV panels used in the simulations. Each PV panel has an effective area of about 0.87m^2.

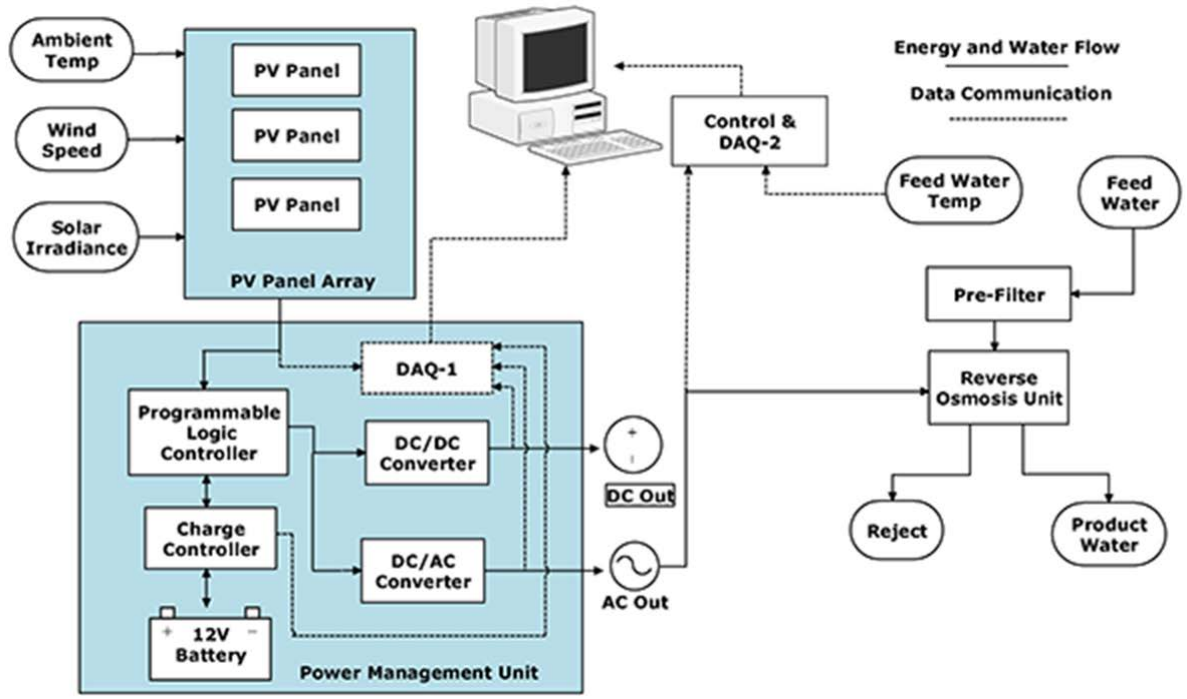

Figure 2.1 - Overall layout of system showing components modelled and data acquisition.[3]

[3] Refer to Appendix D for Chapter 2 system MATLAB/Simulink model.

Figure 2.2 - Experimental setup with the RO unit and the data acquisition system.

Parameter	Value	Parameter	Value
ISC (Irradiance constant)	1367 W/m2	Longtiude (location)	115.8°
ID (diffuse radiation)	0.25IB (bean radiation)	Latitude (location)	-31.75°
A (model constant)	1000	B (model constant)	0.18

Table 2.1 - Solar irradiance modelling parameters with longitude and latitude parameters for a typical Perth based location.

The PLC tested and modelled incorporates three distinct operational modes. Mode-I involves PV power used to (only) run utilities which may be DC or AC. If PV power is inadequate to meet load demand, the system works in Mode-II with PV power only used to charge energy storage media (e.g., batteries) in this stand-alone system. If PV power is in excess of that to run utilities, the system operates in Mode-III with PV power supplying both utilities (DC or AC) and charging energy storage media. Whilst power control may fluctuate between these operational modes through the day, the likelihood of running systems in Mode-III increases during summer when good solar irradiance exists.

Energy storage in small scale renewable energy systems is commonly achieved using batteries, although other forms of energy storage also exist including capacitors, flywheels or hydrogen [29]. Energy storage becomes important when there is excess solar energy available that is not utilised or when there exists a mismatch between solar energy and load demand. Excess energy is defined as energy available from the solar panel/s which is not used by the Reverse Osmosis unit (the load demand) or not stored which happens either when no storage media exists or is already at full capacity. Figure 2.3 helps demonstrate these concepts for data on the 21st of December. The stand-alone system tested and modelled incorporates a lead acid battery (make: Banner- Germany, model: SBV 12-55) with a 55 Ah capacity (C=20h/12Volts). Subsequent simulations will consider characteristics derived from experiments for discharging and charging in addition to a maximum battery leakage of 10% per month, which appears to be a reasonable estimate [30].

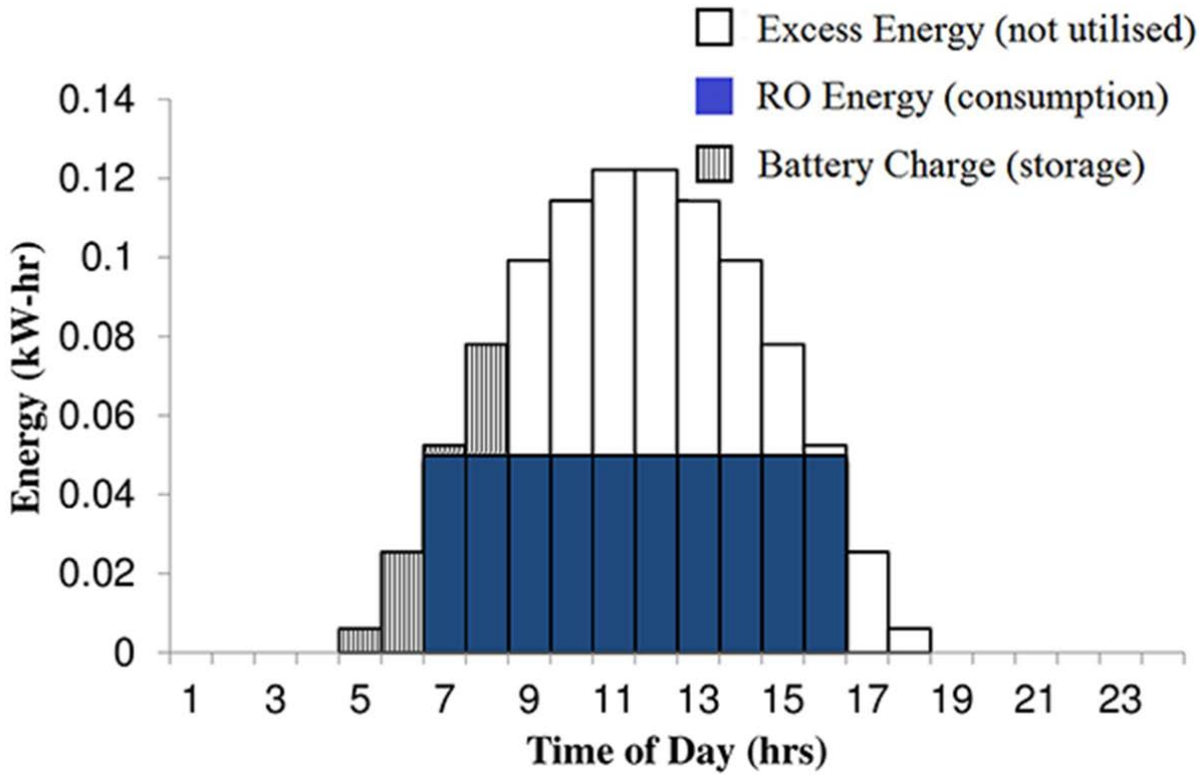

Figure 2.3 - Definition of excess energy using the 21st of December data (hourly resolved) for $A_{PV}=1m^2$ after RO operation and 55Ah battery charging.

A laboratory-scale Reverse Osmosis unit (make: Katadyn- Switzerland, model: Power Survivor 40E) was used to desalinate simulated saline water. Small-scale RO units typically include pre-filters (for particulate removal), a pump to yield the needed osmotic membrane pressures and energy recovery to reduce specific energy consumption (kW/m^3). This DC powered RO unit has a nominal (potable) water production rate of 5.5litres/hr and a nominal power rating of 50W at 12VDC. The unit however operates using a reciprocating piston which means a highly dynamic (fluctuating) current draw is realised at 12VDC. Figure 2.4 shows one complete cycle of the pump for a constant 12V supply with the operational frequency of the RO unit equal to 0.5Hz. The water recovery ratio of 10% (potable water produced relevant to total feedwater) was found through monitoring.

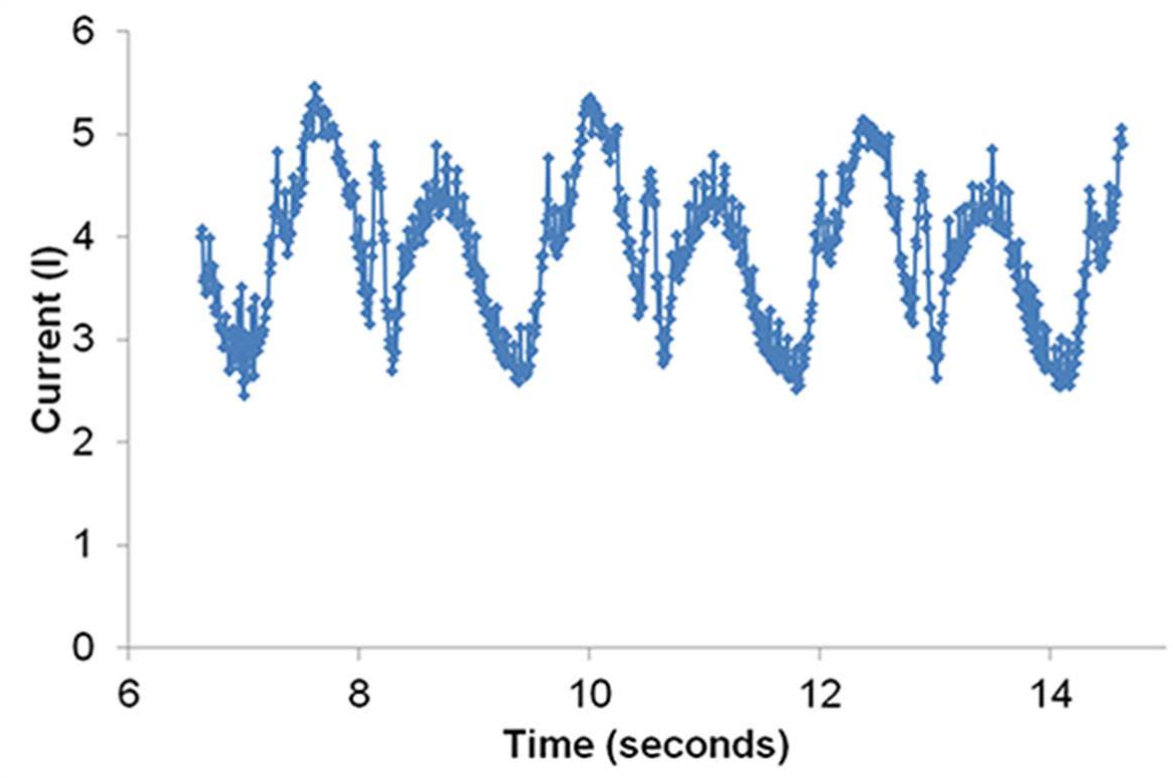

Figure 2.4 - RO current profile measured at the battery with 10ms sampling rate (sample data shown for demineralised feedwater at T_A=25°C).

The battery charging rate characteristics shown in Figure 2.5a are achieved in the lab by using a power supply to charge the batteries thereby simulating the (DC) input solar current that would alternatively be supplied via a solar-PV system. The results demonstrate a linear relationship between charging rate and time taken for the battery to be charged to 100%. That

is if the charging rate is doubled then the time taken to fully charge the battery is halved. The rate of battery discharge from testing at 50W was done with DC testing at a nominal (time-averaged) 50W load (4A, 12Volts) as well as a dynamic (fluctuating) DC load of 50W±30W. Figure 2.5b shows the effect of fluctuating and time-averaged loads on battery performance with fluctuating loads causing the battery to deplete at an increased rate. The rate at which the battery depletes is an important factor. These two loads with the same mean power characteristic were used to help model the effect of merely using the nominally designated (steady) DC power specifications of an RO unit (50W,4A,12VDC), versus incorporating the exact intricacies associated with a dynamically fluctuating DC load from a reciprocating pump RO unit (50W±30W, 4.17A±2.5A, 12VDC). The battery's State-Of-Charge (BAT_{SOC}) is defined as the amount of energy stored in the battery at a required power rating. To establish the efficiency of the DC convertor embedded within the stand-alone PV energy system, the output power drawn (P_0) by a static (50W) DC load connected to the system was compared to the input power supplied (P_{IN}). Figure 2.6 illustrates the DC-DC conversion process for this system is approximately 99% efficient whilst the DC-AC converter is approximately 82% efficient. Because the RO unit operates under a DC mode, the subsequent simulations therefore considered the DC-DC efficiency.

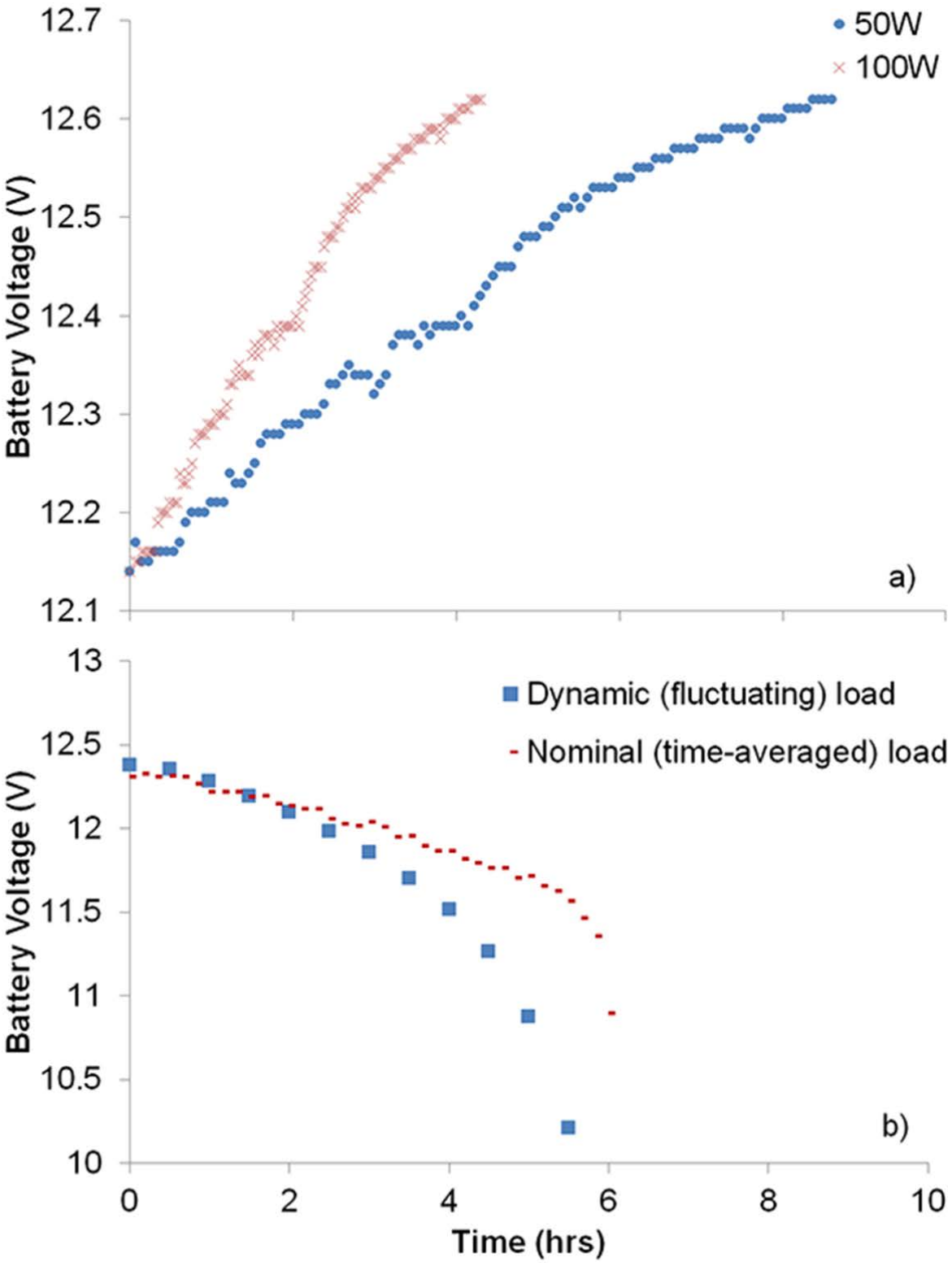

Figure 2.5 - Battery characteristics: a) measured battery charging (55Ah, T_A=25°C) over time at varying input rates. b) Measured battery discharge (55Ah, T_A=25°C) over time at 50W dynamic (fluctuating) load and 50W nominal (time-averaged) load.

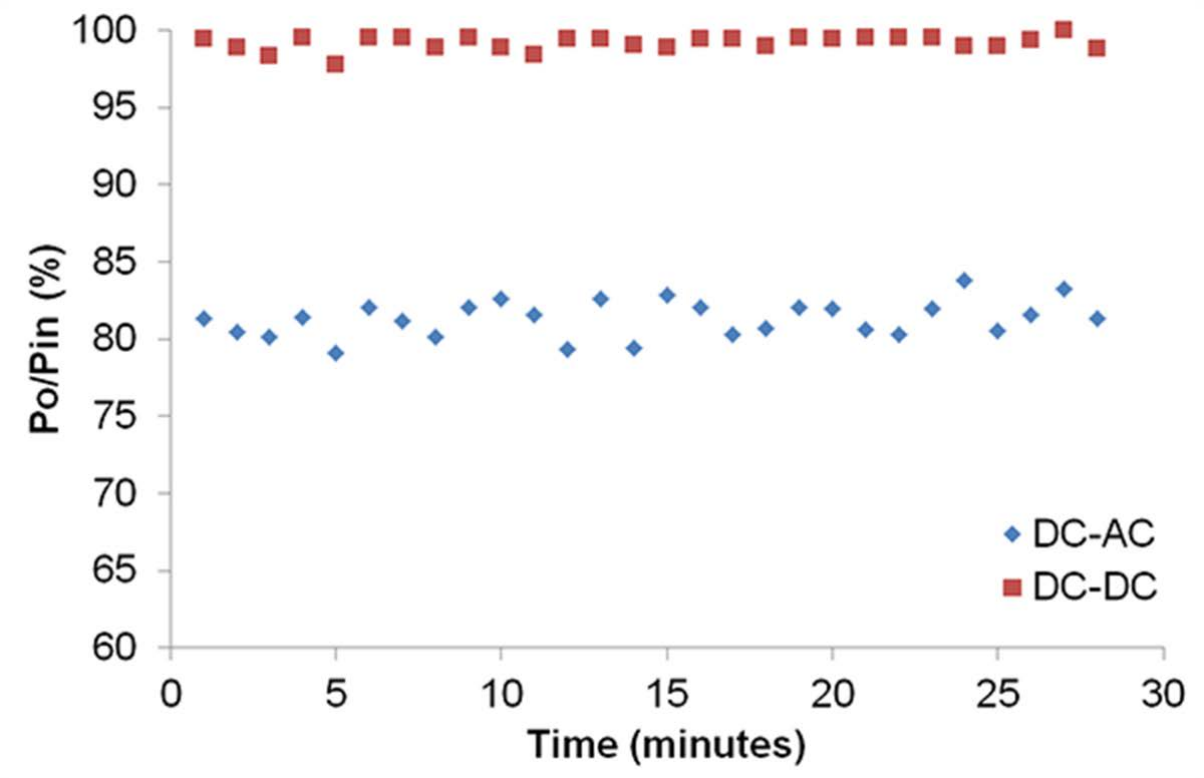

Figure 2.6 - Solar-PV system converter under different modes of operation (DC-DC and DC-AC).

Energy consumption associated with desalination is a major element that contributes to the cost of freshwater production, production rate being dependent on feedwater composition, pre-treatment and pressurising [31-34]. The simulated saline water used to supply the RO unit was prepared using pre-dissolved solutions of (crystallised) rock salt in demineralised water (at different levels of salinity). Total Dissolved Salts (TDS) in the feedwater were measured using a water conductivity meter (make: Eutech Instruments- Singapore, model: CyberScan CON 10 Cond/TDS meter). The range of salinity investigated was from 1% to 4% which resembles brackish to high saline seawater, respectively. To accurately model RO device characteristics, experiments were undertaken to establish the dependence of specific energy consumption (kW-hr/m^3) on feedwater salinity in the range of 25°C to 35°C. Figure 2.7a shows that specific energy consumption increases substantially with an increase in salinity. By referring to Figure 2.7b it can be seen that the feedwater salinity also affects the potable water production rate. An increase in salinity decreases the rate at which potable water is

produced from approximately 5L/hr to 4.2L/hr. Water temperature, potable water production rate and variable salinity is accounted for in the simulations for the annual yield of potable water.

Finally, a data acquisition unit (make: National Instruments- U.S.A, model: CompactRIO cRIO-9072) was incorporated in order to take the measurements of voltage, current and temperatures.

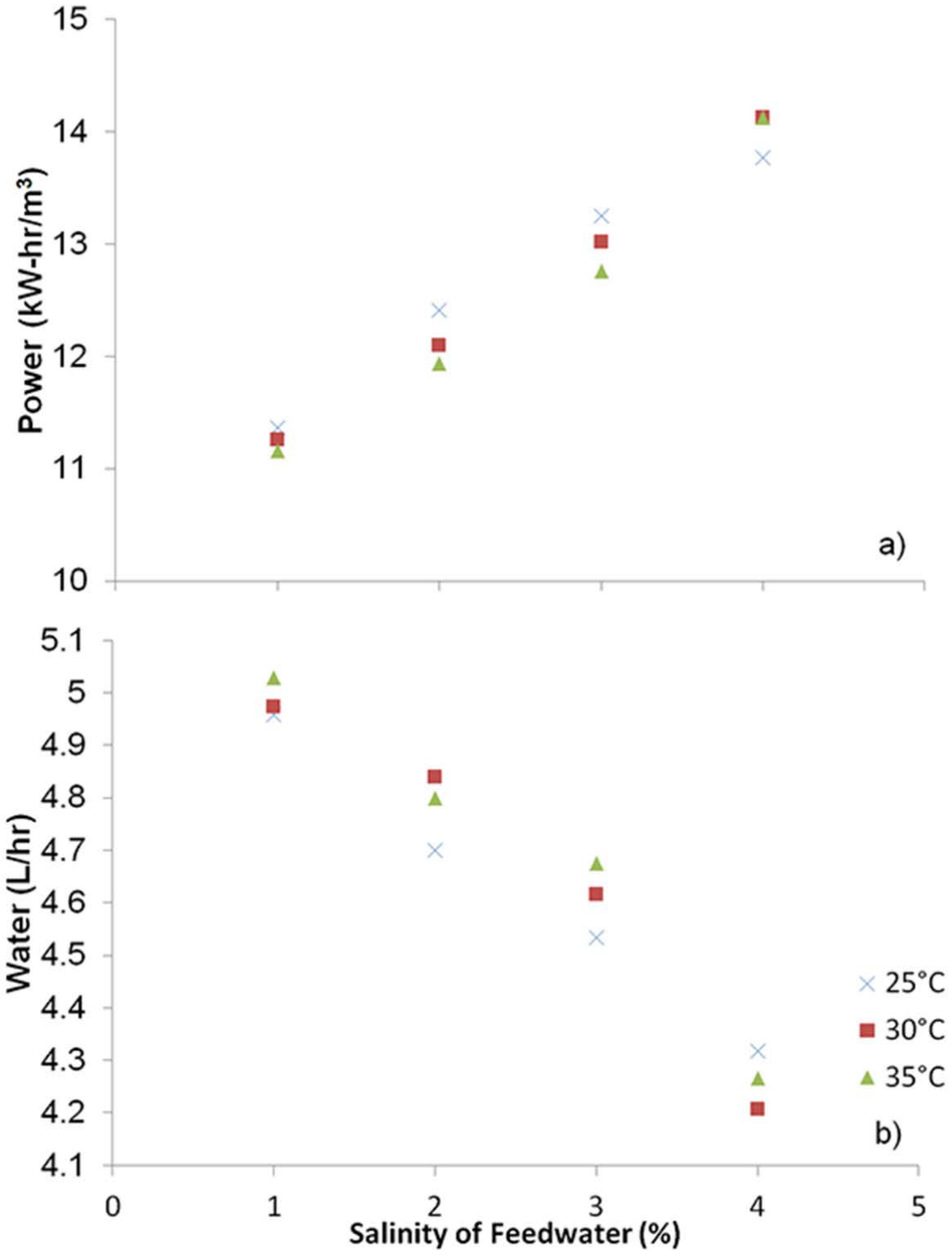

Figure 2.7 - Experiment based characteristics for a) the variation of specific energy consumption for RO at varying T_A and salinity of feedwater. b) The potable water production rate for RO at varying T_A and salinity of feedwater.

2.4 - Modelling- Methodology

Once the device specific characteristics of the PMU and RO unit were resolved, modelling was used to predict the total conversion of solar energy via the PV panels[4] as well as the battery's instantaneous State of Charge (BAT_{SOC}).

Solar irradiance: Solar irradiance is the energy incident upon the earth surface which can be collected via photovoltaic panels and converted to electrical energy. Although (location specific) meteorological data based on cumulative (total) daily solar irradiance is available for a location in Australia (-31.75°, 115.8°), utilizing solar irradiance models can yield (global) irradiance (I_G) resolved to a higher resolution at either 1hr or 1 minute. The utilization of solar irradiance models can therefore allow (energy system) simulations to be hourly or minutely based rather than daily, hence pseudo-dynamic. For this purpose, global irradiation models are used to predict hourly or minutely resolved I_G over 365 days. Solar irradiance can be predicted by various models, many of which modify the ASHRAE clear sky model by proposing location specific factors A, B and C [35]. The ASHRAE model also forms the basis for renewable energy input into the simulations presented in this chapter.

$$I_G = I_N \cos\theta_Z + I_D \qquad \textit{Equ. 2.1}$$

$$I_N = A \times exp\left[\frac{-B}{\cos\theta_Z}\right] \qquad \textit{Equ.2.2}$$

$$I_D = C \times I_N \qquad \textit{Equ.2.3}$$

The hourly global irradiance (I_G, W/m^2), hourly beam radiation (I_N, W/m^2), hourly diffuse radiation (I_D, W/m^2) may be calculated using Equation 2.1 to 2.3 with factors A and B as per Table 2.2. Factor C is also set to zero because this allows predicted daily averages to match those from actual averaged daily data [36]. The zenith angle (θ_Z) is also dependent on the two parameters of latitude (Φ), the hour angle (ω) and may be calculated as per Equation 2.4 to 2.8. The nth day of year (n) is also defined through the declination angle of the sun (c) as given by Equation 2.8:

$$\cos\theta_Z = \sin\Phi \sin\delta + \cos\Phi \cos\delta \cos\omega \qquad \textit{Equ.2.4}$$

[4] Refer to Appendix D for PV panel model.

$$\omega = 15(12 - LAT) \qquad \textit{Equ.2.5}$$

$$LAT = ST + ET \pm 4(STL - l) \qquad \textit{Equ.2.6}$$

$$ET = 229.2(0.000075 + 0.001868\cos x - 0.032077\sin x - 0.014615\cos 2x - 0.04089\sin 2x) \qquad \textit{Equ.2.7}$$

$$\delta = 23.45\sin\left[\frac{360 \times (284 + n)}{365}\right] \qquad \textit{Equ.2.8}$$

The hour angle, which represents the solar angle remaining to solar noon, is equivalent to 15°hr-1 (365°/24hr) and 0.25°min-1 (365°/24*60min). The other parameters are defined as noon based Local Apparent Time (LAT), Standard Time (ST) Standard meridian for Local Time zone (STL), longitude of location (l)and the Equation of Time (ET) correction in minutes where x= (n-1)/360/365.

Parameter	**Value**	**Parameter**	**Value**
P_{MAX}	130 W_P	Efficiency	13.61%
T_{REF} (reference temperature)	25°C	U_{OC} (voltage max load)	17.2V

Table 2.2 - Solar-PV panel specifications (each) and relevant modelling parameters [40].

To validate the veracity of resolved I_G predictions, Figure 2.8a shows the predictions made using the ASHRAE model[5] compared to measured solar irradiance [37]. All solar hours plotted include standard time-zone corrections given by Equation 2.7 [35]. Since daily (averaged) solar irradiance values were verified, all minute resolved are also correct.

[5] Refer to Appendix D for ASHRAE Clear Sky model code.

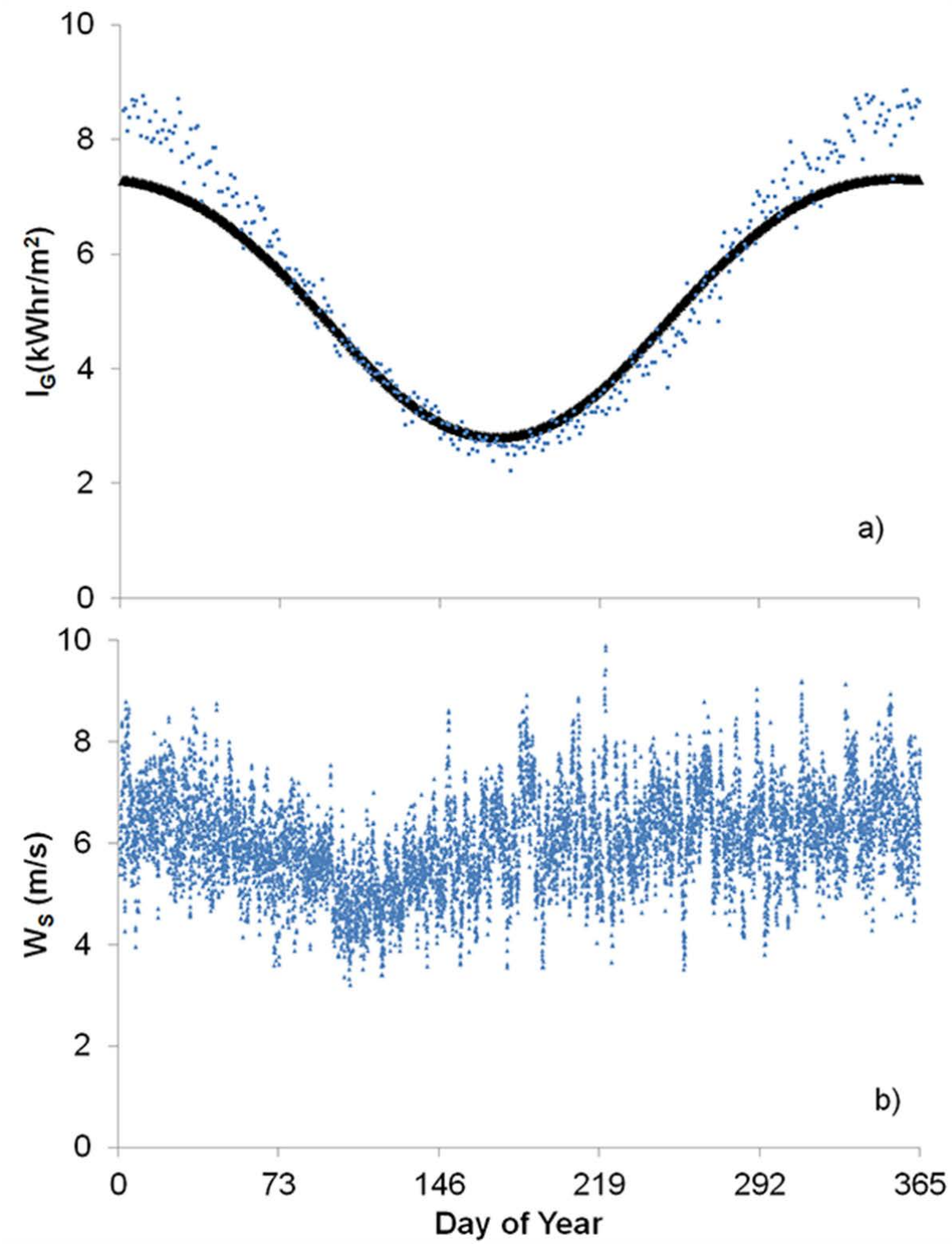

Figure 2.8 - a) Validation of irradiance. Dots: measured daily I_G (data: [37]); line: Daily predicted solar irradiance using the ASHRAE model. b) Annual variation of wind speed for a typical Perth based location (data source: [38]).

PV panels: Photovoltaic cells can be modelled using the single diode equivalent. This model mimics the solar irradiance as a current source connected in parallel with a diode generating electrical current from incident energy [39, 40]. Photovoltaic panels are similarly comprised of many cells (typically 36) which are connected in both series and parallel to produce power, with photocurrent (I_L) directly proportional to the irradiance (I_G) [39-41]. Diode characteristics also set the open circuit voltage of the PV cell thereby determining the cell I-V characteristics. The I-V characteristic curve can be generated as a function of incident solar irradiance, wind speed and the cell temperature using Equation 2.9 to 2.11[22]:

$$I_{pv} = I_L - I_0\left[e^{\frac{U_{pv}+I_{pv}R_S}{a}} - 1\right] - \frac{U_{pv} + I_{pv}R_S}{R_{sh}} \qquad \textit{Equ.2.9}$$

$$a = \frac{nkT}{q} \qquad \textit{Equ.2.10}$$

$$I_L = \frac{I_G}{I_{G.ref}}\left[I_{Lref} + \mu_{Isc}\left(T_{pv} - T_{pv.ref}\right)\right] \qquad \textit{Equ.2.11}$$

In these equations, the parameters are photocurrent (I_L), diode reverse saturation current (I_O), series resistance (R_S) and shunt resistance (R_{sh}) which corresponds to the leakage current and for theoretical modelling purposes is neglected. In addition, other parameters are open circuit voltage (U_{PV}), short circuit current (I_{PV}) and thermal voltage for a given diode quality factor (a). Also $I_{G.ref}$ is reference solar irradiation (1000 Wm^2), $I_{L.ref}$ is the short circuit current at reference temperature and solar irradiation (A), T_{pv} is the operating temperature of the cell (Kelvin), $T_{pv.ref}$ is the reference temperature of 298K and μ_{Isc} is the temperature coefficient of the short circuit current. The saturation current of the diode I_0 is also given by [22]:

$$I_0 = I_{0ref}\left(\frac{T_{pv}}{T_{pv.ref}}\right)^3 e^{\left[\left.\frac{E_g}{kT}\right|_{T_{pvref}} - \left.\frac{E_g}{kT}\right|_{T_{pv}}\right]} \qquad \textit{Equ.2.12}$$

$$I_{0ref} = \frac{I_{sc.ref}}{e^{\frac{qV_{oc\,@\,Tpv.ref}}{nkT_{pv.ref}}} - 1} \qquad \textit{Equ.2.13}$$

In Equation 2.12 to 2.13, the different parameters are the operating temperature of the cell (T_{pv}), the reference temperature from manufacturers specifications ($T_{pv.ref}$), energy band gap

(E_g), short circuit current ($I_{sc.ref}$) and the short circuit voltage ($V_{oc.ref}$) of the PV panel at a reference temperature, typically 298K.

Integrating solar power into the system simulations must take into account the PV panel current-voltage (I_{PV}-V_{PV}) characteristics which are hardware reliant but are strongly affected by incident solar irradiance (I_G), panel temperature (T_{PV}) and wind speed (W_S). Parameters I_G, T_{PV} and W_S are location dependant and dynamic (time dependant and seasonal). In the simulations, panel temperatures were derived using measured (meteorological) ambient temperatures (T_A) and localised wind speed (W_S). Wind speed affects the performance of the solar cell through its effect on PV panel temperature [22]. A sample of the wind data used [38] is plotted in Figure 2.8b. Equations 2.14 to 2.15 express the power (I_{PV}-V_{PV}) characteristics using (T_{PV}), W_S and T_A [22]:

$$T_{pv} = T_{mpv} + \frac{I_G}{I_{G.NOCT}} \Delta T_{pv} \qquad \textit{Equ. 2.14}$$

$$T_{mpv} = T_A + Ge^{(a_c + b_c W_S)} \qquad \textit{Equ. 2.15}$$

In these equations, the parameters are the instantaneous solar irradiation at Nominal Operating Cell Temperature (NOCT) is I_{GNOCT}; T_A is the ambient temperature; ΔT_{pv} is the temperature difference between the cell and the back surface of the PV panel; T_{mpv} is the back surface temperature of the PV module; W_S is the wind speed; and a_c, b_c are empirical constants for cell temperature calculations.

Simulations are later undertaken for panel areas of A_{PV}=1m^2 (unit area of PV panel), A_{PV}= 2.6m^2 (3 panels) and 8.7m^2 (10 panels) in order to show the effects of scalability. The power (I_{PV}-V_{PV}) characteristics are shown as a function of incident solar irradiance in Figure 2.9a and as a function of PV panel temperature (T_{PV}) in Figure 2.9b. Through the models used, later simulations will also incorporate the effects of T_{PV} and W_S on PV panels which gives more accurate representations of overall power P_{PV} (P_{PV} =I_{PV}*V_{PV}), the effects of which are shown in Figure 2.9c. In the systems simulations, values for T_A were based on meteorological data [36] and were set at the peak temperature for each day which is approximately around solar noon.

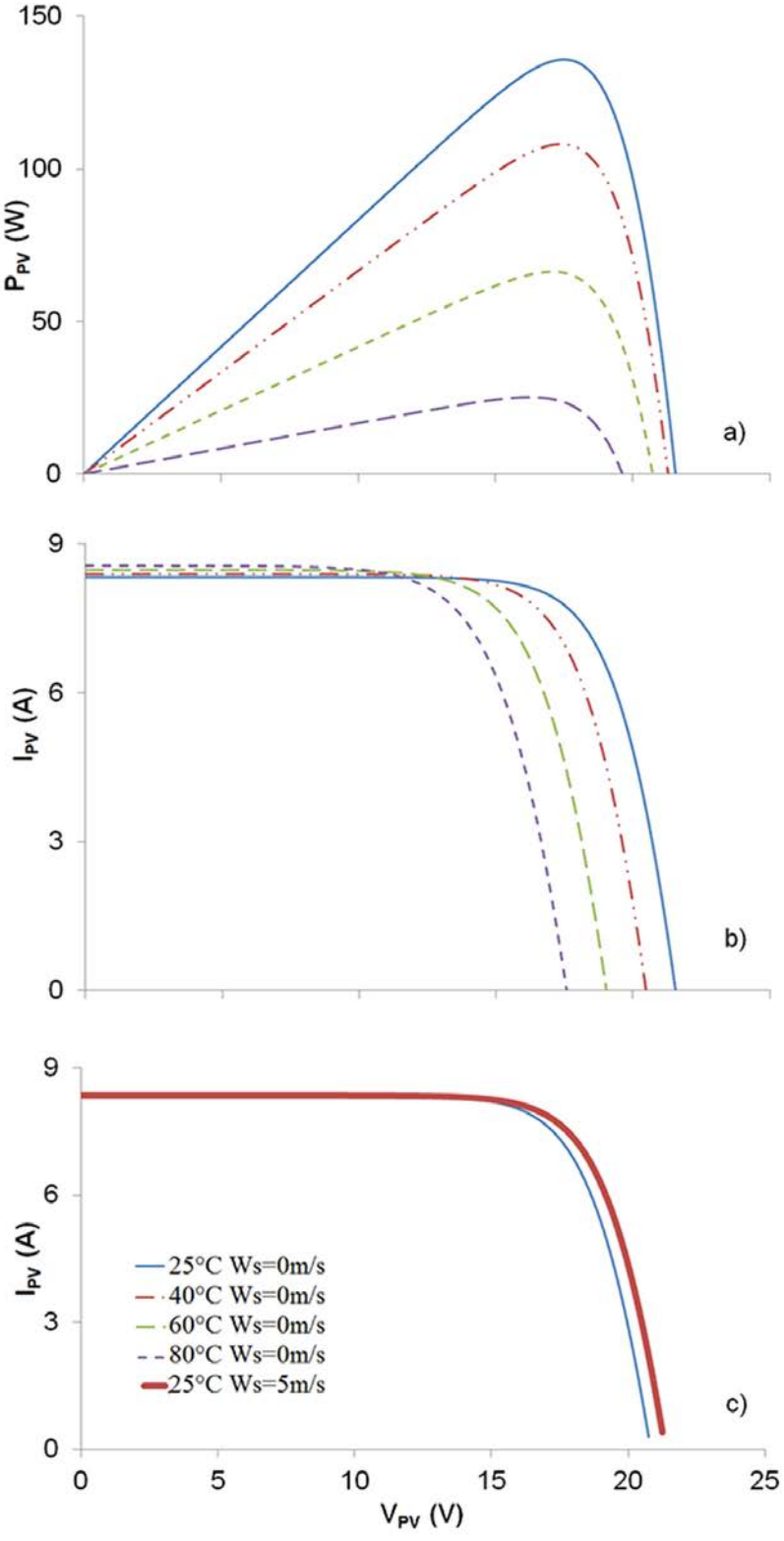

Figure 2.9 - Modelled PV characteristics: a) power versus voltage at varying I_G (T_A=25°C, W_S=0m/s). b) Current versus voltage at varying T_{PV} and W_S=0m/s. c) Current and voltage at varying W_S (IG=1000W/m^2, T_A=25°C.)

Energy storage: Because solar irradiance is highly dynamic, integrating storage media into energy systems is designed to provide supplemental power to RO over periods when incident solar radiation is insufficient to generate enough power. The operational status of the energy system depends on its ability to support utilities (such as RO), maintain energy storage (SOC_{BAT}) at 100% for as long as possible and (potentially) yield excess renewable energy for seasonal storage. Based on the availability of renewable energy and the respective load demand, there may be an excess of renewable energy. This excess should also be utilised through charging batteries which can be used to supply the load under periods of low solar exposure or during the night [42, 43].

The battery voltage is an important consideration in the operation of the reverse osmosis unit. For RO to operate at its rated DC power (P_{RO}=50W), nominal RO device specifications require (battery) potential at 11.0-12.5V. For this reason, the simulations undertaken will also consider the battery as fully-charged at 12.5V (SOC_{BAT}= 100%) and fully depleted beyond "practical" use at 11V (SOC_{BAT}= 0%). As such, monitoring the battery voltage also provides a timeframe over which the RO unit operates on any given day or hour. Battery voltage and State of Charge is defined as [44]:

$$U_B(t) = (1+\propto t)U_{B0} + R_T I_B(t) + K_I Q_R(t) \qquad \textit{Equ. 2.16}$$

$$E(t) = E_{IN} + \int_0^t U_B(x) I_B(x) dx \qquad \textit{Equ. 2.17}$$

$$SOC_{BAT}(t) = SOC_{BAT}(t-1) + \frac{P_B(t) \times \Delta t}{1000 \times C_B} \qquad \textit{Equ. 2.18}$$

Where Equation 2.16 to 2.19, the different terms denote: battery voltage (U_B); self-discharge rate (α); internal resistance (R_T); battery current (I_B); polarisation coefficient (K_I); the rate of accumulated charge (Q_R); and E_{IN} is the battery initial charge (V). Other parameters in these equations are battery State of Charge (SOC_{BAT}); (P_B) is rate power flow (Charging P_B>0, Discharging P_B<0); time step (t); and (C_B) which is the total nominal capacity of battery in kW-hr. When the battery is at full capacity, SOC_{BAT} is 100%.

2.5 - Simulation and Results

Simulations are undertaken to investigate the effects of two factors on the overall performance of the energy system modelled, under the conditions of battery storage of excess

(renewable) energy and no excess energy storage. Temporal resolution (hourly or minute based) is examined in relation to the annual yield of potable water and the battery state of charge. The results apply for a specifically sized RO unit with investigations into the effects of time-resolved, versus time-averaged, characteristics on larger scaled RO units also being warranted in the future. However, results attained even for a lab-scale unit are important as they show the difference of using simulations which are either hour or minute based as well as the effects of incorporating nominally stated I-V (time-averaged power) characteristics (from data derived using device technical sheets) as opposed to actually including measured or dynamic I-V (fluctuating power).

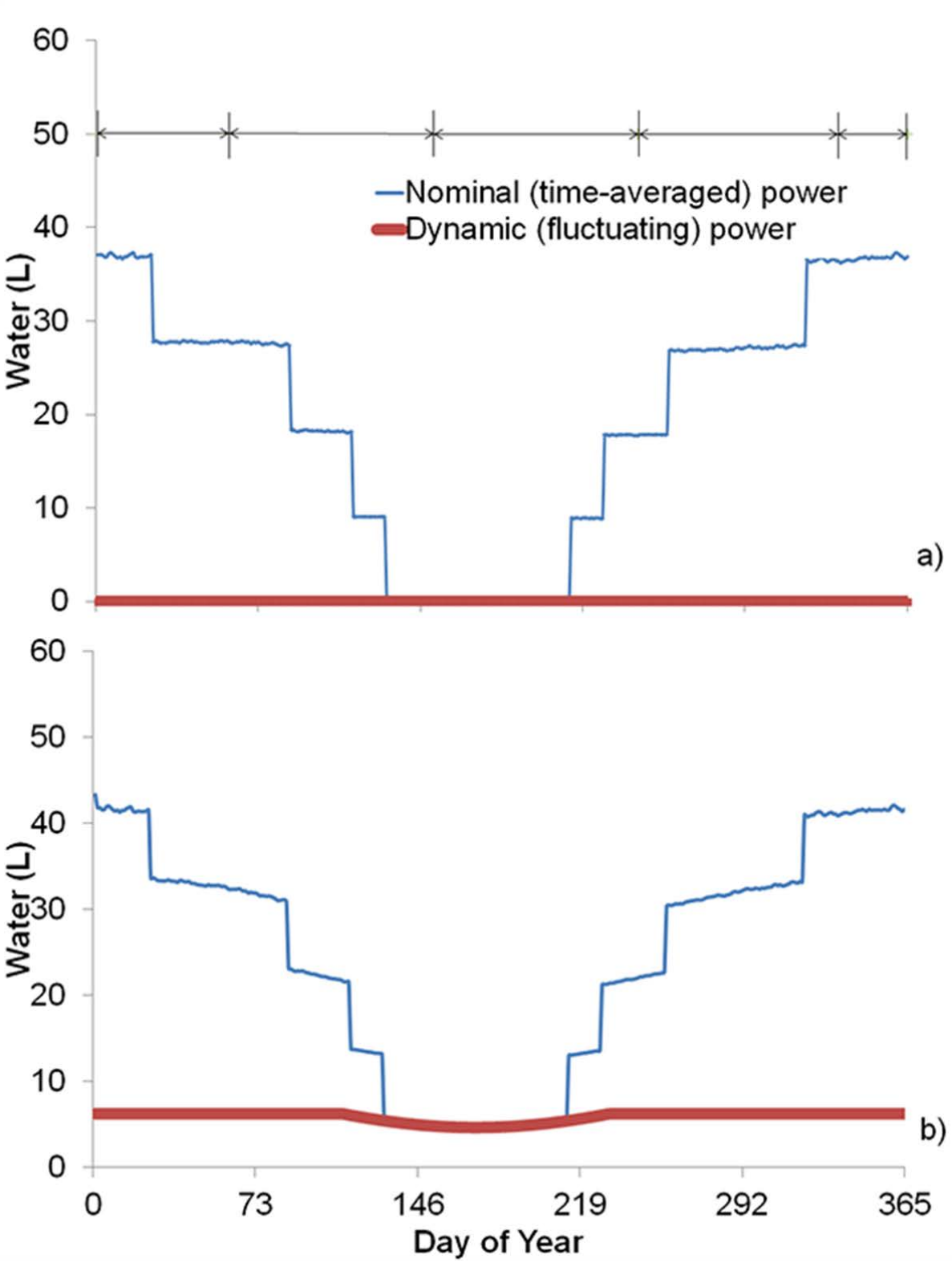

Figure 2.10 - Effect of method used to account for RO device power characteristics on maximum desalinated water produced from 3% salinity feedwater using hourly resolved simulations for a PV panel area of $1m^2$. a) No battery for energy storage; b) Battery incorporated.

Figure 2.10 shows the amount of desalinated water produced (per unit PV area) for both battery and battery-less configurations using hourly resolution. In Figure 2.10a, no battery is implemented (system running in Mode-I) which results in periods whereby the power delivered to the RO unit (by the PV panels) is inadequate and thus no potable water is produced. The incorporation of battery storage results in an increase in potable water production across all days of the year as evident in Figure 2.10b. This shows that energy storage media are needed in such instances to better utilise available renewable energy through, for example, by using 'excesses' to charge batteries or other methods such as energy storage via hydrogen.

A seasonal trend is also observed through a decrease in potable water production in (Australian) winter months due to the lack of low solar irradiance.

			Hourly Resolved Simulations		Minute Resolved Simulations	
	PV Panel Area	Yearly Values	Nominal (time-averaged) power	Dynamic (fluctuating) power	Nominal (time-averaged) power	Dynamic (fluctuating) power
No Battery	$1m^2$	Water (L)	7,302	0	7,340	0
		Excess (kWhr)	140	260	139	260
	$2.6m^2$	Water (L)	14,302	12,072	14,611	12,097
		Excess (kWhr)	446	351	441	350
	$8.7m^2$	Water (L)	17,159	16,696	17,262	16,457
		Excess (kWhr)	1986	1,816	1,990	1,822
Battery	$1m^2$	Water (L)	9,005	2,155	9,037	2,156
		Excess (kWhr)	0	70	0	70
	$2.6m^2$	Water (L)	16,582	14,311	16,882	14,319
		Excess (kWhr)	242	151	238	152
	$8.7m^2$	Water (L)	19,800	18,978	19,543	18,738
		Excess (kWhr)	1782	1,612	1,786	1,618

Table 2.3 - Comparison of yearly totals for excess energy and water production at different A_{PV}.[6]

The inclusion of dynamic I-V RO power characteristics results in a significant impact on annual potable water production. Table 2.3, which presents a summary of all simulation results, shows that using hourly based simulations and $A_{PV}=1m^2$, the use of nominal RO (I-V) characteristics yields approximately 7300L/year (battery-less) and 9000L/year (with battery) of potable water as compared to much lesser values when using dynamic RO (I-V)

[6] Nominal (time-averaged) power of the RO unit was taken from the manufacturers datasheet where dynamic was the result from experimentation.

characteristics. The discrepancy between the PV-systems' performance under two different ways of incorporating the power characteristics of utilities (RO) highlights the need to consider the instantaneous I-V drawn by these utilities. When only nominal power characteristics are considered in the simulations, system performance appears to only be governed by energy balances (energy needed to drive the RO versus total energy available from PV and batteries). When using dynamic power characteristics, there is an additional complexity of whether the instantaneous I-V will also trip the PMU. For a relatively small scale of PV energy conversion (A_{PV}=1m^2), the likelihood that power drawn by utilities will trip the PMU becomes more possible and hence less water appears to be desalinated.

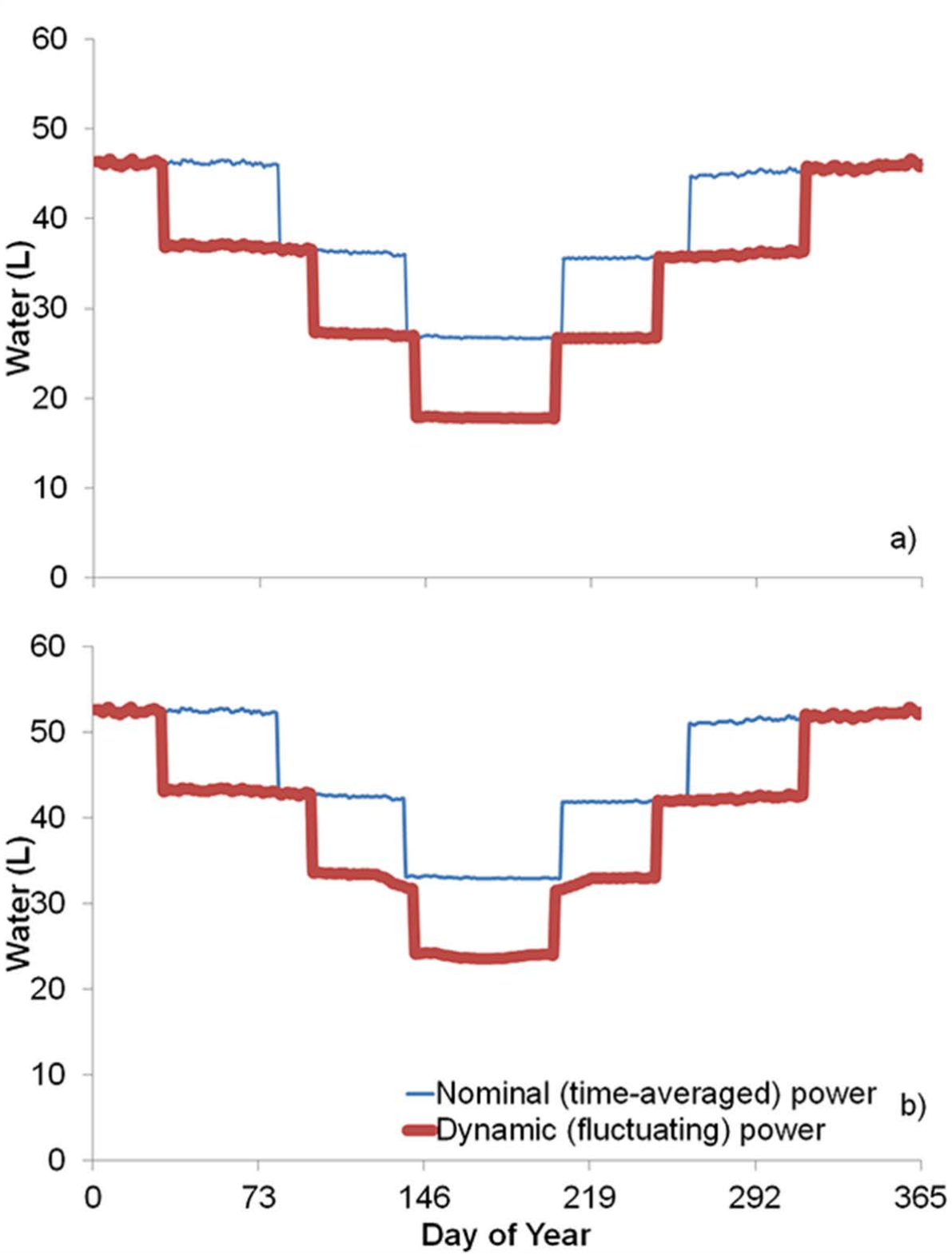

Figure 2.11 - Effect of method used to account for RO device power characteristics on maximum desalinated water produced from 3% salinity feedwater using hourly resolved simulations for a PV panel area of A_{PV}=2.6m^2. a) No battery for energy storage; b) Battery incorporated.

Figure 2.11 similarly shows overall energy system performance but for a PV panel conversion area of A_{PV}= 2.6m^2. Through increasing the scale of the PV array, the conversion of solar irradiance to electrical energy is increased thus providing more power. Increased solar energy results in the RO unit operating during periods where it was unable to do so at A_{PV}=1m^2. With the increase of renewable energy yield, Table 2.3 also shows that using nominal RO (I-V) power characteristics gives predictions with an increase in annual potable water production to approximately 14,300L/year (battery-less) and 16,500L/year (with battery). Similar results also apply for the inclusion of dynamic RO (I-V) power characteristics whereby increasing A_{PV} yields more power and 12,000L/year (battery-less) or 14,300L/year (with battery). Like with the case for A_{PV}=1m^2, the use of dynamic RO (I-V) characteristics at A_{PV}=2.6m^2 also provides less than that using nominal RO (I-V) characteristics. A further examination of the data shown in Table 2.3 (or between Figure 2.10 and Figure 2.11), also indicates that the relative effect of using dynamic RO (I-V) characteristics, as opposed to nominal (I-V) characteristics, appears to diminish as A_{PV} increases. This also indicates that scalability is another consideration which impacts on the effect of including time-resolved device characteristics.

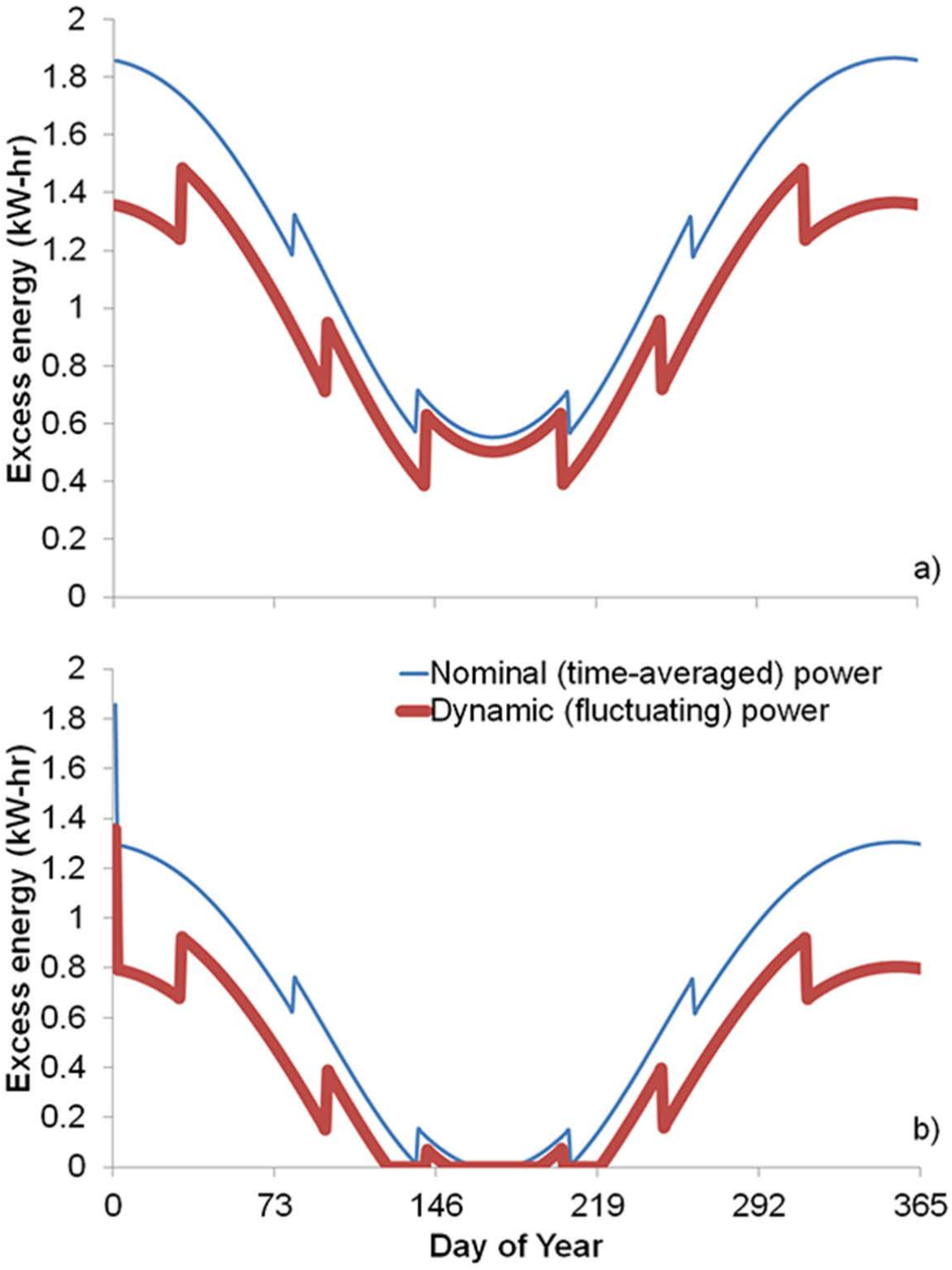

Figure 2.12 - Effect of method used to account for RO device power characteristics on total excess energy using 3% salinity feedwater with hourly resolved simulations for a PV panel area of $A_{PV}=2.6m^2$. Figure 2.12a - No battery for energy storage; Figure 2.12b - Battery incorporated.

Using battery storage improves the system's ability to meet overall utility demand (RO). As shown in Figure 2.3, without the use of battery storage the energy that is not used for desalination becomes excess energy. Figure 2.12 shows these excess energy for $A_{PV}=2.6m^2$. The amount of excess energy predicted with simulations using nominal RO (I-V) power characteristics is significantly more than those using dynamic RO (I-V) power characteristics. Additionally, a seasonal trend similar to annual potable water production is evident with less excess energy in winter months as compared to summer months. With no battery storage, Figure 2.12a illustrates there is more excess that is not captured or used for RO because of insufficient power on any given day compared to the incorporation of battery storage as shown in Figure 2.12b. There are periods where no excess energy is observed (with battery) as in these periods all available energy (not used for RO) is stored. Incorporating battery storage means excess energy can be stored for use under low solar irradiation conditions. However, data in Table 2.3 shows that increasing the scale of the system (more A_{PV}) seems to increase the amounts of water desalinated since battery power supplements solar energy and allows RO to operate for longer periods.

One observation from Figures 2.8 – 2.10 is the occurrence of abrupt (sharp) increases/decreases in the data for freshwater production and excess energy. This is believed to be due to the time step (hourly) used in the simulations presented thus far. However, within the hourly time-step there may exist times when the operational status of utilities, solar energy or battery SOC may change. This suggests the time-scale of resolution is another consideration worthy of further examination in the modelling. Very little evidence exists to show this aspect has been systematically researched in the literature on small scale stand-alone PV energy systems.

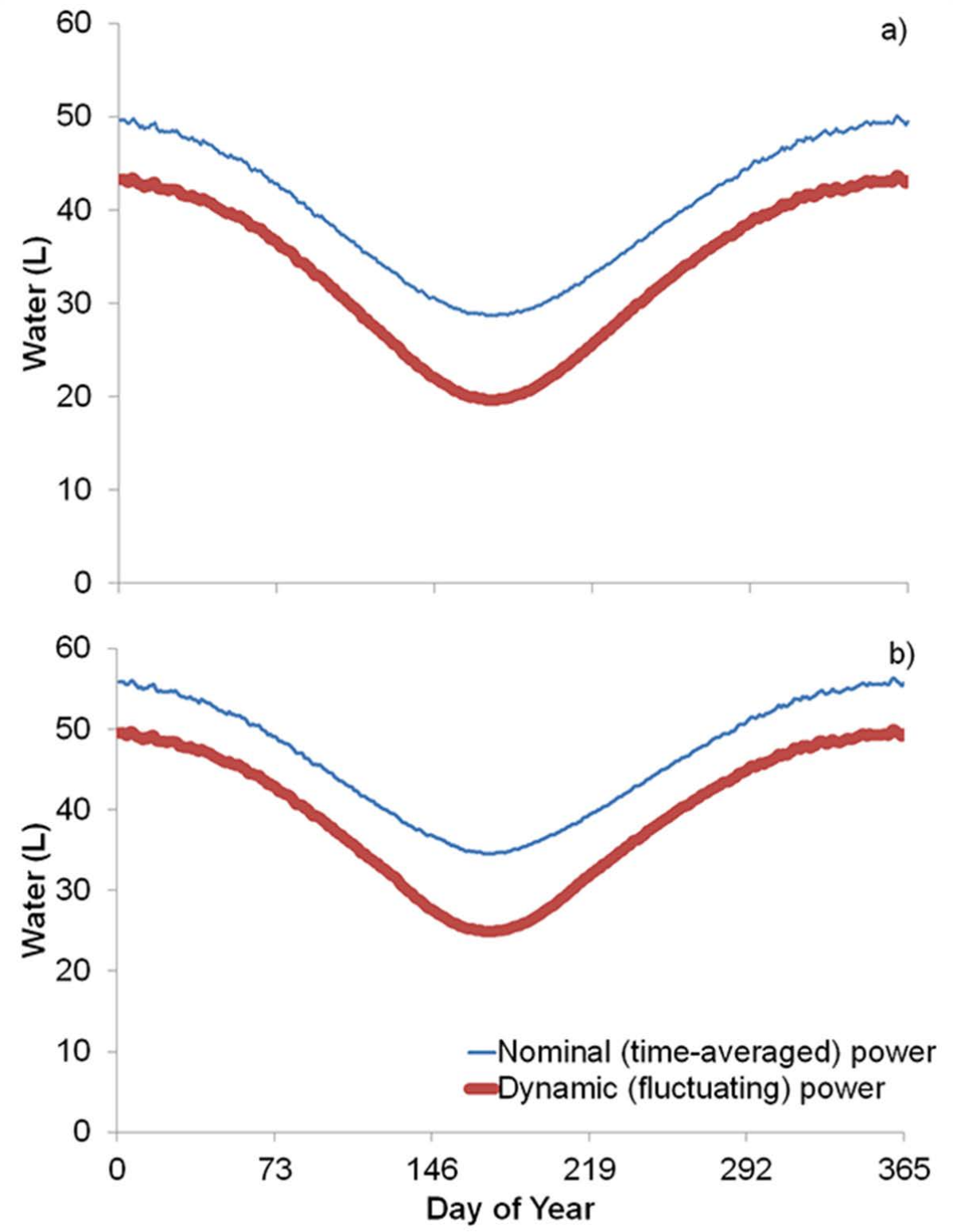

Figure 2.13 - Effect of method used to account for RO device power characteristics on maximum desalinated water produced from 3% salinity feedwater using minute resolved simulations for a PV panel area of $A_{PV}=2.6m^2$. a) No battery for energy storage; b) Battery incorporated.

Figure 2.13 shows data for water production using minute based simulations of solar irradiance and battery SOC. The minute resolution provides smoother results compared to Figure 2.11 (also for A_{PV}=2.6m^2). Table 2.3 also shows summary data for both predicted (annual) water desalination as well as excess energy (not utilised) using both minute based simulations and hourly. The data indicates that whilst some differences do exist (both with and without batteries); these are only insignificant for the system scale investigated.

2.6 - Conclusions

The modelling methodology has been presented for small-scale solar-PV systems with RO. Simulations are used to study the effects of different modelling methodologies on system performance over a period of one year. Overall system performance has been analysed in terms of total water produced (litres) and excess renewable energy stored (kW-hr), both with and without battery storage and for different scales of solar-PV conversion.

Simulations indicate that time-resolved power characteristics of system components should be measured and incorporated when analysing system performance, rather than merely using power derived from nominal (time-averaged) I-V specifications. The implications of ignoring (dynamic) sub-component power characteristics, such as the instantaneous current and voltage drawn by RO or other utilities and merely resorting to time-averaged nominal I-V levels such as those featured in device specifications, appears to significantly perturb the analyses for the range of conditions tested. Simulations also show these effects are more pronounced for solar-PV/RO systems with smaller PV conversion capacity (e.g., per metre square of panels). System scalability therefore appears to affect the sensitivity of simulations as well as the type of I-V characteristics used.

The simulations also confirm that including media to store excess renewable energy (such as batteries) appears to have greater impact on the performance of smaller systems compared to larger ones. In the systems modelled, energy storage was implemented via lead-acid batteries. Further investigation is warranted into the utilisation of longer-term storage technologies within solar-PV/RO systems, including the use of hydrogen which may be more suitable for prolonged storage and the effects of time-resolved, versus time-averaged, characteristics on larger scaled RO units. The need for excess energy storage is exacerbated as the power needed to run utilities increases (more water or less efficient RO) and renewable energy availability falls.

2.7 - Chapter References

[1] Saidur R, Elcevvadi ET, Mekhilef S, Safari A, Mohammed HA. An overview of different distillation methods for small scale applications. Renewable and Sustainable Energy Reviews. 2011;15:4756-64.

[2] Fritzmann C, Löwenberg J, Wintgens T, Melin T. State-of-the-art of reverse osmosis desalination. Desalination. 2007;216:1-76.

[3] He T-x, Yan L-j. Application of alternative energy integration technology in seawater desalination. Desalination. 2009;249:104-8.

[4] International Energy Agency. Key world energy statistics. 2010. DOI:

[5] Soric A, Cesaro R, Perez P, Guiol E, Moulin P. Eausmose project desalination by reverse osmosis and batteryless solar energy: design for a 1 m^3 per day delivery. Desalination. 2012;301:67-74.

[6] Bourouni K, Chaibi M. Solar energy for application to desalination in Tunisia: description of a demonstration project. Renewable Energy in the Middle East: Enhancing Security through Regional Cooperation. 2009:125-49.

[7] Davies PA, Hossain AK. Development of an integrated reverse osmosis-greenhouse system driven by solar photovoltaic generators. Desalination and Water Treatment. 2010;22:161-73.

[8] Saffarini RB, Summers EK, Arafat HA, Lienhard V JH. Technical evaluation of stand-alone solar powered membrane distillation systems. Desalination. 2012;286:332-41.

[9] Abdallah S, Abu-Hilal M, Mohsen MS. Performance of a photovoltaic powered reverse osmosis system under local climatic conditions. Desalination. 2005;183:95-104.

[10] Mahmoud M. Solar electric powered reverse osmosis water desalination system for the rural village, Al Maleh: design and simulation. International Journal of Sustainable Energy. 2003;23:51-62.

[11] Bourouni K, Ben M'Barek T, Al Taee A. Design and optimization of desalination reverse osmosis plants driven by renewable energies using genetic algorithms. Renewable Energy. 2011;36:936-50.

[12] Gude VG, Nirmalakhandan N, Deng S. Renewable and sustainable approaches for desalination. Renewable and Sustainable Energy Reviews. 2010;14:2641-54.

[13] Ma Q, Lu H. Wind energy technologies integrated with desalination systems: Review and state-of-the-art. Desalination. 2011;277:274-80.

[14] Davies PA. A solar-powered reverse osmosis system for high recovery of freshwater from saline groundwater. Desalination. 2011;271:72-9.

[15] Fahmy FH, Ahmed NM, Farghally HM. Optimization of renewable energy power system for small scale brackish reverse osmosis desalination unit and a tourism motel in egypt. Smart Grid and Renewable Energy. 2012;3:43-50.

[16] Kalogirou SA. Seawater desalination using renewable energy sources. Progress in Energy and Combustion Science. 2005;31:242-81.

[17] Kershman S, Rheinlander J, Gabler H. Seawater reverse osmosis powered from renewable energy sources-hybrid wind/photovoltaic/grid power supply for small scale desalination in Libya. Desalination. 2002;153:17-23.

[18] Manolakos D, Mohamed ES, Karagiannis I, Papadakis G. Technical and economic comparison between PV-RO system and RO-Solar Rankine system. Case study: Thirasia island. Desalination. 2008;221:37-46.

[19] Mathioulakis E, Belessiotis V, Delyannis E. Desalination by using alternative energy: Review and state-of-the-art. Desalination. 2007;203:346-65.

[20] Ghermandi A, Messalem R. Solar-driven desalination with reverse osmosis: The state of the art. Desalination and Water Treatment. 2009;7:285-96.

[21] National Centre of Excellence in Desalination. Australian Desalination Research Roadmap. 2011:p. x. DOI:

[22] Deshmukh SS, Boehm RF. Review of modeling details related to renewably powered hydrogen systems. Renewable & Sustainable Energy Reviews. 2008;12:2301-30.

[23] Ben M'Barek T, Bourouni K, Ben Mohamed KB. Optimization coupling RO desalination unit to renewable energy by genetic algorithms. Desalination and Water Treatment. 2012:1-13.

[24] Koroneos C, Dompros A, Roumbas G. Renewable energy driven desalination systems modelling. Journal of Cleaner Production. 2007;15:449-64.

[25] Geovanni S, Orlando L, Rafeal P, Alberto S, Sebastian P. Analysis of the current methods used to size a wind/hydrogen/fuel cell-integrated system: a new perpective. International Journal of Energy. 2010;34:1042-51.

[26] Hrayshat ES. A Wind-Powered System for Water Desalination. International Journal of Green Energy. 2007;4:471-81.

[27] Hoevenaars EJ, Crawford CA. Implications of temporal resolution for modeling renewables-based power systems. Renewable Energy. 2012;41:285-93.

[28] Turki M, Ben Rhouma A, Belhadj J. Experimental characterization of a Reverse Osmosis desalination process fed by hybrid power source. 6th International Multi-Conference on Systems, Signals and Devices. Tunisia 2009. p. 1-6.

[29] Hadjipaschalis I, Poullikkas A, Efthimiou V. Overview of current and future energy storage technologies for electric power applications. Renewable & Sustainable Energy Reviews. 2009;13:1513-22.

[30] Power Sonic. Sealed lead-acid batteries. 1998. DOI:

[31] Gude VG. Energy consumption and recovery in reverse osmosis. Desalination and Water Treatment. 2011;36:239-60.

[32] Qiu TY, Davies PA. The scope to improve the efficiency of solar-powered reverse osmosis. Desalination and Water Treatment. 2011;35:14-32.

[33] Avlonitis SA, Avlonitis DA, Panagiotidis T. Experimental study of the specific energy consumption for brackish water desalination by reverse osmosis. International Journal of Energy Research. 2012;36:36-45.

[34] Laborde HM, França KB, Neff H, Lima AMN. Optimization strategy for a small-scale reverse osmosis water desalination system based on solar energy. Desalination. 2001;133:1-12.

[35] Jamil Ahmad M, Tiwari G. Solar radiation models- a review. International Journal of Energy Research. 2011;35:271-90.

[36] Bureau of Meteorology (Australia). Temperature data for Wanneroo, Western Australia. 2011b. DOI:

[37] Bureau of Meteorology (Australia). Solar exposure data for Wanneroo, Western Australia. 2011a. DOI:

[38] Mahmoud Y, Xiao W, Zeineldin HH. A simple approach to modeling and simulation of photovoltaic modules. IEEE Transactions on Sustainable Energy. 2012;3:185-6.

[39] Walker GR. Evaluating MPPT converter topologies using a MATLAB PV model. Journal of Electrical & Electronics Engineering, Australia. 2001;21:49-55.

[40] Heckert Solar. HS-PL Solar Panel Datasheet. 2009. DOI:

[41] Bureau of Meteorology (Australia). Wind speed data for Ocean Reef, Western Australia.: Bureau of Meteorology; 2011c.

[42] Singh SN, Singh AK. Optimal design of a cost effective solar home power system - an alternative solution to DG for grid deprived rural India. International Journal of Research and Reviews in Applied Sciences. 2010;2:60-6.

[43] Achaibou N, Haddadi M, Malek A. Lead acid batteries simulation including experimental validation. Journal of Power Sources. 2008;185:1484-91.

[44] Pedrazzi S, Zini G, Tartarini P. Complete modeling and software implementation of a virtual solar hydrogen hybrid system. Energy Conversion and Management. 2010;51:122-9.

Chapter 3. The Impact of Renewable Energy Intermittency on the Operational Characteristics of a Stand-Alone Hydrogen Generation System with On-site Water Production

Daniel P. Clarke*, Yasir M. Al-Abdeli and Ganesh Kothapalli

This chapter was published as a full research paper in Desalination. Whilst all efforts were made to retain the original features of this article, minor changes such as the layout, number formats, font size and style were implemented in order to maintain consistency in the formatting style of the thesis.

3.1 - Abstract

In renewably powered remote hydrogen generation systems, on-site water production is essential so as to service electrolysis in hydrogen systems which may not have recourse to shipments of de-ionised water. Whilst the inclusion of small Reverse Osmosis (RO) units may function as a (useful) dump load, it also directly impacts the power management of remote hydrogen generation systems affecting operational characteristics.

This research investigates the impact on the hydrogen generation system when simulations utilise different methods to account for solar power needed to drive the system as well as varying scales of (short-term) battery capacity. The simulations, in MATLAB/Simulink, utilise two specific methods of irradiance prediction (ASHRAE clear sky model and Neural Networks) and are benchmarked against measured irradiance data for Geraldton (Western Australia). This imposes different levels of accuracy and intermittency. Laboratory testing and device-level models help simulate the operational characteristics of a hydrogen generation system including on-site water production. Operational characteristics studied include: total energy available for PEM electrolysis, ontime of the electrolyser in steady-state, the number of start/stop cycles for the electrolyser and its duty factor (litres of hydrogen generated over the total number of start/stops).

Results show that increasing systems' battery capacity only affects the operational characteristics of a PEM electrolyser up to a threshold capacity (Ah). Increasing battery capacity generally allows for more renewable energy penetration. Additionally, the hydrogen generation system behaviour is (generally) more accurately predicted, across all battery

capacities, when Neural Networks are used to predict the availability of solar irradiance. The ability to predict accurate levels of solar irradiance becomes more important in winter when irradiance is at its lowest. The results also highlight the need to use highly resolved (temporal) simulations which are able to better capture device-level operational characteristics.

3.2 - Introduction

Renewable energy is attracting increased attention to meet growing global energy demand by providing cleaner power generation options and decreasing dependence on fossil-based fuels [1]. However, the intermittent and seasonal nature of renewable energy sources (e.g. wind and solar) presents the need for effective (long-term) energy storage [2, 3] in addition to the appropriate sizing of (short-term) battery capacity to help cater for very short transients. Intermittency arises in numerous ways such as when there is no sunlight during night periods, if wind power fluctuates or cloud cover causes a variation in the output of Photovoltaic (PV) panels. To help mitigate against the effects of intermittency and seasonal variations, batteries are predominately used in renewable energy systems but these are not ideal for long-term storage due to high losses [4] as well as reliability issues and environmental impact [5].

Hydrogen has the potential to become one of the main energy carriers in the near-term, with literature covering different aspects of what has been termed the “Hydrogen Economy” [6-8]. Hydrogen fuel cells and electrolysers have been coupled with hydrogen storage and minimal battery capacity to yield stand-alone (renewable) energy systems. These systems may feature a single means of primary energy conversion, such as solar-PV [9-11] or wind turbines [12, 13], as well as hybridised architectures consisting of more than one primary energy conversion pathway [2, 14, 15]. In any of these hydrogen-based systems, there will often be a surplus of power in periods of low load (demand) or high renewable energy availability. These excesses which are not utilised arise when hydrogen storage tanks or batteries reach their fully charged capacity and results in less renewable energy penetration. Such excesses are normally diverted to a dump load so as to maintain energy system balance and avoid having to repeatedly start-up/shut-down system components. Depending on the hardware configuration and Power Management Strategy (PMS) employed, the dump load most commonly takes the form of an energy storage or dissipation device such as batteries [16-19], super capacitors [20], electrolysers [15, 21-23] or even resistive circuits [3].

Despite the critical reliance of stand-alone hydrogen energy systems on the availability of suitably pure feed water for electrolysis, there appears to be very little published research linking water desalination (as a form of dump load) to stand-alone hydrogen energy systems [24]. Such a linkage is necessary bearing in mind hydrogen systems are mostly intended for operation in stand-alone mode and based at remote locations. In such an operational landscape, continual shipments of deionised water may not be possible. This scenario means that integrating small-scale desalination into the energy system not only provides the necessary water for electrolysis (hydrogen generation) but can also be a (useful) dump load serving potable water requirements. From an operational perspective, the result is increased renewable energy penetration through better utilisation of primary energy sources such as solar.

There is scarcity of research into energy modelling of systems linking water production to hydrogen despite that such linkages are worth pursuing [25]. Additionally, many aspects of electrolysers have also been simulated such as power characteristics, operational temperatures and pressures as well as factors affecting hydrogen flow rates [9, 10, 26-28]. However, the factors influencing the cyclic operation of electrolysers when integrated into energy systems have not been adequately addressed in the published literature. Although PEM electrolysers suffer from degradation [29], the detrimental effects of start-stop cycles on PEM electrolysers appear to have received little attention in the literature. Under low-duty cycles which result in less severe intermittency compared to that anticipated with solar-PV and wind energy systems [30], some studies have revealed the number of start-stop does not significantly impact the electrolyser performance [28, 31]. One reason for this lack of research into PEM electrolyser durability may be the fact that such devices have historically been used in controlled (laboratory) environments to generate hydrogen for analytical use and not subjected to the intermittency of stand-alone systems. However, start-stop cycles become an important factor in other PEM devices such as fuel cells whereby the number of start-stops has been more extensively researched [32, 33] and found to limit the lifetime of such devices [12, 13]. As such, more work is needed to discern the impact of energy intermittency on hydrogen generation systems.

This chapter investigates the effect of solar energy intermittency and battery capacity on the operational characteristics of a solar-PV powered hydrogen generation system. The system architecture modelled is similar to that which would typically be integrated within a

remotely-based stand-alone energy system or hydrogen refuelling station. The system modelled is (conceptually) directly coupled with an RO device and its operation simulated over two seasons (winter and summer) to highlight two levels of solar energy intermittency and yield. Two specific solar prediction techniques are also deployed and compared to measured irradiance data so as to demonstrate the impact of the prediction technique on the operational characteristics of a hydrogen generation system. The methods used over the same timeframe are the ASHRAE (clear sky) model and Neural Networks , both of which are benchmarked against measured solar irradiance data for Geraldton, Western Australia [34]. The effects of superimposing different scales of (short-term) battery storage within the hydrogen generation system are also studied to ascertain its impact on the operational characteristics of a PEM electrolyser. System operational characteristics investigated include: number of start/stop cycles for electrolysis; hydrogen generation duty cycles (litres generated/start-stop); total water produced as feedstock for electrolysis; plus the total excess solar energy not utilised.

3.3 - Methodology

The renewably powered, stand-alone, hydrogen generation system which provides the basis for the simulations is shown in Figure 3.1[7]. This system consists of three solar-PV panels and a Power Management Unit (PMU), whereby a PEM electrolyser is driven through the PMU. More details on the subcomponents for this solar-hydrogen system (make: Heliocentris - Germany; model: Solar Hydrogen Extension) are noted below. If conceptually integrated with Reverse Osmosis (RO) and water de-ionisation, the overall hydrogen generation system can potentially be applied to coastal locations where an abundance of seawater is available to provide water for electrolysis. In establishing the relevant modelling parameters and (hardware specific) operational characteristics for system components, a range of laboratory-based measurements are undertaken, with some recourse to using physical models derived from the literature[8] (where indicated below). MATLAB/Simulink is used as the basis for all simulations conducted which extends to applying the ASHRAE model and Neural Networks to predict solar irradiance availability as well as modelling time-resolved energy flows.

[7] Refer to Appendix D for Chapter 3 system MATLAB/Simulink model.

[8] Refer to Appendix C for error analysis methods.

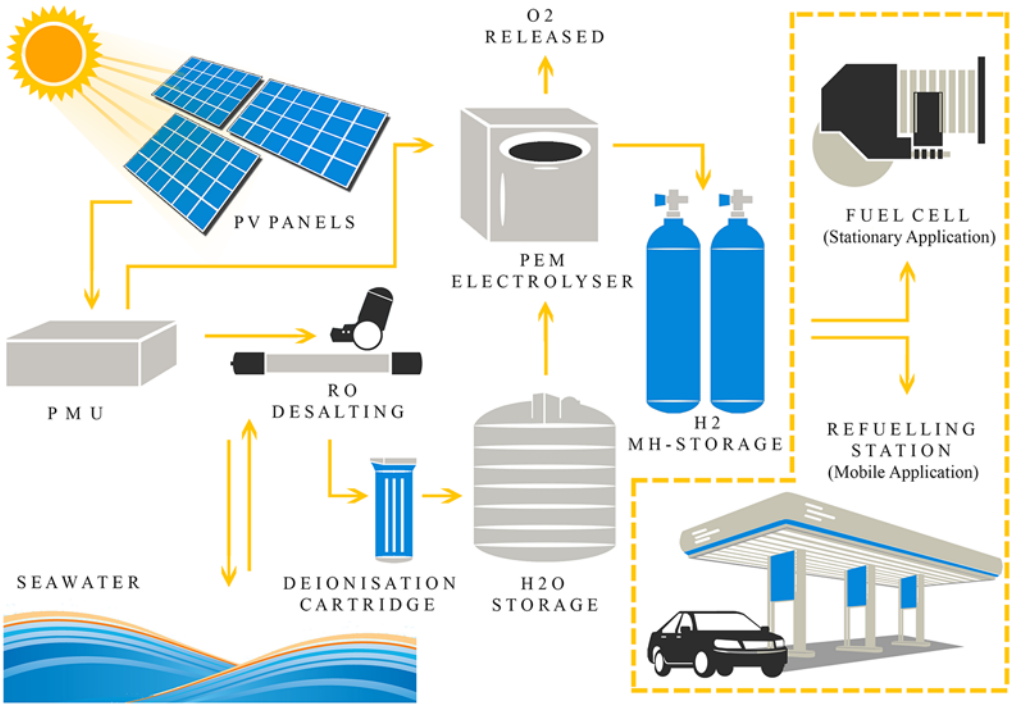

Figure 3.1 - Stand-alone hydrogen generation system with on-site Reverse Osmosis. The dashed box indicates potential integration scenarios into refuelling stations (mobile applications) or fuel-cells (off-grid power generation).

A. System-Level Simulation

To simulate the stand-alone hydrogen generation system, each component is first modelled (individually) before integrating all components into a single system-level simulation. The simulations aim to resolve four operational characteristics across the different seasons modelled and under the influence of varying intermittency in solar energy:

1. Total energy (kW-hr) and electrolyser ontime (T_0, minutes);
2. The number of start/stop cycles for electrolysis;
3. The duty factor for hydrogen production (litres/ start-stop); and
4. Desalinated water (litres) available for electrolysis.

Some general aspects related to implementing the simulations are noted below:

- To estimate the power generated by the PV-array and which forms the energy (input) into the entire system, the magnitudes and time-series for solar energy data should be based on irradiance measurements. However, because techno-economic studies conducted for establishing (new) energy systems might not always have access to measured solar irradiance, recourse can then sometimes be to predictions. This research uses three types of solar energy (input) data: measured irradiance sourced from the Bureau of Meteorology and predicted irradiance derived using Neural Networks or the ASHRAE (clear sky) model[9]. All irradiance data, whether measured or predicted, is for a specific Western Australian location. The measured irradiance data provides a benchmark to calculate the accuracy of predictions and identify the implications of different predictive techniques on the operational characteristics of the system. The two predictive methods also serve to impose two levels of intermittency for solar irradiance. All irradiance data, whether measured or predicted, is minute resolved and spans the Australian summer (December, January and February) and winter (June, July and August).

- A Power Management Strategy (PMS) is needed to control the activation of various hardware components and is normally implemented through the PMU. The simulation uses the hardware characteristics of the PMU which consists of four components: a Programmable Logic Controller (make: Beckhoff- Germany, model: BC9000); converters (DC-DC and DC-AC); a charge controller (make: SMART Power Systems-Germany, model: SMART MS 300) to limit maximum (solar) charging current for batteries to 30A at 12V and protect batteries from over-depletion; and some lead-acid battery capacity (12V, 55Ah). To further resolve the impact of battery scale on the operational characteristics of the hydrogen generation system, total battery capacity is numerically scaled in the simulations between 0Ah (no battery) and 200Ah (equivalent to 2.4kW-hr). Figure 3.2 presents this strategy.

- Pre-set power thresholds are typically used in a logic-based PMS to represent the minimum power requirements for activating/deactivating various components. In the present investigation, the pre-set power threshold in the PMS is not dynamically varied as it does not constitute an objective of this research. The utilisation of a different PMS will however (likely) impact the relative operational characteristics of a

[9] Refer to Appendix D for ASHRAE Clear Sky model code.

hydrogen system and has already been investigated elsewhere [3, 35]. In the PMS adopted and depicted in Figure 3.2, provided there is sufficient renewable energy to run the electrolyser for an operational time greater than ten minutes (i.e., about twice the transient start-up time for this device) and there exists a sufficient amount of deionised water, the PMS dictates the system generates hydrogen. The de-ionised water storage capacity is defined at an upper limit of 50L which is sufficient to supply the PEM electrolyser for 2 days. The simulations assume a cartridge type de-ioniser. The lower threshold of reserve water capacity below which the electrolyser will not function is set at 25L (a single day of operation in case RO is under preventive maintenance). Any energy not used to power the electrolyser is used to desalinate seawater and thereafter to charge batteries. At 10 bar output, the electrolyser draws about 250W. Where the total available power over the next time-steps is less than that which is sufficient to operate both the electrolyser and RO unit, the PMS diverts any excess power to raise the battery State-of-Charge (SOC). The simulations assume the battery is used for the short-term energy storage (only) and not long-term (seasonal) storage. Once the battery SOC reaches 100%, any power not utilised to operate the PEM electrolyser or RO unit is wasted and flagged as “excess energy not utilised”. Within the PMS, various counters are used to count amounts of hydrogen produced, water desalinated, component operational times, device start-stops, the battery SOC and excess energy not utilised.

- At the start of the simulations for any season (T=0mins), the battery State-Of-Charge (BAT_{SOC}) is assumed to be 100% with a defined minimum depth of discharge of 20% of rated capacity in any time-step.

- Laboratory-based testing is used to derive converter efficiencies (DC-DC and DC-AC), solar panel performance and battery characteristics. Details for how these were resolved in addition to the linkage between solar irradiance and PV panel output power used in simulations are reported elsewhere [19].

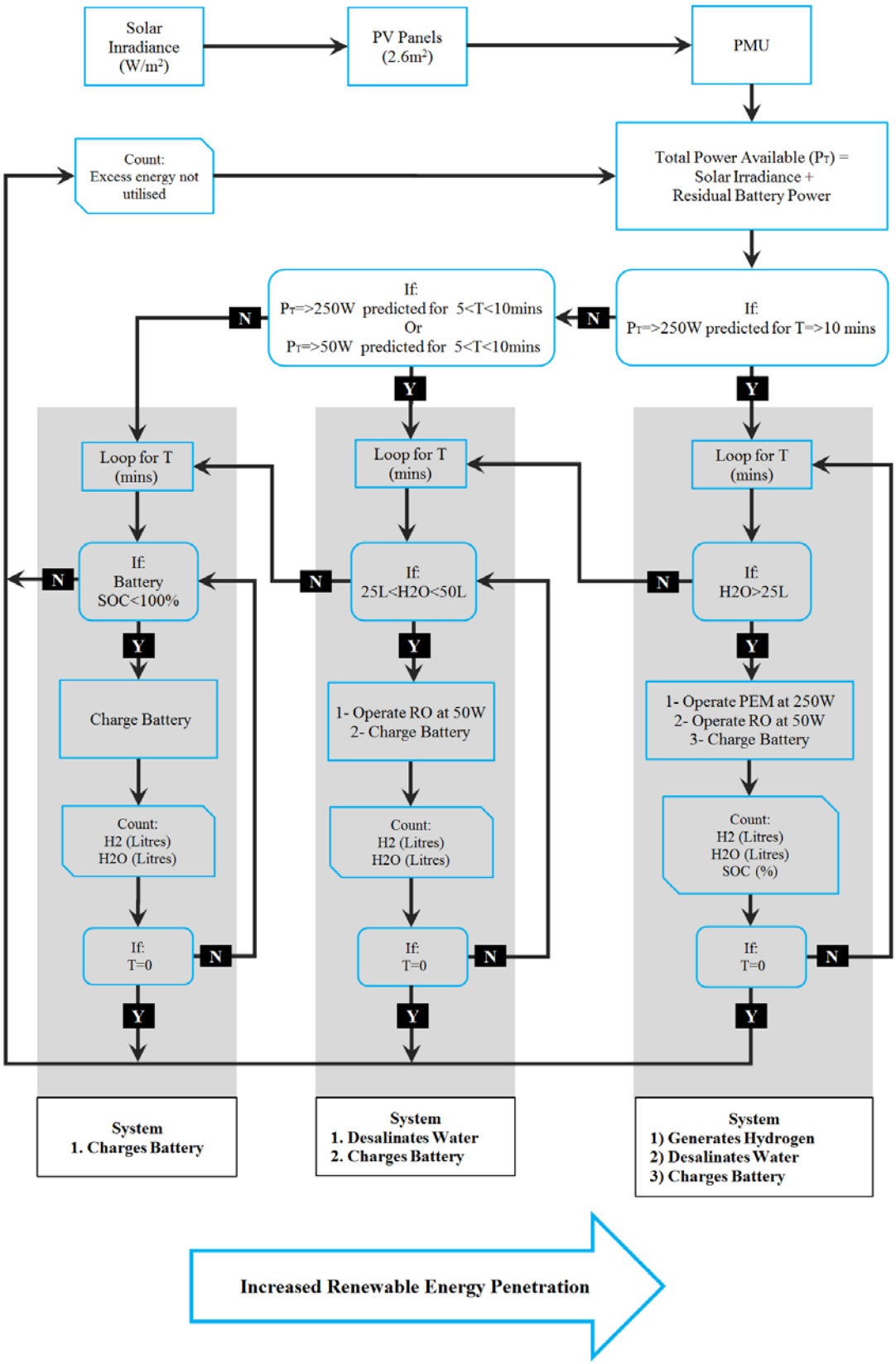

Figure 3.2 - The Power Management Strategy (PMS) used in the systems-level simulations. The time-scale for simulations is one minute applied over an entire season.

B. Electrolysis

PEM electrolysers, because of their favourable start-up characteristics and relatively lower power demand, have the potential to allow simple integration into small stand-alone hydrogen generation systems. In the present research, one of the aims is to identify how seasonal fluctuations of solar irradiance and electrolyser (device) start-up/shutdown characteristics affect the maximum amount of hydrogen which can be generated. As such, hydrogen storage capacity is considered unlimited in the simulations so as not to artificially limit the ability of the electrolyser to operate due to storage capacity. The basic model for the amount of hydrogen generated via electrolysis (in litres) is defined by Equation 3.1 [3]:

$$n_{H2} = \frac{n_C \times I}{n \times F} \times n_F \qquad \textit{Equ. 3.1}$$

In this regard, the hydrogen flow rate (n_{H2}) is designated in mol/s, whilst the other parameters are Faradays efficiency (n_F), number of electrolyte cells (n_C), operation current (I) in Amps, electrons per mole of H_2O (n=2) and Faradays constant (F= 9.65 x 10^4 C/mol).

Whilst Equation 3.1 has been extensively used in published research to simulate the production rate of hydrogen for a given energy input and efficiency across electrolysis, this (physics) representation does not include other electrolyser specific characteristics such as start-up time and inefficiencies arising from Balance of Plant (BOP) components which constitute (parasitic) power consumption. Such considerations are important for the integration of PEM electrolysers in stand-alone systems, particularly for small-scale systems but are often overlooked in simulations. Where intermittency is present, which is generally true for all electrolysers operated outside a laboratory environment via renewables, the need to consider such factors becomes imperative and can mean the electrolyser is likely to shut-off and require multiple starts per day. In the simulations undertaken in this study, the PEM electrolyser (make: DBS - Italy, model: NMH2 500) is part of the solar-hydrogen generation system and coupled with water supply. This AC powered electrolyser has a nominal hydrogen flow rate of 30L/hr and a maximum nominal power rating of 250VA at 10bar delivery pressure. Figure **3.3** shows data from laboratory derived tests for the current profile of the PEM electrolyser at an operating pressure of 10bar. The electrolyser is assumed to operate at this operating pressure throughout these results so as to limit the effects of BOP components on overall electrolyser efficiency (based on laboratory testing). The data shows a significant transient (approximately 275 seconds) associated with each start-up. For a

renewably powered hydrogen generation system, this transient puts a constraint on the ability to utilise the electrolyser every time it is started. As such, the PMS adopted for the simulations stipulates that only when (foreseeable) power levels are sufficient to maintain the PEM electrolyser in operation for 10 minutes or greater, will this device be activated. A 10min block essentially caters for a little over twice the length of the transient start-up. Laboratory testing also revealed that deionised water temperature (T_W) has no effect on electrolyser performance in the range of 25°C to 35°C. This temperature is assumed to be the average daily ambient temperature on any day in the simulations.

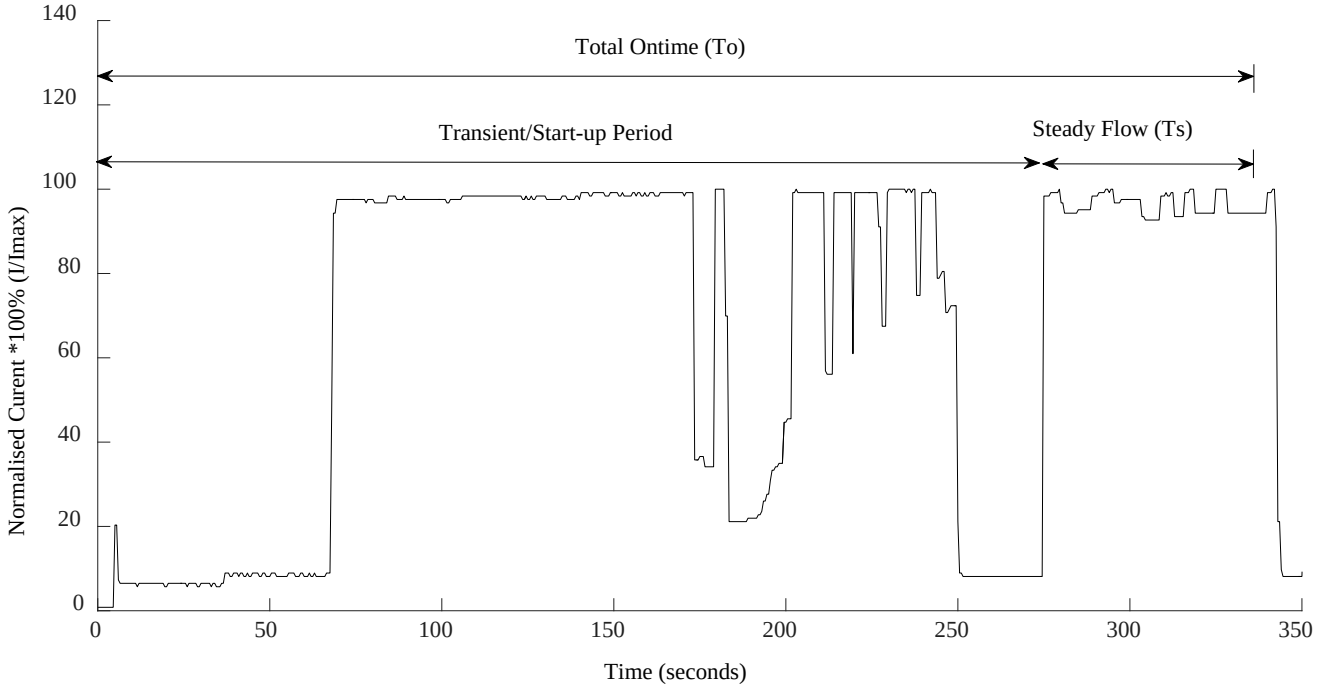

Figure 3.3 - Electrolyser current profile measured from start-up to steady flow. Data acquired at a sampling interval of 0.5s. Electrolyser operates at 10 bar internal pressure, 0.2psi/min pressure rise and T_W=22°C.

C. Reverse Osmosis

Reverse Osmosis (RO) is the most commonly integrated water purification technique in renewably powered desalination [36-39]. The scale of an RO unit determines the water volume flow rate and hence also impacts on feedstock available for hydrogen generation via electrolysis. The system-level simulations conducted incorporate a RO device (make: Katadyn – Switzerland, model: PowerSurvivor 40E). The device has a nominal desalinated water production rate of 5.5L/hr with a power rating of 50W and a recovery ratio of 10 %

potable water [40]. The recovery ratio for the RO device is defined as the amount of desalinated water produced for a given amount of input (saline) water. Selecting a relatively small RO device ensures the PMS maximises the use of solar energy for hydrogen generation and not water production. However, a number of factors which affect RO performance also need to be taken into consideration, and those include water salinity and temperature as well as its dynamic power (draw) characteristics. System simulations use the dynamic time-resolved characteristics which have been experimentally derived earlier for this RO device [19]. Because the hydrogen generation system being modelled is for a coastal location, the availability of saline water is considered unlimited. Feed water is assumed to have a Total Dissolved Salt (TDS) concentration of 3% corresponding to seawater. The tank storage capacity for desalinated water is set to 50L in the simulations with a minimum threshold of 25L considered. The initial capacity of 30L is assumed in the first time-step of simulations.

D. Powering the Hydrogen Generation System

In simulations of solar-PV hydrogen systems, the solar irradiance incident upon a horizontal or tilted surface at the location of interest is an important parameter as it largely determines the input power to the system. Due to the highly stochastic nature of solar irradiance, many models have been developed for the prediction of this energy input. In the research presented here, a minute-based temporal resolution is used throughout the simulations to provide an accurate system response to varying real-time conditions. Additionally, two specific methods of solar irradiance prediction are compared not only because of their different accuracies, but also because they impose two levels of intermittency on solar energy input. The impact of using both the ASHRAE clear sky model and NN on system operational characteristics is then benchmarked against that derived from measured data. The solar energy is converted via the PV array (make: Heckert Solar - Germany, model: HS-PL 135) which has three panels (total 2.6m^2) and supplies electrical energy to the PMU[10].

The ASHRAE clear sky model has the merit of being a mathematical model with (some) empirically refined constants used to predict solar irradiance, but the distinct disadvantage of not being able to predict the generally stochastic nature of solar irradiance or susceptibility to varying cloud cover. The second method selected to predict the solar irradiance is based on a Neural Network (NN) which although requires very large amounts of (historical) training

[10] Refer to Appendix D for PV panel model.

data, can also be designed to account for the likely occurrence of cloud cover by considering rainfall data in the same time-series. Historical rainfall and irradiance data is therefore used in the current study to provide a likely measure for cloud cover on total solar energy yield used to drive the hydrogen generation system. Neural Networks[11] are typically used in applications where analyses would be difficult when applied to nonlinear systems which exhibit stochastic behaviour and which are dependent on a large number of process parameters. In this manner, the present chapter also investigates the role which different solar energy prediction methods can have in relation to the cyclic operation of stand-alone hydrogen generation systems. Whilst the ASHRAE clear sky model provides a relatively simple approach for estimating minute-resolved solar irradiance for any location [41], applying the model to the Western Australian coastal city of Geraldton requires accurate values for three (local) model parameters (A, B and C). Representative values for these parameters have been derived for many locations around the world [42-44], however have not been published to date for Australia. This research has derived the parameters for Geraldton, Western Australia, and is given in the Section 3.7.

[11] Further details of the theory of Neural Networks are given in Appendix E

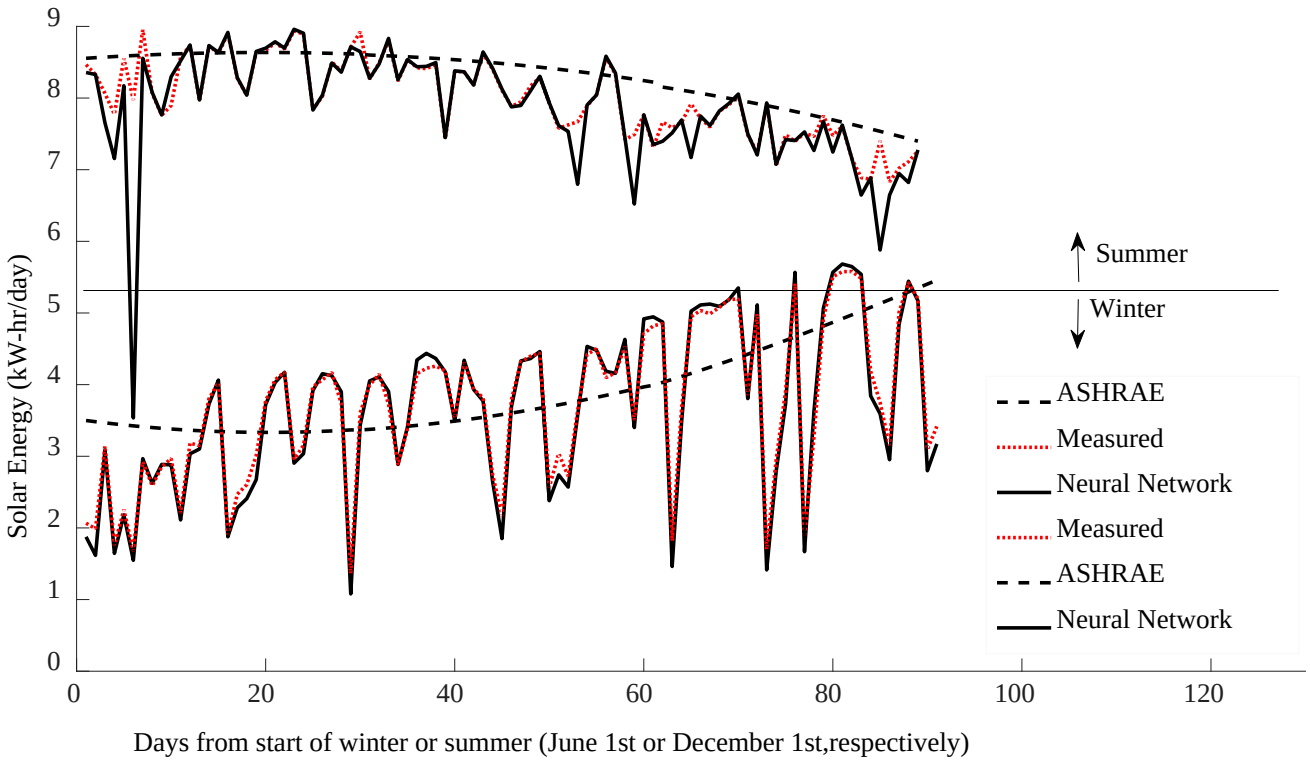

Figure 3.4 - Validations of the minute resolved solar irradiance data predicted (daily totals) for Geraldton, Western Australian. Predictions from the ASHRAE model and Neural Networks are benchmarked against measured data from the Bureau of Meteorology.

Figure 3.4 shows the daily irradiance totals obtained from summing up minute-resolved irradiance over a 24hr period for both Australian winter (1 June - 31 August) and summer periods (1 December - 28 February). Figure 3.5 depicts a typical daily profile for minute-resolved irradiance during a winter and summer day and highlights the stochastic nature of measured irradiance data. These results reveal that the NN predictions are able to better predict the time-averaged (Figure 3.4) and time-resolved (Figure 3.5) fluctuations in the measured irradiance data compared to the ASHRAE model across both seasons. The ensuing results will demonstrate that accurately representing strong variability heavily impacts on the operational characteristics of a hydrogen generation system.

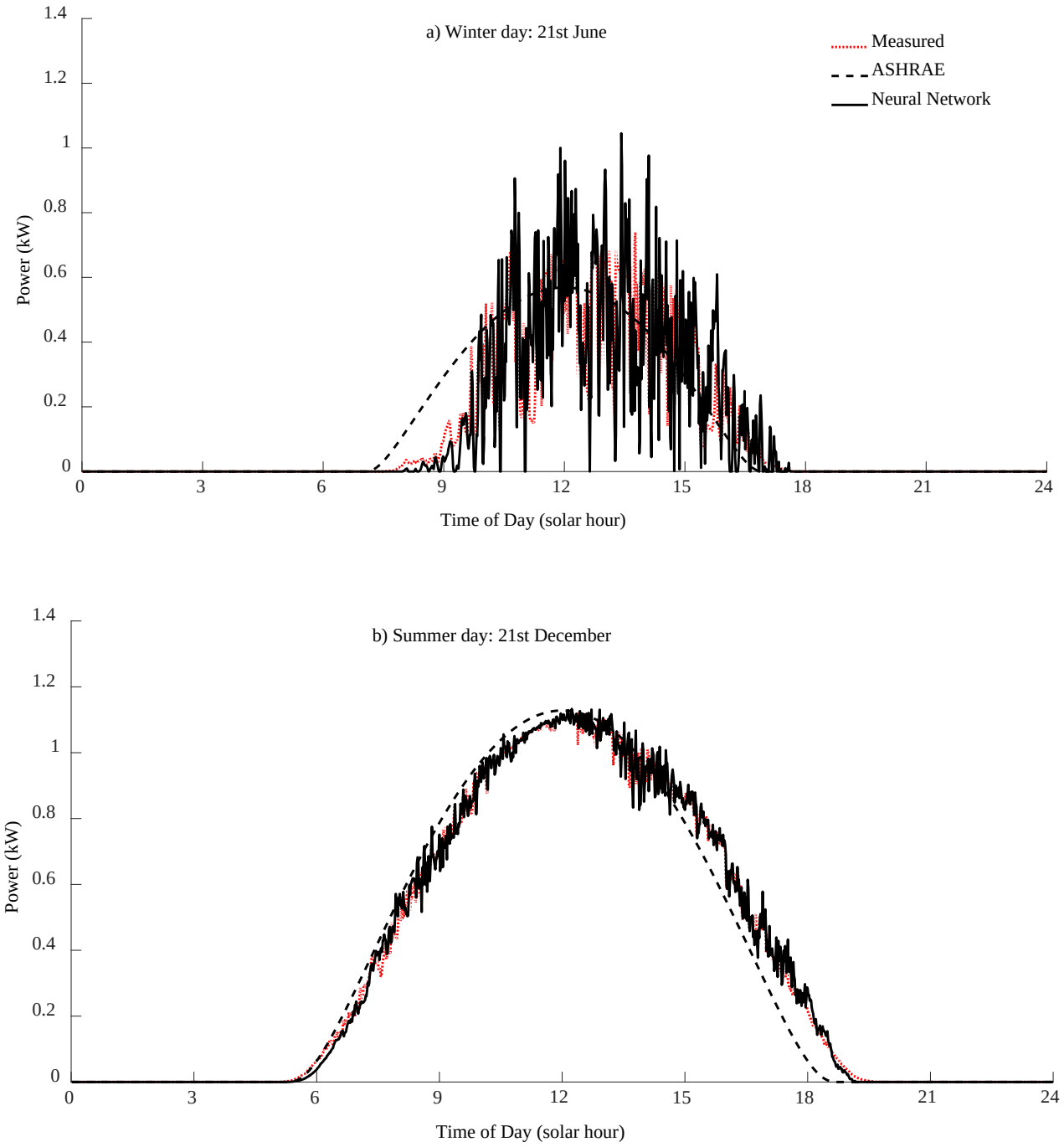

Figure 3.5 - Comparison of different minute resolved solar irradiance prediction methods for the summer and winter solstice: a) 21st June and b) 21st December. Location: Geraldton, Western Australia.

The use of Neural Networks with renewable energy systems is a well-researched area [6, 45-48], but the effects arising from prediction accuracy onto the cyclic operation of a hydrogen generation system have not been investigated before. In this regard, preliminary testing conducted (results not shown here) has revealed that if a Neural Network is used to predict

(future) solar irradiance data by being trained on historical irradiance data alone, it may be less accurate than if trained on historical irradiance data and another meteorological parameter, related positively or negatively to solar irradiance. As such, there is a positive impact expected on prediction accuracy when the number of input parameters is increased because the accuracy of a Neural Network depends on its ability to resolve relationships between independent inputs (such as calendar date) and dependant outputs (such as solar irradiance). The network then uses the perceived relationship between these input-outputs to predict future values of the dependant parameter, which in this study is minutely resolved solar irradiance needed to drive the hydrogen generation system. This method can be adapted to any location providing that access to meteorological data exists [45-48]. A Nonlinear AutoRegressive network with eXogenous inputs (NARX) is a type of recurrent dynamic network which is commonly used in time-series modelling and uses a feedback process to self-iterate. The defining equation for the NARX model is given below in Equation 3.2, whereby the output signal *y*(*t*) is regressed on previous (historical) values of the output signal and previous values of an independent (exogenous) input signal u(t):

$$y(t) = f(y(t-1), y(t-2), \ldots, y(t-n_y), u(t-1), u(t-2), \ldots, u(t-n_u)) \qquad \textit{Equ. 3.2}$$

In this research, the NN training dataset is derived from meteorological data for Geraldton-Western Australia [34] and spans a period of five years (2001-2005, minute resolved). To highlight seasonal effects on the hydrogen generation system, results for only the two extreme seasons of summer and winter will be presented. In predicting the solar irradiance at any time-step I(t), the Neural Network considers historical data as far back as I(t-60). This means the NN considers historical data for an equivalent hour (60 minutes) for each prediction of solar irradiance in the next minute (ahead). Additionally, the Neural Network also uses historical (daily total) rainfall data to help refine its predictions of minute resolved solar irradiance. Daily rainfall data is available from the Bureau of Meteorology for the same locality [49]. Total measured rainfall and solar energy in each season are given in Table 3.1. This data is also compared to predicted irradiance derived from the ASHRAE model as well as Neural Networks. Again, summer and winter seasons are used in simulations to help provide a contrast between the effects of high and low cloud cover (seasonal) rainfall on the

hydrogen generation system[12]. Figure 3.6 shows that for both winter and summer, the NN model with the inclusion of rainfall more accurately predicts irradiance compared to the ASHRAE clear sky model. Because the amount of rainfall in winter far exceeds that in summer, it is also seen the biggest errors (peaks) associated with the ASHRAE model correspond with calendar weeks of increased rainfall. It is during such periods of strong rainfall where NN out-performs the ASHRAE model for solar energy input into the hydrogen generation system. Alternatively, for the summer season where rainfall is minimal, the results derived from both the ASHRAE and NN predictions are mixed in terms of accuracy. To calculate the percentage error depicted in Figure 3.6, Equation 3.3 is used:

$$Error\ (\%) = \frac{|Predicted\ Value - Measured\ Value|}{Measured\ Value} \times 100 \qquad \textit{Equ. 3.3}$$

Sournce of Irradiance Data	**Total Solar Energy Across Season (kW-hr)**	
	Summer	**Winter**
Measurements	255	121
ASHRAE Model	264	127
Neural Networks	251	119
Total Rainfall (mm)	**5**	**222**

Table 3.1 - Total solar energy[13] (across summer and winter) as predicted by the ASHRAE model and Neural Networks. Measured (annual) solar energy data, averaged over 2001 to 2005, is also given against these for comparison. Predictions are for a system comprising three solar panels (2.6m^2). Annual average seasonal rainfall is also shown. Location for data is the Western Australian city of Geraldton (latitude: -28.77°, longitude: 114.61°).

[12] To check the robustness of the predictions when applied to other geographical locations, preliminary analyses (not given here) were also undertaken for another city (latitude: -31.75°, longitude: 115.8°) [19].

[13] Total solar energy received (kW-hr) by the 2.6m^2 PV array

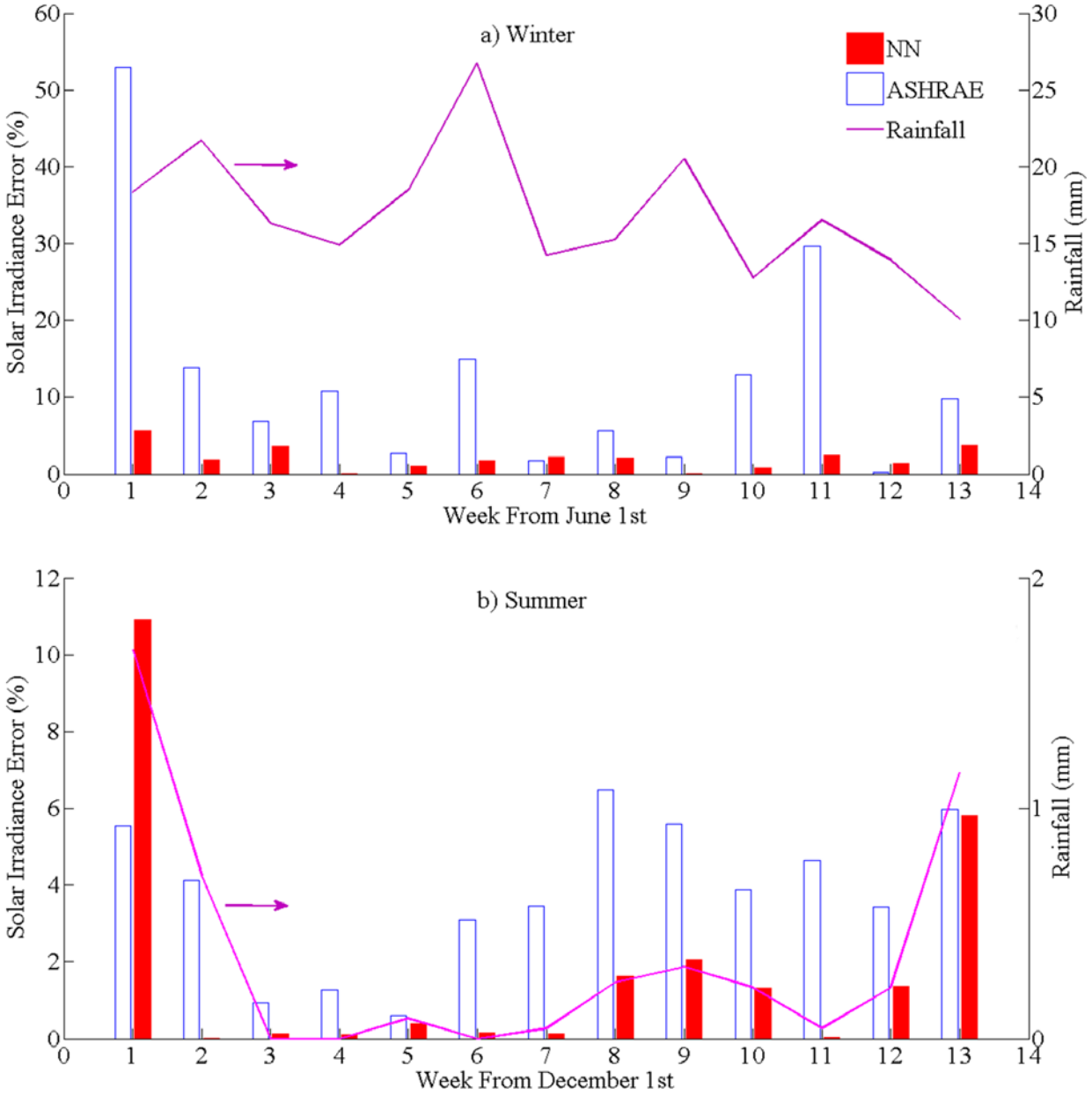

Figure 3.6 - Errors for different solar irradiance prediction methods relative to measured irradiance data: a) Australian winter (June-August) and b) Australian summer (December-February).

3.4 - Results and Discussion

Figure 3.7 presents data for the effect of different irradiance prediction techniques and varying battery capacity on the energy available to operate the PEM electrolyser and the excess energy not utilised during winter. Similarly Figure 3.8 gives the same results but for

summer. At the “systems-level”, results presented in Figure 3.7 and Figure 3.8 indicate that predicting energy availability for electrolysis can more accurately be done when Neural Networks are used compared to the ASHRAE model. The effect of including a larger battery capacity means greater penetration of renewable energy which in turn allows a greater available energy for driving the PEM electrolyser. In both winter (Figure 3.7) and summer (Figure 3.8), there appears to be a threshold battery capacity whereby further increases to the short-term energy storage (battery scale) do not appear to significantly influence the energy available for electrolysis.

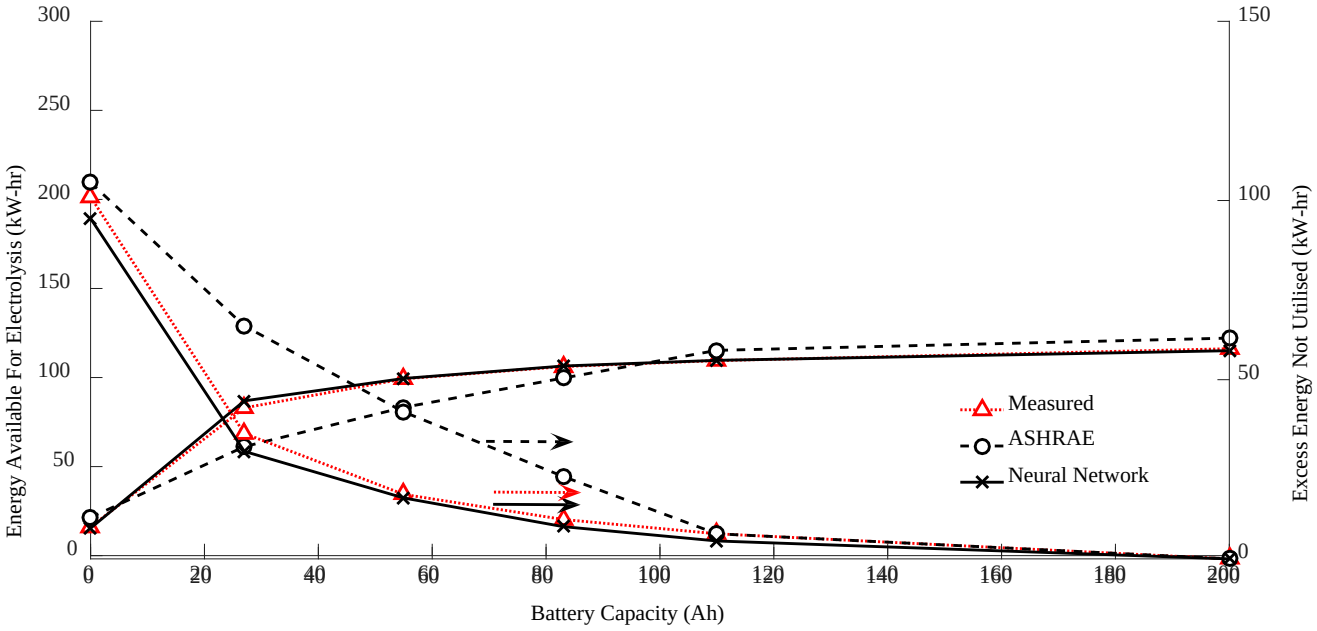

Figure 3.7 - Total predicted energy available for PEM electrolysis in winter (June-August). Three methods have been used to calculate incident irradiance at varying battery capacity.

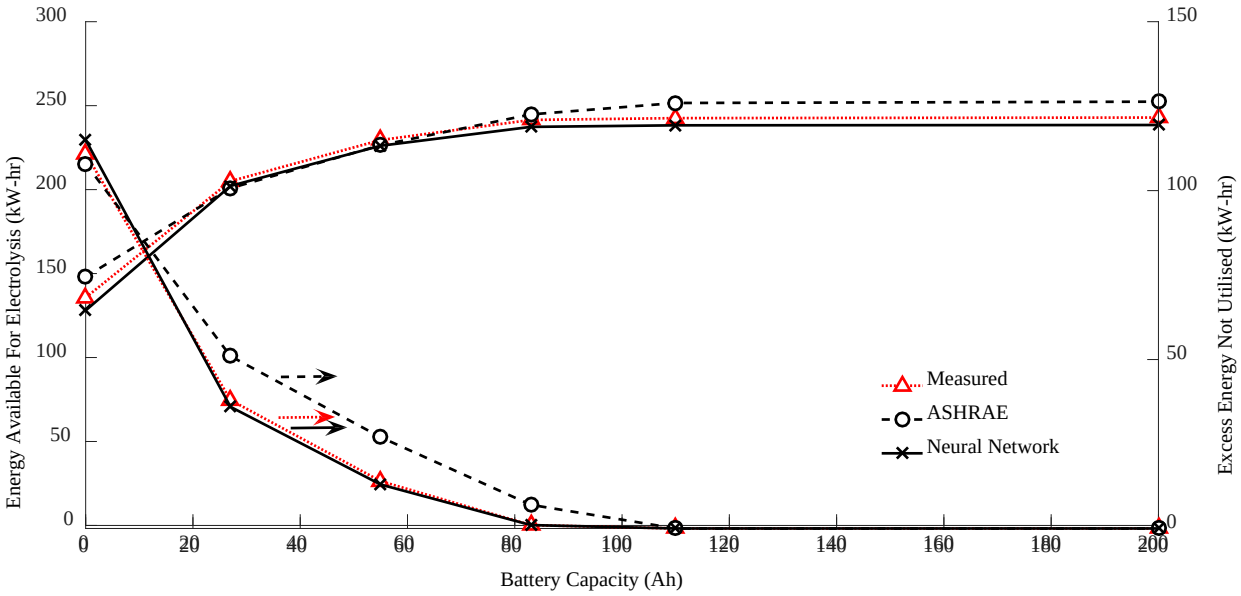

Figure 3.8 - Total predicted energy available for PEM electrolysis in summer (December - Febuary). Three methods have been used to calculate incident irradiance at varying battery capacity.

Across winter and summer, the threshold (saturation) battery capacity when derived from the more accurate NN or measured irradiance data appears to be around 83Ah. The excess energy not utilised also appears to approach minimal values at this level of battery capacity. Whilst increasing battery capacity in winter increases the total energy available for electrolysis from around 16kW-hr (at 0Ah) to 116kW-hr (at 200Ah), Table 3.2 shows that energy available for RO only increases from 1kW-hr (at 0Ah) to 9kW-hr (at 200Ah).Table 3.2 also shows that for summer, those values similarly increase only from around 9-10 kW-hr (at 0Ah) to 17-18 kW-hr (at 200Ah). This confirms the effectiveness of the PMS adopted in that, with the increase in battery capacity, the majority of solar energy is diverted for hydrogen generation. It should be noted here that in the absence of start-up transients for a reciprocating piston RO device, the amount of desalinated water produced is proportional to the energy available as dictated by the PMS. However, the capacity to generate hydrogen is dependent on three factors, namely the amount of (renewable) energy to run the electrolyser, the availability of de-ionised/desalinated water and the start-up characteristics of the electrolyser.

Battery Capacity (Ah)	Source of Irradiance Data	Reverse Osmosis Ontime (min)		Energy to RO (kW-hr)		RO Water Produced (Litres)	
		Summer	Winter	Summer	Winter	Summer	Winter
0	Meas.	5,957	604	10	1	459	46
	ASHRAE	6,678	923	11	2	514	71
	NN	5,496	581	9	1	423	45
27	Meas.	9,051	3,534	15	6	697	272
	ASHRAE	9,045	2,543	15	4	697	195
	NN	8,991	3,630	15	6	693	279
55	Meas.	10,054	4,261	17	7	774	328
	ASHRAE	9,735	3,438	16	6	750	264
	NN	9,736	4,196	16	7	750	323
83	Meas.	10,496	4,568	17	8	809	352
	ASHRAE	10,567	4,283	18	7	814	329
	NN	10,301	4,569	17	8	794	352
110	Meas.	10,585	4,797	18	8	815	369
	ASHRAE	10,884	5,067	18	8	838	390
	NN	10,539	4,731	18	8	812	364
200	Meas.	10,523	5,140	18	9	811	396
	ASHRAE	10,923	5,380	18	9	841	414
	NN	10,334	5,010	17	8	796	386

Table 3.2 - Total desalinated water produced, ontime and energy distributed for the Reverse Osmosis unit over both winter (June - August) and summer (December – Febuary) for one year. Three methods have been used to calculate the incident irradiance at varying battery capacity.

Battery Capacity (Ah)	Source of Irradiance Data	Steady Flow Time (mins)	Total Ontime (mins)	Start-Stops over Ontime (number)	Duty Factor (Litres/Start-Stop)	Specific Energy Consumption (kW-hr/m^3)	Total Hydrogen Produced (Litres)
0	Meas.	3,474	3,859	55	28	10.41	1,545
	ASHRAE	4,927	5,144	31	76	9.1	2,355
	NN	3,336	3,700	52	29	10.37	1,486
27	Meas.	19,016	19,912	128	71	9.16	9,060
	ASHRAE	14,043	14,687	92	73	9.13	6,700
	NN	19,736	20,856	160	58	9.34	9,308
55	Meas.	22,864	23,823	137	80	9.06	10,953
	ASHRAE	19,303	19,982	97	96	8.94	9,312
	NN	22,699	23,875	168	64	9.24	10,762
83	Meas.	24,484	25,478	142	83	9.04	11,745
	ASHRAE	23,279	23,930	93	122	8.81	11,314
	NN	24,495	25,552	151	78	9.08	11,719
110	Meas.	25,448	26,281	119	103	8.9	12,308
	ASHRAE	27,018	27,662	92	143	8.74	13,187
	NN	25,295	26,317	146	83	9.04	12,137
200	Meas.	27,131	27,880	107	127	8.56	13,566
	ASHRAE	28,671	29,315	92	152	8.72	14,014
	NN	26,736	27,618	126	103	8.9	12,927

Table 3.3 - Operational characteristics of the PEM electrolyser over the winter season (June-August) for one year. Three methods have been used to calculate incident irradiance onto three solar panels (2.6m^2) at varying battery capacity.

In addition to the observations derived at the systems-level, the simulations undertaken also provide a valuable insight into the device-level operational characteristics associated with hydrogen generation. These device-level characteristics are based on the results presented in Table 3.3 which also shows the effect different irradiance prediction techniques, as well as battery capacity, on the operational characteristics of the electrolyser which include electrolyser steady flow time (T_S, minutes) as defined in Figure 3.3, number of start/stop cycles, specific energy consumption (kW-hr/m^3) and total hydrogen generated (litres) for winter. Table 3.4 presents a similar compilation of data but for summer. These data show that greater battery capacity allows better renewable energy penetration resulting in an increase in steady flow time. This appears true across all battery storage capacities and for all methods of predicting solar irradiance. An interesting outcome is also shown in Figure 3.9 whereby it is seen that with greater (short-term) battery storage, which allows the electrolyser to operate for longer steady-flow periods (Table 3.2 and Table 3.3), results in a fewer number of

start/stop cycles, but there appears to be a plateau effect. There is a threshold whereby the number of start/stop cycles seems to taper off (or fall). This threshold also coincides with conditions where optimal renewable energy penetration is approached (Figure 3.7 and Figure 3.8). The data also helps define another operational (device-level) characteristic for the electrolyser, namely, the electrolyser duty factor which is the total accumulated amount of hydrogen generated per total number of start/stop cycles. Figure 3.10 shows the duty factor generally increases for larger battery capacity probably because of the availability of larger energy for hydrogen generation (Figure 3.7) for the same or fewer number of start/stop cycles (Figure 3.9).

Battery Capacity (Ah)	Source of Irradiance Data	Steady Flow Time (mins)	Total Ontime (mins)	Start-Stops over Ontime (number)	Duty Factor (Litres/Start-Stop)	Specific Energy Consumption (kW-hr/m^3)	Total Hydrogen Produced (Litres)
0	Meas.	31,583	32,570	141	108	8.87	15,298
	ASHRAE	34,920	35,543	89	193	8.64	17,149
	NN	29,477	30,730	179	79	9.07	14,112
27	Meas.	48,423	49,203	108	221	8.61	23,822
	ASHRAE	47,575	48,205	90	261	8.56	23,473
	NN	47,802	48,523	103	229	8.59	23,541
55	Meas.	53,832	55,085	161	163	8.73	26,290
	ASHRAE	53,132	54,345	145	179	8.72	25,960
	NN	53,078	54,270	148	175	8.72	25,943
83	Meas.	56,690	57,959	159	174	8.71	27,711
	ASHRAE	57,506	58,748	168	167	8.70	28,132
	NN	55,742	56,946	160	170	8.71	27,260
110	Meas.	56,966	58,216	176	158	8.71	27,858
	ASHRAE	59,137	60,380	169	171	8.69	28,947
	NN	55,968	57,188	170	161	8.70	27,374
200	Meas.	57,171	58,298	155	181	8.67	28,022
	ASHRAE	59,332	60,569	169	172	8.69	29,048
	NN	56,151	57,232	151	182	8.66	27,535

Table 3.4 - Operational characteristics of the PEM electrolyser over the summer season (December-Febuary) for one year. Three methods have been used to calculate incident irradiance onto three solar panels (2.6m^2) at varying battery capacity.

Figures 3.7 – 3.10 show that whilst using different methods to account for the power needed to run a hydrogen generation system result in more subtle inaccuracies in relation to some characteristics such as electrolyser ontime (T_0) as shown in Table 3.2 and Table 3.3, the use

of different methodologies has a relatively stronger impact on device-level (electrolyser) operational characteristics. These more notable impacts include the number of start/stops (Figure 3.9) and the duty factor (Figure 3.10). From these data, it is also clear that methods such as Neural Networks allow for a higher prediction accuracy of various electrolyser operational characteristics. This indicates the need to consider which of these tools to use when establishing techno-economic analysis targeted at stand-alone hydrogen generation systems. Alternatively, electrolyser ontime, duty factor as well as total hydrogen generated and the number of start/stops is less accurately predicted with the ASHRAE model than with Neural Networks. This can be attributed to the ASHRAE models' inability to accurately follow the stochastic nature of the solar irradiance (Figure 3.5). This may also indicate that using highly resolved (temporal) simulations may yield different outcomes in relation to device-level operational characteristics, when compared to less resolved simulations which may be hourly based (for example). This is because of the limiting effect of low-resolution simulations to represent the highly fluctuating nature of renewable energy sources.

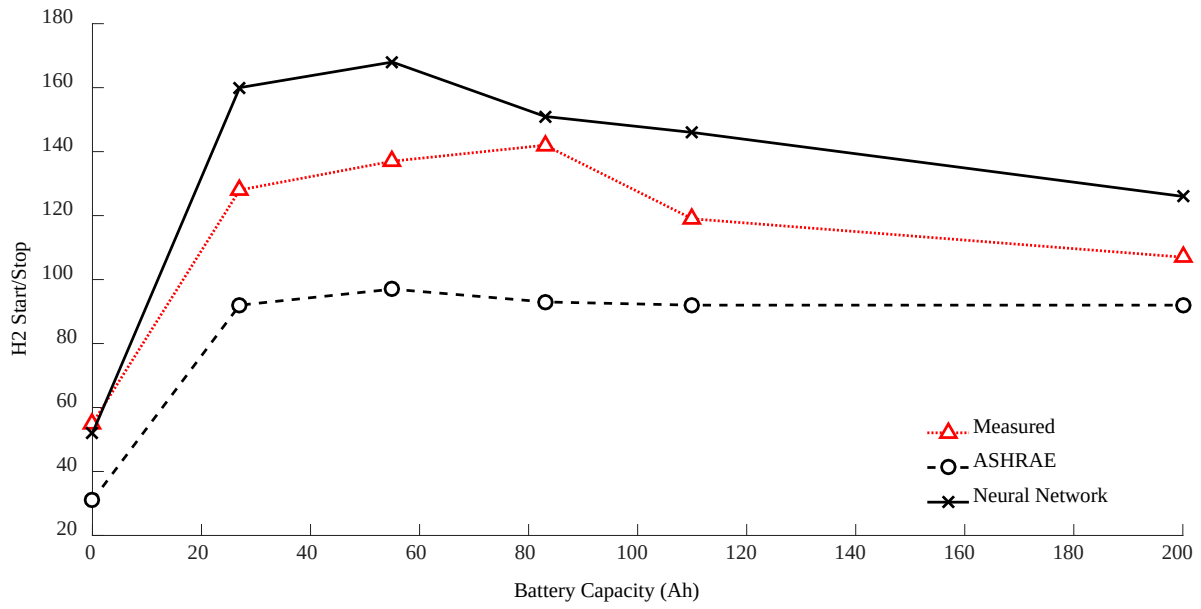

Figure 3.9 - Total predicted number of start/stop cycles for the PEM electrolyser in winter (June-August). Three methods have been used to calculate incident irradiance at varying levels of battery capacity.

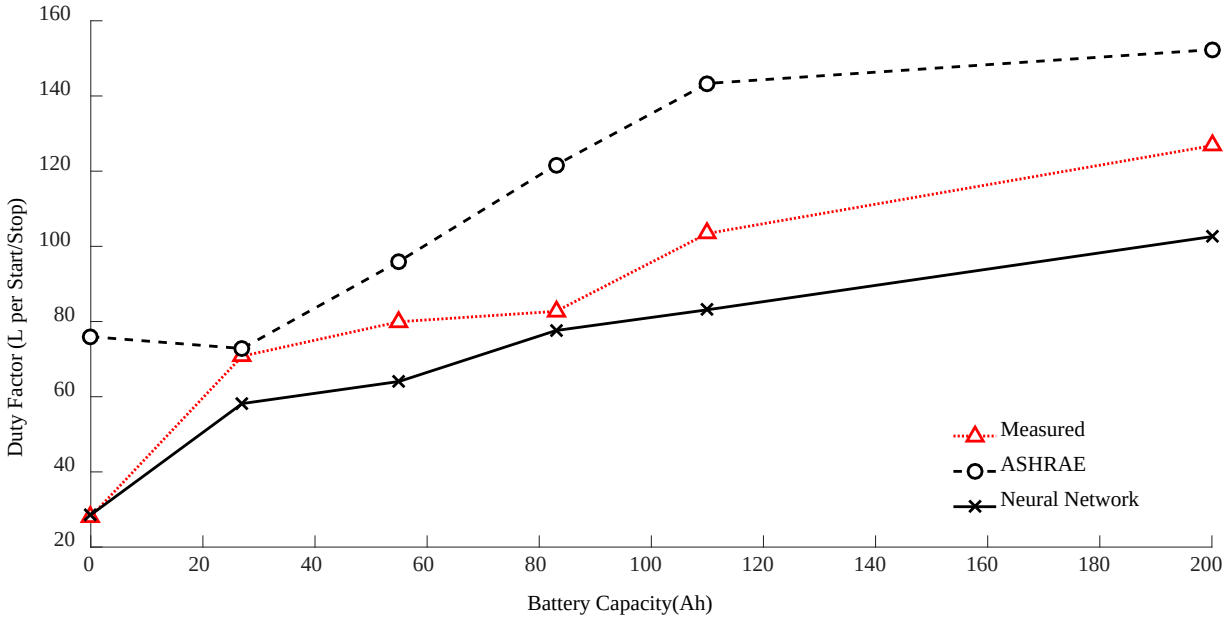

Figure 3.10 - Predicted duty factor for the PEM electrolyser in winter. Three methods have been used to calculate incident irradiance at varying levels of battery capacity.

To best utilise the available renewable energy, the electrolyser duty factor should be maximised, so that less power is consumed in start-up processes whilst simultaneously maximising hydrogen generation. This can be facilitated by using an “optimum” battery capacity which also results in decreasing electrolyser specific energy consumption (kW-hr/m^3) as shown in Table 3.3 because less energy is directed to parasitic start-up processes.

3.5 - Conclusions

The effect of solar energy intermittency and battery capacity on the operational characteristics and energy utilisation of a solar-PV powered hydrogen generation system have been explored. The methodologies used in this research include laboratory-based testing to resolve device-level operational characteristics as well as minute resolved simulations conducted using MATLAB/Simulink. The focus of the research is a (conceptual) renewably powered hydrogen generation system intended for use in conjunction with a refuelling station or via a fuel cell, but operated at a coastal location. The hydrogen generation system is directly coupled with a RO device and simulated over two seasons (winter and summer) for a specific Western Australian location. Very few studies have been conducted to analyse hydrogen generation systems with water production also integrated. Two specific solar prediction techniques, highlighting two levels of intermittency are chosen. This helps identify

the impact of prediction accuracy on the renewable power generated and the operational characteristics of the hydrogen system. Both methods are benchmarked against using meteorological data. Low levels of intermittency are obtained via implementing the ASHRAE (clear sky) model whilst severe intermittency is derived from using Neural Networks. The above effects are also analysed with different scales of (short-term) battery storage[14] and benchmarked against operational characteristics obtained from measured irradiance data.

Results indicate the importance of considering which methods are used to predict the solar irradiance needed to run the system when forecasting device-level operational characteristics in stand-alone hydrogen generation systems. Two issues appear to be relevant here: (i) the general accuracy of the method and (ii) its ability to forecast fluctuation. Using a simplistic solar prediction technique (ASHRAE) produces larger relative errors in energy availability than Neural Networks when compared to measured irradiance data. The larger errors produce an overestimation of hydrogen production when using ASHRAE compared to NN or measured data. This can be attributed to the fact that ASHRAE is unable to account for dynamic fluctuations in solar irradiance. Solar energy intermittency and varying battery scale impacts the operational characteristics of a PEM electrolyser as well as the energy distribution between system components. Specifically, results (Table 3.3) highlight that start-stop cycles and duty factor (litres/start-stops) are more accurately predicted using methods (NN) which forecast intermittency in the renewable energy resource. The merit of using such methods, compared to others (ASHRAE), however appears less significant when deriving specific energy consumption (kW-hr/m^3). The effects of such solar irradiance prediction techniques have varying influence depending on season. The ability to predict accurate levels of solar irradiance becomes important in winter where irradiance is at its lowest levels with high levels of fluctuation and less of an impact in summer where irradiance is at its maximum as well as minimal fluctuation.

An increase in battery storage capacity allows for greater renewable energy penetration resulting in increased hydrogen yield with higher hydrogen generation in both seasons and steady flow time also increases across all battery storage capacities. The inclusion of battery storage capacity in both summer and winter allows the electrolyser to operate for more

[14] Battery storage capacities are scale multiples (i.e. 1 battery 2 batteries etc.)

extended periods (operational times) and a greater duty factor. The increase in duty factor subsequently results in a decrease in the PEM electrolyser specific energy consumption.

Further investigations are warranted into the optimisation of the Power Management Strategy as another means for helping optimise systems and device-level operational characteristics. An “intelligent” PMS may also lead to better scaling of hydrogen and water storage capacities as well as devices such as electrolysers. Although desalinated water is exclusively used for electrolysis in this study, an adaptive PMS strategy may also consider using the RO unit to service further water requirements (i.e. drinking).

3.6 - Chapter References

[1] Flannery T, Sahajwalla V. The critical decade: generating a renewable Australia. Available from, http://climatecommission.gov.au/wp-content/uploads/Renewables-report_lowres.pdf; 2012. [cited March,2013].

[2] Mehrpooya M, Daviran S. Dynamic modeling of a hybrid photovoltaic system with hydrogen/air PEM fuel cell. Iranica Journal of Energy & Environment. 2013;4:104-9.

[3] Ipsakis D, Voutetakis S, Seferlis P, Stergiopoulos F, Elmasides C. Power management strategies for a stand-alone power system using renewable energy sources and hydrogen storage. International Journal of Hydrogen Energy. 2009;34:7081-95.

[4] Dufo-López R, Bernal-Agustín JL, Contreras J. Optimization of control strategies for stand-alone renewable energy systems with hydrogen storage. Renewable Energy. 2007;32:1102-26.

[5] Gray EM, Webb CJ, Andrews J, Shabani B, Tsai PJ, Chan SLI. Hydrogen storage for off-grid power supply. International Journal of Hydrogen Energy. 2011;36:654-63.

[6] Akdemir B, Cetinkaya N, Kulaksiz AA. Forcasting renewable energy potential of Turkey using artificial neural network up to 2030. In: IPCBEE, editor. International Conference on Clean and Green Energy. Singapore: IACSIT Press; 2012. p. 30-5.

[7] McLellan B, Shoko E, Dicks AL, Costa JCDd. Hydrogen production and utilisation oppurtunities for Australia. International Journal of Hydrogen Energy. 2005;30:669-79.

[8] Penner SS. Steps towards the hydrogen economy. International Journal of Energy. 2006;31:33-43.

[9] Paul B, Andrews J. Optimal coupling of PV arrays to PEM electrolysers in solar-hydrogen systems for remote area power supply. International Journal of Hydrogen Energy. 2008;33:490-8.

[10] Garcia-Valverde R, Miguel C, Martinez-Bejar R, Urbina A. Optimized photovoltaic generator-water electrolyser coupling through controlled DC-DC converter. International Journal of Hydrogen Energy. 2012;33:5352-62.

[11] Nafeh AE-SA. Hydrogen production from a PV/PEM electrolyzer system using a neural-network-based MPPT algorithm. International Journal of Numerical Modelling: Electronic Networks, Devices and Fields. 2011;24:282-97.

[12] Geovanni S, Orlando L, Rafeal P, Alberto S, Sebastian P. Analysis of the current methods used to size a wind/hydrogen/fuel cell-integrated system: a new perpective. International Journal of Energy. 2010;34:1042-51.

[13] Genç G, Çelik M, Serdar Genç M. Cost analysis of wind-electrolyzer-fuel cell system for energy demand in Pınarbaşı-Kayseri. International Journal of Hydrogen Energy. 2012;37:12158-66.

[14] Pedrazzi S, Zini G, Tartarini P. Complete modeling and software implementation of a virtual solar hydrogen hybrid system. Energy Conversion and Management. 2010;51:122-9.

[15] Jalilzadeh S, Rohani A, Kord H, Nemati M. Optimum design of a hybrid Photovoltaic/Fuel Cell energy system for stand-alone applications. 6th International Conference on Electrical Engineering/Electronics, Computer, Telecommunications and Information Technology, ECTI-CON 2009. p. 152-5.

[16] Qi ZY, Lin E. Integrated power control for small wind power system. Journal of Power Sources. 2012;217:322-8.

[17] Li C-H, Zhu X-J, Cao G-Y, Sui S, Hu M-R. Dynamic modeling and sizing optimization of stand-alone photovoltaic power systems using hybrid energy storage technology. Renewable Energy. 2009;34:815-26.

[18] Kaldellis JK, Zafirakis D. Optimum sizing of stand-alone wind-photovoltaic hybrid systems for representative wind and solar potential cases of the Greek territory. Journal of Wind Engineering and Industrial Aerodynamics. 2012;107:169-78.

[19] Clarke DP, Al-Abdeli YM, Kothapalli G. The effects of including intricacies in the modelling of a small-scale solar-PV reverse osmosis desalination system. Desalination. 2013;311:127-36.

[20] Glavin ME, Hurley WG. Optimisation of a photovoltaic battery ultracapacitor hybrid energy storage system. Solar Energy. 2012;86:3009-20.

[21] Patsios C, Antonakopoulos M, Chaniotis A, Kladas A. Control and analysis of a hybrid renewable energy-based power system. 2010 XIX International Conference on Electrical Machines (ICEM). Rome 2010. p. 1-6.

[22] Zhou T, Francois B. Modeling and control design of hydrogen production process for an active hydrogen/wind hybrid power system. International Journal of Hydrogen Energy. 2009;34:21-30.

[23] Tao Z, Francois B, el Hadi Lebbal M, Lecoeuche S. Real-time emulation of a hydrogen-production process for assessment of an active wind-energy conversion system. Industrial Electronics, IEEE Transactions on. 2009;56:737-46.

[24] Kyriakarakos G, Dounis AI, Arvanitis KG, Papadakis G. A fuzzy logic energy management system for polygeneration microgrids. Renewable Energy. 2012;41:315-27.

[25] Carter D, Ryan M, Wing J. The fuel cell industry review Available from, http://www.fuelcelltoday.com/media/1713685/fct_review_2012.pdf; 2012. [cited March,2013].

[26] Garcia-Valverde R, Espinosa N, Urbina A. Simple PEM water electrolyser model and experimental validation. International Journal of Hydrogen Energy. 2012;37:1927-38.

[27] Clarke RE, Giddey S, Badwal SPS. Stand-alone PEM water electrolysis system for fail safe operation with a renewable energy source. International Journal of Hydrogen Energy. 2010;35:928-35.

[28] Millet P, Mbemba N, Grigoriev SA, Fateev VN, Aukauloo A, Etiévant C. Electrochemical performances of PEM water electrolysis cells and perspectives. International Journal of Hydrogen Energy. 2011;36:4134-42.

[29] Oliveira LFL, Laref S, Mayousse E, Jallut C, Franco AA. A multiscale physical model for the transient analysis of PEM water electrolyzer anodes. Physical Chemistry Chemical Physics. 2012;14:10215-24.

[30] Millet P, Grigoriev SA, Porembskiy VI. Development and characterisation of a pressurized PEM bi-stack electrolyser. International Journal of Energy Research. 2013;37:449-56.

[31] Lee B, Park K, Kim H-M. Dynamic simulation of PEM water electrolysis and comparison with experiments. International Journal of Electrochemical Science. 2013;8:235-48.

[32] Wu J, Yuan XZ, Martin JJ, Wang H, Zhang J, Shen J, Wu S, Merida W. A review of PEM fuel cell durability: degradation mechanisms and mitigation strategies. Journal of Power Sources. 2008;184:104-19.

[33] de Bruijn FA, Dam VAT, Janssen GJM. Review: durability and degradation issues of PEM fuel cell components. Fuel Cells. 2008;8:3-22.

[34] Bureau of Meteorology (Australia). Solar exposure data for Geralton, Western Australia. Available from, http://reg.bom.gov.au/climate/reg/oneminsolar/index.shtml; 2012. [cited October,2012].

[35] Shabani B, Andrews J, Watkins S. Energy and cost analysis of a solar-hydrogen combined heat and power system for remote power supply using a computer simulation. Solar Energy. 2010;84:144-55.

[36] Fahmy FH, Ahmed NM, Farghally HM. Optimization of renewable energy power system for small scale brackish reverse osmosis desalination unit and a tourism motel in Egypt. Smart Grid and Renewable Energy. 2012;3:43-50.

[37] Soric A, Cesaro R, Perez P, Guiol E, Moulin P. Eausmose project desalination by reverse osmosis and batteryless solar energy: design for a 1m^3 per day delivery. Desalination. 2012;301:67-74.

[38] Avlonitis SA, Avlonitis DA, Panagiotidis T. Experimental study of the specific energy consumption for brackish water desalination by reverse osmosis. International Journal of Energy Research. 2012;36:36-45.

[39] Qiu TY, Davies PA. The scope to improve the efficiency of solar-powered reverse osmosis. Desalination and Water Treatment. 2011;35:14-32.

[40] Katadyn. PS-40E Manual Available from, http://katadynch.vs31.snowflakehosting.ch/fileadmin/user_upload/katadyn_products/Downloads/Manual_Katadyn_PS-40E_EN.pdf; 2011. [cited April 2011].

[41] Jamil Ahmad M, Tiwari G. Solar radiation models- a review. International Journal of Energy Research. 2011;35:271-90.

[42] Amarananwatana P, Sorapipatana C. An assessment of the ASHRAE clear sky model for irradiance prediction in Thailand Nuntiya. Asian Journal on Energy and Environment. 2007;8:523-32.

[43] Nijegorodov N. Improved ashrae model to predict hourly and daily solar radiation components in Botswana, Namibia, and Zimbabwe. Renewable Energy. 1996;9:1270-3.

[44] Al-Sanea SA, Zedan MF, Al-Ajlan SA. Adjustment factors for the ASHRAE clear-sky model based on solar-radiation measurements in Riyadh. Applied Energy. 2004;79:215-37.

[45] Martin L, Zarzalejo LF, Polo J, Navarro A, Marchante R, Cony M. Prediction of global solar irradiance based on time series analysis: Application to solar thermal power plants energy production planning. Solar Energy. 2010;84:1772-81.

[46] AbdulAzeez MA. Artificial neural network estimation of global solar radiation using meteorological parameters in Gusau, Nigeria. Archives of Applied Science Research. 2011;3:586-95.

[47] Yona A, Senju T, Sabar AY, Funabashi T, Sekine H, Kim C-H. Application of neural network to one-day-ahead 24 hours generating power forecasting for photovoltaic system. In:

IEEE, editor. The 14th International Conference on Intelligent System Applications to Power Systems. Kaohsiung, Taiwan: IEEE; 2007.

[48] Krishnaiah T, Rao SS, Madhumurthy K, Reddy KS. Neural network approach for modelling global solar radiation. Journal of Applied Sciences Research. 2007;3:1105-11.

[49] Bureau of Meteorology (Australia). Rainfall data for Geralton, Western Australia. Available from, http://www.bom.gov.au/jsp/ncc/cdio/weatherData/av?p_display_type=dailyZippedDataFile&p_stn_num=008051&p_c=-12975576&p_nccObsCode=136&p_startYear=2013; 2012. [cited October,2012].

3.7 - Chapter Appendix

To accurately resolve the A, B and C parameters, minute resolved meteorological data for Geraldton [34] was used to benchmark against the ASHRAE prediction. The A, B and C parameters were then iteratively refined. The method for the calculation of the A, B and C values of the ASHRAE model is defined in [42], whereby:

$$I_N = A \times exp(-B \times \sec\theta_Z) \qquad \textit{Equ. A1}$$

$$\ln I_N = \ln A - B \times \sec\theta_Z \qquad \textit{Equ. A2}$$

In the relations above, parameters denote minutely beam radiation (I_N, W/m^2), zenith angle (θ_Z, deg) with A (W/m^2) and B (dimensionless) as model correction factors. The zenith angle is approximately the same as the hour angle for the 21st day of each month [42]. When meteorological data is plotted in the form of Equation A2, values for A and B can be visualised, whereby parameter A is the inverse natural logarithm of the vertical axis intercept and B the slope of this line. The last parameter C, which is the diffuse radiation parameter, is obtained by averaging the ratio of the diffuse irradiance to the direct normal irradiance which can be obtained from the meteorological dataset. Table 3.5 shows the A, B and C parameters derived using this method across the summer and winter periods and subsequently used in the simulations.

Australian Season	Month	A (W/m2)	B (dimensionless)	C (dimensionless)
Summer	December	1,379	0.290	0.070
	January	1,253	0.220	0.090
	February	1,089	0.125	0.070
Winter	June	1,120	0.173	0.570
	July	1,000	0.122	0.740
	August	1,600	0.370	0.790

Table 3.5 - The A, B, C parameters used in the ASHRAE model when applied to the Western Australian city of Geraldton (latitude: -28.77°; longitude:114.61°).

Chapter 4. The Impact of using Particle Swarm Optimisation on the Operational Characteristics of a Stand-Alone Hydrogen System with On-site Water Production

Daniel P. Clarke*, Yasir M. Al-Abdeli and Ganesh Kothapalli

This chapter was published as a full research paper in International Journal of Hydrogen Energy. Whilst all efforts were made to retain the original features of this article, minor changes such as the layout, number formats, font size and style were implemented in order to maintain consistency in the formatting style of the thesis.

4.1 - Abstract

In Chapter 3, we analysed the impact of renewable energy intermittency on the operational characteristics of hydrogen energy systems with pre-set Power Management Strategies not subject to optimisation. This follow-up chapter demonstrates the validity of successfully applying Particle Swarm Optimisation (PSO) to size and optimise these systems. Specifically, PSO is used to iteratively converge on the (short-term) battery capacity (Ah) and hydrogen storage (L) in addition to defining the switching parameters which a Power Management Strategy (PMS) uses. The PSO algorithm is guided by three operational objective functions and conducted using MATLAB/Simulink. Simulations also incorporate laboratory resolved device characteristics.

Results are benchmarked against earlier deployed methods and show improvements with a PSO optimised PMS depend on system scale, with greater relative benefits arising at smaller scales. The choice of PSO acceleration parameters also affects the time to reach an optimal solution.

4.2 - Introduction

Due to dispersed population within Australia, remote communities are heavily reliant on stand-alone diesel-based power generation with access to the utility grid sometimes being uneconomical. Where such communities are also located at coastal locations, combining energy provision with potable water production becomes an attractive option. Society is becoming more environmentally aware of carbon emissions and the need for sustainable power generation practises to replace fossil fuels. The utilisation of renewable sources [1] has

been identified as the best candidate for achieving stand-alone power generation with reduced emissions. Renewable energies such as wind and solar are perpetual, clean and can be used in stand-alone energy systems. However, the inevitable intermittency and unpredictability of energy sources [2] results in periods where load demand cannot be fully met via available renewables or when surpluses may exist during periods of low load (demand). This highlights the need to incorporate energy storage media such as batteries and hydrogen [3, 4] coupled with better renewable resource predictions.

In such application scenarios and for a given resource and load profile, the overall penetration of renewables, reliability of meeting external loads and indeed the operational characteristics (switching, performance) of the energy system components are a function of both the Power Management Strategies (PMS) deployed and the scale of hardware. Therefore, optimisation techniques are essential to maximise system performance and reduce the likelihood of unnecessarily cycling devices into On/Off mode such as fuel cells due to degradation issues [5, 6].

With the above in mind, the sizing and operational strategies of a stand-alone energy system have been achieved using various optimisation techniques including iterative, probabilistic, as well as intelligent methods which rely on genetic algorithms, fuzzy logic and neural networks [7, 8]. In this regard, Particle Swarm Optimisation (PSO) has been deployed to optimise some aspects of stand-alone energy systems as it offers many advantages such as PSO having fewer tuneable parameters compared to other intelligent techniques [9]. However, two important challenges present themselves in this regard. Firstly, the effective use of PSO still requires tuning “acceleration parameters” to achieve accurate results and the impact of such (acceleration) parameters in relation to stand-alone hydrogen energy systems has largely not been addressed in the literature [10, 11]. Secondly, the merit of using PSO to help scale hydrogen energy system components and optimise the operational characteristics of the energy system (as a whole) has not been adequately addressed to date. The current research aims to address both these deficiencies.

Outside the scope of the present chapter which analyses the use of PSO to size and optimise power management strategies, most other published research with PSO focusses on its impact from a techno-economic perspective. Within stand-alone hydrogen systems, the use of PSO has been shown to positively affect total system costs [12-16], with the cost of electricity improving by 18.5% [17] or to shorten the payback time from 12.3 years to 5.7 years [18].

Additionally, the use of PSO has been shown to reduce environmental impact from the running, production and installation of renewable energy systems over a 25 year lifetime by increasing total carbon emissions saved from approximately 3,260 tons to 3,980 tons [18]. In order to increase the probability of meeting an electric load demand, most research done to date on hydrogen systems has predominantly been based on Power Management Strategies (PMS), which are themselves not optimised [8, 19-21]. Optimising the PMS by adjusting specific control set-points used in stand-alone hydrogen systems further maximises system performance whilst reducing system costs [22, 23]. However, rarely has the effect of optimising a PMS onto the operational characteristics (and longevity) of energy system components been addressed in the literature. For hybrid systems, a PSO optimised PMS can minimise dependence on diesel generators [22] by 10%, when compared to HOMER, and reduce Loss of Load (T_{LOL}) [15] for the smallest total system cost possible [6]. Additionally, some research has indicated that an optimised PMS results in better component switching (On/Off) to meet a load, for the lowest system cost [9], but overlooked incorporating the dynamic operational characteristics of system components. Also, PSO has been used to identify the best inclination angle of solar-PV arrays to maximise available energy [24]. Despite the above, the simultaneous optimisation of both system size and the PMS control set-points has received little attention.

This chapter aims to extend the analyses done in our previous work [25] by additionally using Particle Swarm Optimisation to simultaneously optimise battery scale and hydrogen storage capacity as well as the Power Management Strategy in a stand-alone power generation system. In this context, three objective functions are used to guide and help assess the impact of PSO on system performance. Objective-1 maximises hydrogen generation (litres/season) whilst Objective-2 is to minimise the PEM electrolysers' duty factor for a given hydrogen target (litres/season). With the addition of an electric external load demand, Objective-3 aims to minimise the Loss-Of-Load time (T_{LOL}) and the number of fuel cell start-stops whilst maximising an electrolysers' duty factor. For all these objective functions, the PSO acceleration parameters are also varied to analyse their influence. The simulations are implemented for a specific set of hardware components and geographical locations and cover the Australian winter season.

[15] Defined elsewhere in this chapter

4.3 - Methodology

Figure 4.1 depicts the renewably powered, stand-alone, hydrogen energy system which provides the basis for the study[16]. This system integrates two main sub-configurations. The first (shown outside the dashed box) is the "hydrogen generation assembly" investigated in our previous work into the impact of renewable energy intermittency on operational characteristics [25]. In that earlier analysis and as commonly found in published works, the energy system operated to a Power Management Strategy with pre-set control points to govern the switching of various hardware components. There was also no external electric load connected. The second sub-configuration in Figure 4.1 (shown inside the dashed box) is an additionally interfaced electric load and water demand (to satisfy the water needs of electrolysis and drinking). The system simulations presented in the current study consider the characteristics of a number of hardware components and consist of solar-PV panels[17] (Make: Heckert Solar - Germany, Model: HS – PL 135), a PEM electrolyser (Make: DBS – Italy, Model: NMH2 - 500), a Reverse Osmosis (RO) unit (Make: Katadyn - Switzerland, Model: PowerSurvivor 40E) and a PEM fuel cell (Make: Ballard Power Systems - Canada, Model: 1.2kW). The switching of these components is typically controlled through a connected Power Management Unit (PMU) which typically implements the Power Management Strategy (PMS). The PMU is simulated through this research using MATLAB/Simulink on a desktop PC having an Intel i3 processor. The operational characteristics and details of these hardware components have been laboratory tested[18] and reported elsewhere [25, 26].

[16] Refer to Appendix D for Chapter 4 system MATLAB/Simulink model.

[17] Refer to Appendix D for PV panel model.

[18] Refer to Appendix C for error analysis methods.

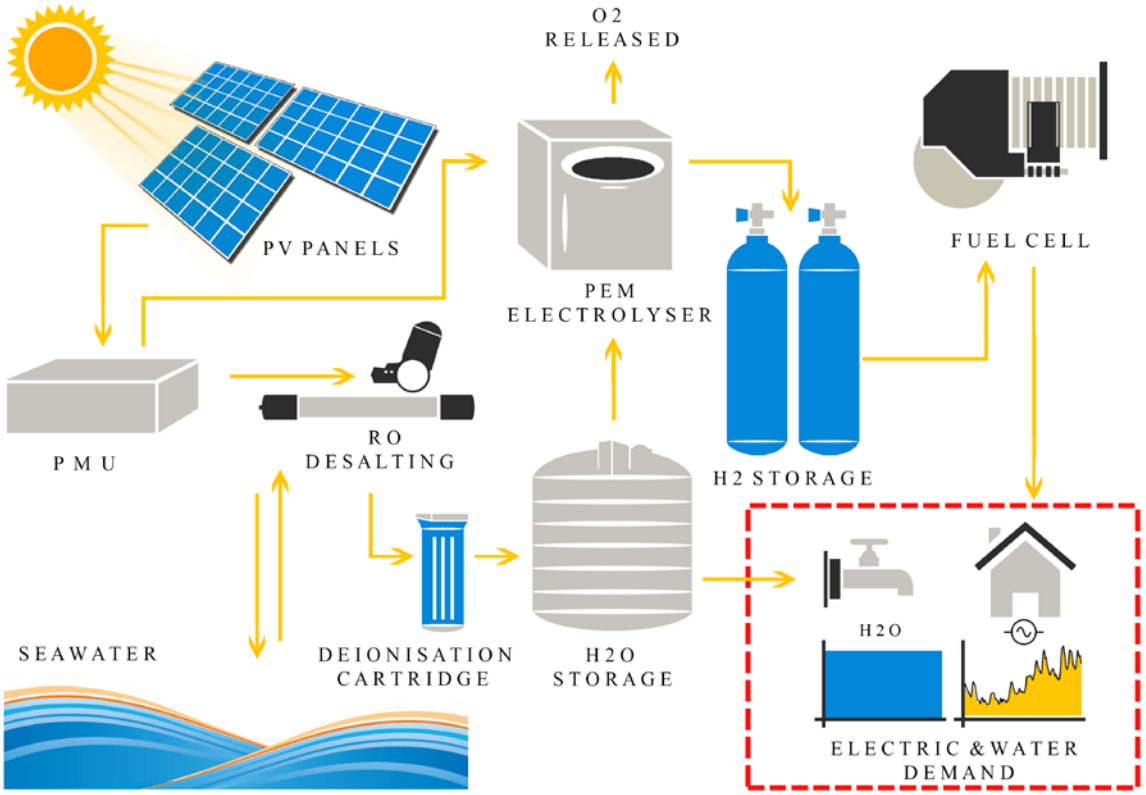

Figure 4.1 - Stand-alone hydrogen energy system with on-site water production. All energy system components outside the dashed box constitute the “hydrogen generation assembly”. The dashed box indicates an electric load and water demand that is interfaced with the “hydrogen generation assembly”.

4.3.1 - The Hydrogen Energy System

A single system-level simulation aims to resolve six characteristics over a period spanning an entire calendar season. The outputs from the simulation are:

1. Total PEM electrolyser hydrogen output (O_H) to go into storage and run a fuel cell (litres/season);
2. Number of start/stop cycles for a PEM electrolyser (O_{ESS});
3. Total desalinated water output (O_W) by RO (litres/season);
4. Minute resolved hydrogen consumption (O_{FC}) by a PEM fuel cell (litres);
5. Number of start/stop cycles for a PEM fuel cell (O_{FCSS}); and

6. Likelihood for meeting a dynamic electric load (T_{LOL}).

Using (1) and (2) the duty factor for the electrolyser (O_{EDF}) is calculated (total hydrogen generated relative to the number of electrolyser start-stops). All simulations are implemented using a temporal resolution of one minute, whereby these time steps can be summed to also provide hourly, daily or seasonal totals. Due to the physical and operational limitations of the modelled hydrogen system, there is a set of constraints that each of the six variables above must satisfy to form any plausible solution. These upper and lower bounds are given in the Table 4.1, whereby those relating to the max battery capacity (200Ah) and min (transient) electrolyser runtime (5 minutes) are derived based on hardware characteristics which were laboratory resolved earlier [25].

Decision Variable Components	**Lower Bound**	**Upper Bound**
Battery Capacity, CB (Ah)	0	200
Min Water Threshold, Ch20 (L)	5	49
Min runtime for electrolyser, TE (min)	5	500
Max Hydrogen Capacity, CH (L)	0	500
Min Hydrogen Capacity, CMH (% of CH)	0	100

Table 4.1 - Upper and lower bounds of the decision variables used to limit the solution space for the Particle Swarm Optimisation algorithm.

Solar Irradiance Data: The power generated by the PV-array forms the energy (input) into the system. In this regard, minute resolved irradiance data is sourced from the Bureau of Meteorology [27] and converted using the photovoltaic array model [26]. The photovoltaic array for both configurations has a nominal area of 2.6m^2 which is the same as that in the small-scale, stand-alone energy system tested earlier (without PSO) [25]. Figure 4.2a shows the distribution of seasonal minute resolved solar irradiance over any day whereby the large unpredictability of this resource over a single season is apparent from the spread of values over any time step. All data spans winter (June, July and August: 132,480 minutes) for a specific Western Australian coastal location (Geraldton). Winter is chosen because the susceptibility of cloud cover results in stronger uncertainty in solar irradiance (fluctuations) and highlights the effect of using an (intelligent-based) method such as PSO to derive the Power Management Strategy and size hydrogen energy system components. Although

measured (historical) solar irradiance at Geraldton, Western Australia is used, the methods presented here can also be integrated with predictive models and methods to consider (future) predictions of irradiance data using techniques such as ASHRAE clear sky (irradiance) model or Neural Networks [25].

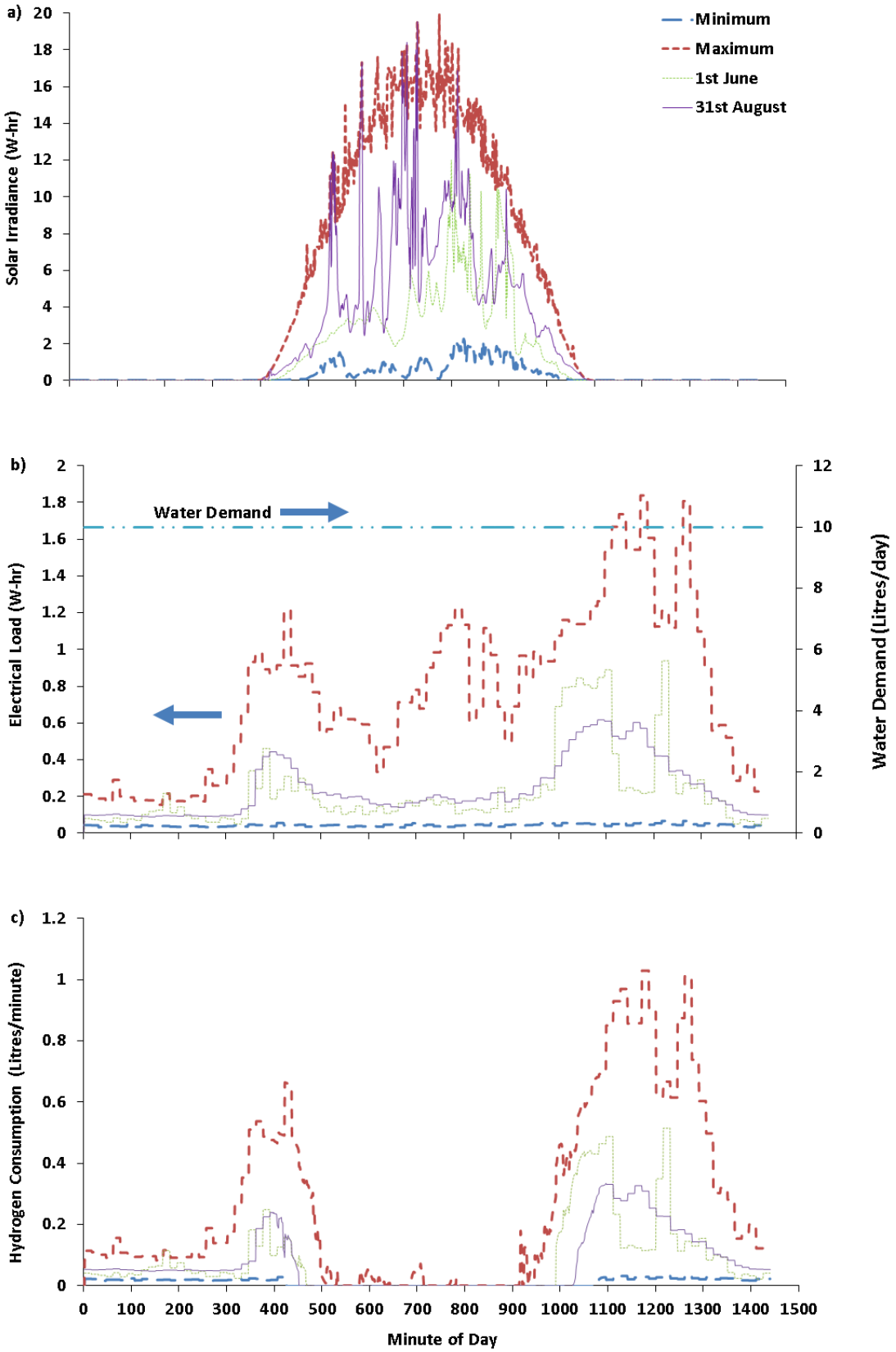

Figure 4.2 - Minute resolved daily distribution of solar irradiance (a), external electric load (b) and fuel cell hydrogen consumption (c). Fuel cell operation meets the gap between available renewables (a) and the external electric load (b).

PEM Electrolyser: The major advantage of a PEM electrolyser in a small-scale, stand-alone energy system is its ability to generate hydrogen at pressures compatible with storage via metal hydrides which may negate the need for an additional compressor. This not only reduces external power consumption but allows simple integration into smaller stand-alone systems. However, the continual cyclic operation of a PEM electrolyser results in higher (parasitic) power expenditure due to start-up times associated with these devices. This also highlights the need to maximise the duty factor in these devices (hydrogen generated per number of start-stop cycles). The start-up time for the electrolyser used in the present simulations is 5 minutes and has been previously laboratory derived [25].

Reverse Osmosis Unit: Reverse Osmosis is commonly integrated into stand-alone solar-PV systems [28-31]. The integration of a Reverse Osmosis (RO) unit with hydrogen systems negates the need for regular deionised water shipments to support electrolysis and allows for such systems to be sustainably deployed in off-grid coastal locations where seawater is abundant. Moreover, on-site water desalination alongside an energy system can also provide drinking water requirements. This is an important consideration as most energy management analyses published on hydrogen systems, with the exception of a few [11, 32], do not even consider the provision of water that is critical to the operation of these systems. In this regard, excess energy not utilised to meet (electric) load demand can be diverted to power RO units, rather than dump loads, and the water produced can be further processed by a (static, gravity fed) cartridge type de-ioniser. In addition to the (daily fluctuating) water needs for the electrolysis, the simulations will therefore consider a (fixed seasonal) water demand of 10L per day to meet the immediate drinking needs for three persons in a small stand-alone system [33]. An alternate drinking water usage can be tested using the simulations if needed.

Energy Storage: Solar irradiance is highly dynamic and only available over specific hours of the day, thus integrating energy storage media into renewable energy systems is primarily designed to provide supplemental power in periods when incident solar radiation is insufficient. Some (secondary) needs for energy storage media also include short-time energy supplements to smooth intermittency, emergency shutdown or maintaining sensors and actuators. For this purpose, hydrogen systems typically implement a metal hydride or compressed gas storage combined with mostly lead-acid batteries, and rarely Li-Ion batteries [34]. The incorporation of hydrogen storage allows the fuel cell to meet the electric load demand by using the hydrogen reserves produced from surplus solar-PV energy. In these

simulations, PSO will define the scale needed of hydrogen storage as well as converging onto an optimal (secondary needs) battery capacity within the hardware bounds (Table 4.1).

PEM Fuel Cell: Whilst other types of fuel cells exist (alkaline, molten carbonate and solid oxide), PEM technology offers the advantages of low operational temperatures, fast start-up times and water as a by-product [35, 36]. However, the longevity of a fuel cell is affected by accumulative operational hours and the number of start/stop cycles [5, 37]. Fuel cell durability has been the focus of much investigation in terms of dynamic loads, transients and parameters affecting performance [6, 37-41]. Hence, the present study also investigates the effects of using (intelligent) optimisation of the PMS on the operational characteristics of a PEM fuel cell. In this regard, the instantaneous electrical power supplied by the PEM fuel cell is fundamentally defined as:

$$P_{FC} = V_{FC} \times I_{FC} \qquad \textit{Equ. 4.1}$$

Where, (P_{FC}) is the output of the fuel cell, (V_{FC}) is the fuel cell voltage and (I_{FC}) the fuel cell operating current. However, this approach neglects the power losses attributed to on-board components such as the air pump, cooling fan, sensors, actuators and controllers which vary as the fuel cell power output changes. In this regard, it is necessary to consider the Balance of Power (BOP) components of the fuel cell to ascertain the net power supplied to an external load after satisfying the power requirements of the fuel cell stack. Using the fuel cell manufacturers' polarisation (V_{FC} vs. I_{FC}) and efficiency curves [42], hydrogen consumption and efficiency are plotted up to a maximum net power of 1.2kW in Figure 4.3 and considered in the simulations. In this manner the simulations use fuel cell characteristics which incorporate the power losses associated with BOP. The duty factor for the fuel cell can also be calculated (total power supplied by the fuel cell relative to the number of fuel cell start-stops for the same time period). Because the lifetime of a fuel cell is largely dependent on the operational hours and number of start-stops, a higher fuel cell duty factor means fewer start-stops for the same operational hour limit.

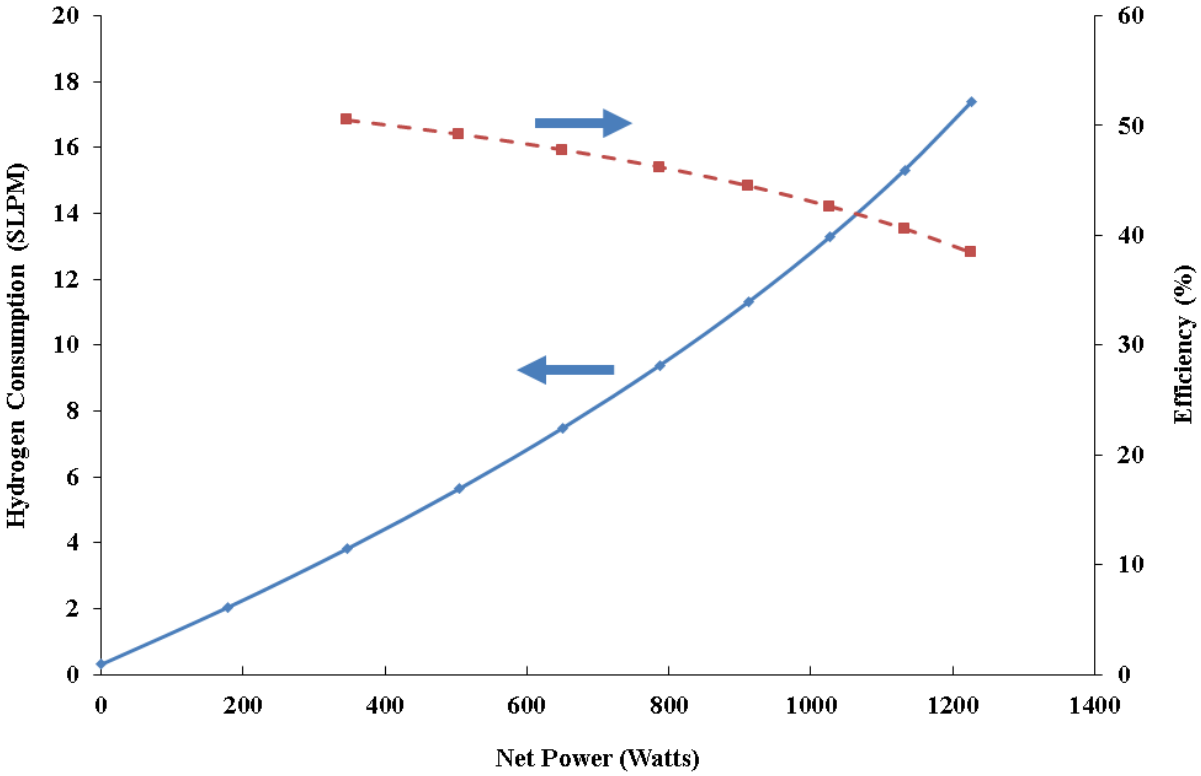

Figure 4.3 - Net system efficiency and hydrogen consumption of a 1.2kW PEM fuel cell as a function of net power output. The system efficiency is defined by the ratio of net power output to the lower heating value of hydrogen consumed in the fuel cell. SLPM: Standard Litres Per Minute; LHV: Lower Heating Value of hydrogen (3.00 kWh/Nm^3).

Power Management Strategy: A Power Management Strategy (PMS) is needed to control the activation of various energy system hardware components and is typically implemented through a PMU (which is mostly represented by a Programmable Logic Controller, PLC). The PMS applied within the hydrogen energy system is depicted in Figure 4.4, and except for the (dashed) part of this which is needed to satisfy the electric load and water demand, is tested against that (non PSO optimised) PMS applied in our earlier study [25]. In the current investigation, PSO is integrated into the simulation to optimise four (operational) control set-points within this PMS (Figure 4.4) in addition to the size of energy system components. These four parameters are:

1. **Minimum delay time before the PEM electrolyser operates (T_E):** Before the PEM electrolyser can operate, it is desirable to secure a continuous period of sufficient solar-PV energy which lasts longer than its start-up time (5 minutes). This helps ensure the power requirement of the electrolyser (device rating of 250W) are satisfied. However, prolonging these delays prior to start-up means less hydrogen produced

over any single day. Any energy not used to power the PEM electrolyser is used to desalinate seawater up to a maximum given water storage tank capacity (50L).

2. **Minimum water capacity threshold (C_{H2O}):** For the PEM electrolyser to operate, the reserve of suitable (desalinated, deionised) water must be higher than a threshold to ensure continuity of operation. If the reserve falls below this threshold, hydrogen generation is terminated and energy is diverted to water production which is then prioritised. However, if water capacity is at the water storage tank maximum (50L), any surplus energy is used to charge batteries. Once the battery State-of-Charge reaches SOC=100%, any power not utilised to operate the PEM electrolyser or RO unit is then dumped and deemed a surplus.

3. **Maximum hydrogen storage capacity (C_H):** Once the maximum hydrogen storage capacity of the metal hydride canisters (500L) is reached, the PEM electrolyser is switched off with power diverted to the production of desalinated water (device rating of DC 50W) or otherwise used to charge the battery. Other peak storage capacities can be built into the simulations.

4. **Define minimum hydrogen capacity threshold (C_{MH}):** Through the use of a minimum threshold, the electrolyser remains off until the hydrogen stored once again falls to a minimum threshold at which point electrolysis is reactivated.

5. **Battery capacity (C_B):** Battery storage allows for short-term energy supplements to power system components such as the PEM electrolyser and RO unit. This allows greater renewable energy penetration which results in extended operational time. However, batteries are not used in this system (Figure 4.1) to directly supply electric load demand.

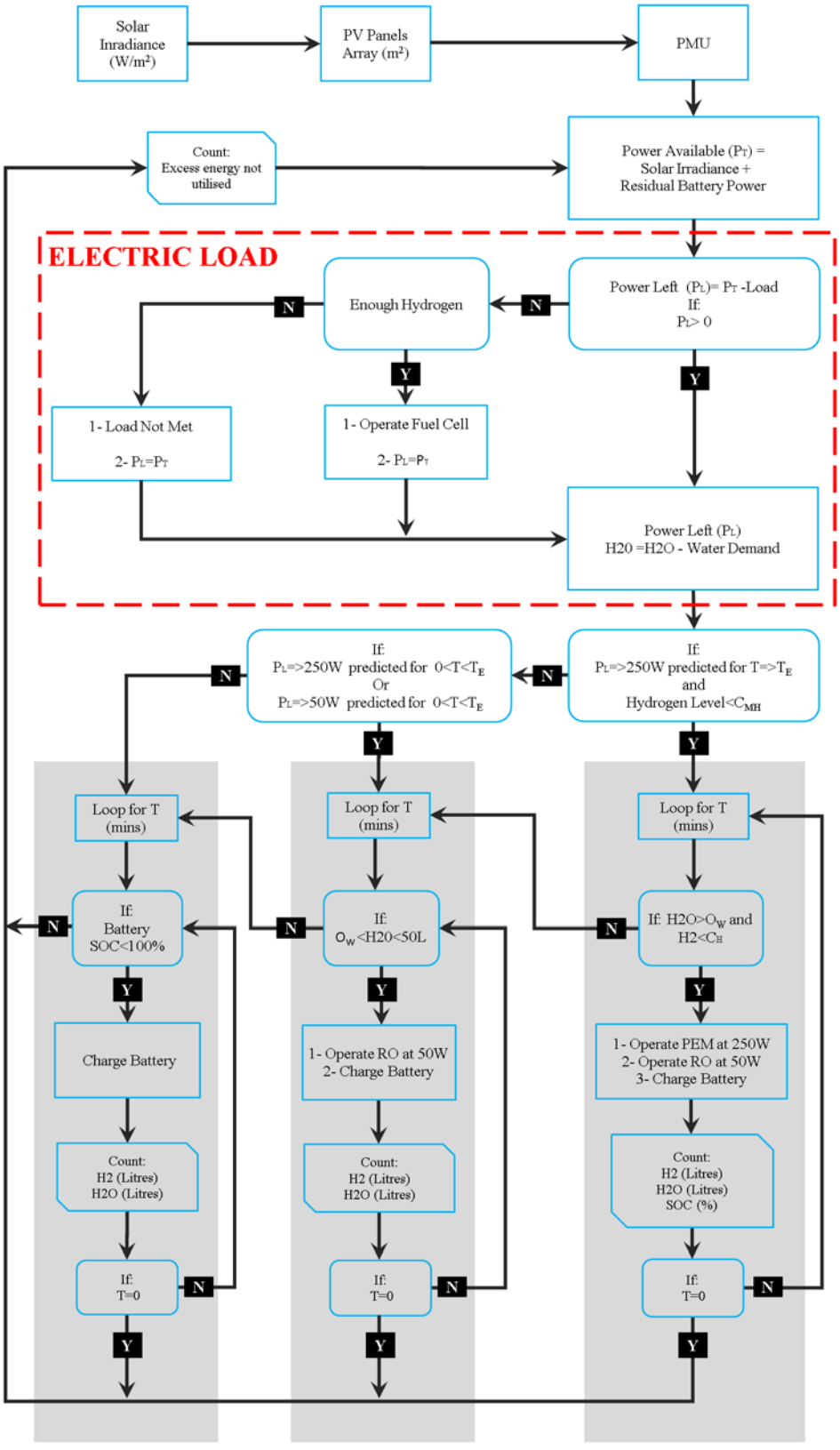

Figure 4.4 - Power Management Strategy (PMS) for the stand-alone hydrogen energy system. The dashed box indicates the addition of a fuel cell to a hydrogen generation system to meet a (electric) load demand.

Obviously the above noted hardware limits can be revised up/down if needed. At the start of the simulations (T=0mins), the battery, water and hydrogen capacity is assumed to be 100% (Table 4.1) with the battery having a pre-set minimum depth of discharge over any time-step at SOC=20%. To optimise the Power Management Strategy, the PSO algorithm seeks out within the search space of plausible solutions, the set of parameters (C_B, C_{H2O}, T_E, C_H and C_{MH}) which maximise system performance for a given operational objective function. This optimal solution is termed (X) and expressed in Equation 4.2 and more on the methodology used by the PSO to seek out this optimal solution (X) is described in the next section.

$$X = [C_B, C_{H2O}, T_E, C_H, C_{MH}] \qquad \textit{Equ. 4.2}$$

4.3.2 - The Particle Swarm Optimisation Algorithm

The algorithm mimics a number of particles which move in a search space, defined by the range of hardware and dynamic operational constraints described above. The number of particles is typically in the range of 20 – 40 [43]. The overall aim for these particles is to each "land on" (find) an optimal solution. The grid position of any single particle throughout this search space represents one possible solution for it and the best solution for this particle is represented by (P_{best}). The movement of particles is governed by the operational objective functions (described in this section). The global best (G_{best}) solution is obtained out of all the (P_{best}) solutions for the entire swarm [13, 44, 45]. In the PSO algorithm, the updated position and velocity of the (i-th) particle are represented in Equation 4.3 [44] as:

$$V_t{}^{k+1} = K(V_i{}^k \times w + c_1 \times R_1 \times \left(P_{best}(i) - X_i{}^k\right) + c_2 \times R_2 \times \left(G_{best} - X_i{}^k\right)) \qquad \textit{Equ. 4.3}$$

Where ($V_t{}^k$) is the possible dimension for (i) particles with position ($X_i{}^k$) and velocity ($V_i{}^k$), a constriction factor (K) which controls the velocity magnitude, the individual best position of particle (i) is (P_{best}), the global best position across all particles is (G_{best}) and the inertia weight (w) controls how much of the particles previous velocity (speed which particle moves in the search space) is retained. Additionally, the iteration number is denoted by (k) and non-negative acceleration factors (c_1 and c_2) are specific to the PSO with random numbers (R_1 and R_2) in the range of [0 to 1]. The cognitive acceleration constant (c1) controls how much the particle heads towards its own personal best position. The social acceleration constant (c2) alternatively controls the tendency of that same particle to head towards the global best

position across all particles[19]. The acceleration parameters of the PSO algorithm are selected based on a "grid search" method whereby each parameter (c1 and c2) are changed in intervals of 0.5 to a maximum of 2. The result is 16 combinational pairs of c1 and c2 with the population size remaining constant throughout at 24 particles. The PSO has parameters in Equation 4.3 which can be adapted to yield better results for optimisation and the algorithm starts by generating random positions and velocities for the particles, within the bounds (Table 4.1). During the main loop of the algorithm, the velocities and positions of the particles are iteratively updated until one of two stopping criteria is met: (i) a maximum iteration number of 100 or (ii) no change in 30 iterations for G_{best}. Throughout the simulations conducted it was observed that the maximum number of iterations whereby G_{best} remains unchanged is more likely to cause the PSO to meet the stopping criteria. This indicates the number of iterations stipulated (100) was sufficient to attain an optimised solution. The PSO algorithm is run 3 times for each objective after which an average output value is established (O_H, O_{ESS}, O_W, O_{FC}, O_{FCSS}, T_{LOL}) along with its associated optimisation time.

Operational Objective Function 1: *Optimise the PMS by finding X which maximises hydrogen generation (litres/season)*

For the "hydrogen generation assembly" (Figure 4.1) an operational objective which may arise in an application scenario is to maximise hydrogen generation for a given solar irradiance profile. This scenario would materialise where a hydrogen refuelling station needs to meet specific reserves to guarantee fuel stock availability. This operational objective function is expressed as:

$$Optimal\ System\ Performance = Max \sum_{i=day}^{n=season} [(O_H)] \qquad \textit{Equ. 4.4}$$

The terms of Equation 4.4 denote total hydrogen generation (O_H) and the PEM electrolysers' duty factor (O_{EDF}) over the entire season. This objective is tested for up to six battery scales (C_B= 0Ah battery-less operation, 0-27Ah, 0-55Ah, 0-83Ah, 0-110Ah and 0-200Ah) which will form a comparison with the non PSO optimised PMS system [25].

[19] Refer to Appendix F for further details on PSO.

Operational Objective Function 2: *Optimise the PMS by finding X which maximises the PEM electrolysers' duty factor for a target hydrogen generation (litres/season)*

Generating the maximum possible hydrogen for a given solar irradiance profile in a given season is not always possible in stand-alone renewable hydrogen systems due to storage limits. Any hydrogen that is generated beyond what is required would be considered surplus to requirements. In such instances it would be more beneficial to target a needed hydrogen quantity but achieve this at increased hardware component efficiencies. The aim of PSO here is to find X (Equation 4.2) that accurately generates the target hydrogen yield (O_{HT}) whilst maximising the PEM electrolysers' duty factor (O_{EDF}). A higher PEM electrolyser duty factor means fewer start-stops to generate the same amount of hydrogen. A higher duty factor therefore increases process efficiency by reducing start-up transients and the ability to divert power to other uses. This scenario is likely to occur when multiple load demands (i.e. water desalination and power generation) are needed as with a remote residential house. Equation 4.5 is utilised to find X for a given hydrogen target:

$$Optimal\ System\ Performance = Min \sum_{i=day}^{n=season} [|O_H - O_{HT}|]\ and\ Max \sum_{i=day}^{n=season} [\ (O_{EDF})] \qquad Equ.\ 4.5$$

The additional terms in Equation 4.5 denote the daily total of desalinated water (O_W) and total hydrogen generation (O_H) over the entire season. The effectiveness of PSO in optimising this operational objective function is tested at C_B=0, 27, 55, 83, 110 and 200Ah over the winter season for comparison with the rule-based system.

Operational Objective Function 3: *Optimise the PMS by finding X which minimises the Loss of Load time and the PEM fuel cell start/stops but maximises the PEM electrolysers' duty factor*

For a given (dynamic, minute resolved) electric and water load demand (Figure 4.2b), the PSO aims to find X (Equation 4.2) that best meets the electric load and drinking water requirements. For most cases, the PSO is able to find a unique solution to X. However, in some instances, where a number of plausible solutions exist for X, the algorithm then filters these solutions seeking out those which minimise the number of PEM fuel cell start/stops (O_{FCSS}) or (thereafter) maximise the PEM electrolysers' duty factor (O_{EDF}). The time (in

minutes) in which the electric load (powering an external load and RO unit) is not satisfied is defined as the Loss of Load (T_{LOL}). Equation 4.6 is utilised to find X:

$$Optimal\ System\ Performance = Min \sum_{i=day}^{n=season} T_{LOL} \qquad Equ.\ 4.6$$

4.4 - Results and Discussion

Optimisation for maximum hydrogen generation: Figure 4.5 presents data derived by applying Operational Objective Function-1 which uses a variety of c1 and c2 PSO acceleration parameters and constraints (C_B, C_{H2O}, T_E, C_H, C_{MH}) to govern the optimal solution X. As noted earlier, the optimisation derived from Operational Objective Function-1 focusses on maximising O_H without considering other performance parameters. Results indicate that using PSO to optimise the control set-points in the PMS allows the system to generate more hydrogen compared to a Power Management Strategy with merely pre-set control points [25]. The improvement occurs across all levels of battery capacity and is accompanied by an increase in electrolyser duty factor. The greater duty factors achievable with PSO mean the optimised Power Management Strategy delivers more hydrogen for lesser electrolyser start-stops. The percentage increase in hydrogen generation, as a function of various combinations of PSO acceleration parameters (c1 and c2), is shown in Figure 4.6a. In general, results indicate that when battery scale (C_B) is decreased, the use of PSO to optimise a PMS has more (relative) impact resulting in a higher percentage increase in hydrogen generation. In this regard, the choice of acceleration parameters appears to have an insignificant effect. This highlights that optimisation of a Power Management Strategy is more significant in smaller scale systems. Figure 4.6b shows the time needed to achieve a PSO derived solution can vary from around 510 seconds to 711 seconds. A performance decrement in duty factor (negative % improvement) is observed when using PSO (compared to a pre-set PMS) at C_B=0 to 110Ah. Careful examination of the raw data at this condition indicates that whilst the PSO algorithm identifies an increased O_H (Figure 4.6a) compared to the non-optimised PMS [25], this improvement in hydrogen generation comes at the expense of duty factor. Such a behaviour is due to the nature of the Operational Objective Function-1 which only seeks to optimise for hydrogen generation. Such limitations may be overcome by using multi-objective function optimisation methods which are beyond the scope of the present work but worthy of pursuit.

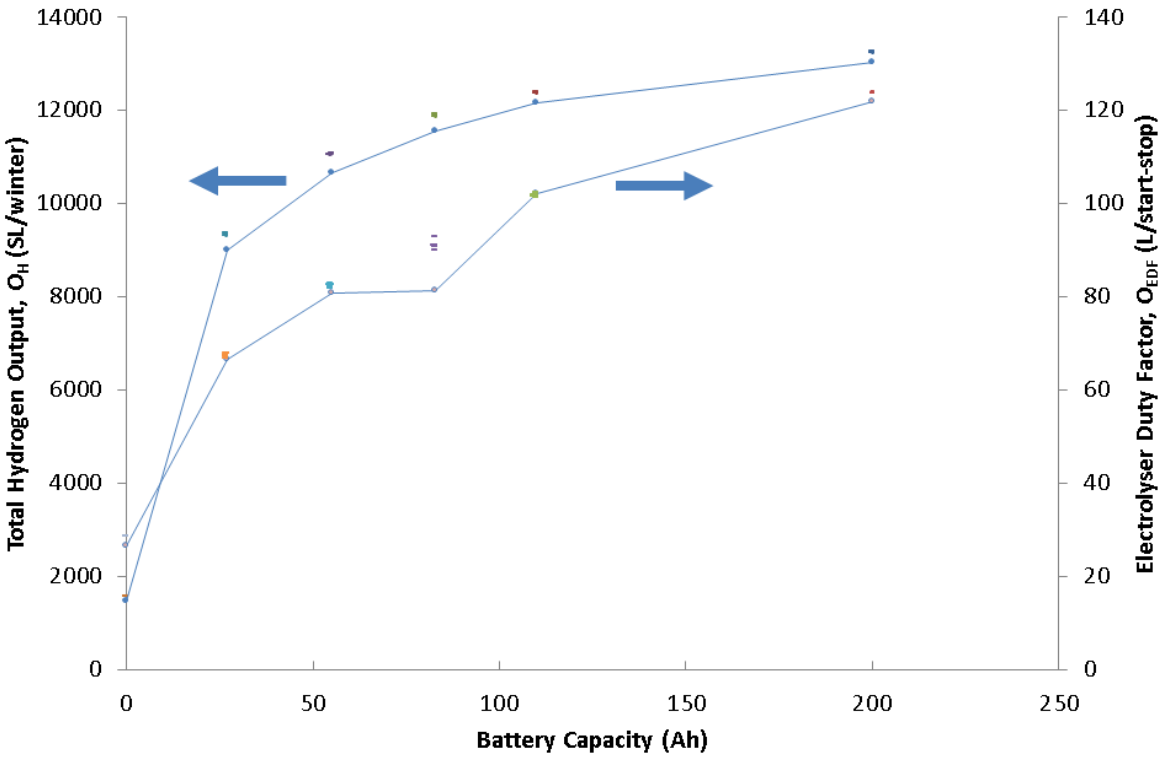

Figure 4.5 - A comparison between an optimised, and non-optimised, PMS on the hydrogen generated (per season) and the electrolysers' duty factor. Results for PSO (unconnected markers) are derived based on a variety of c1 and c2 acceleration parameters (Operational Objective Function-1) and compared to data for a non-optimised PMS (trend lines, [25]).

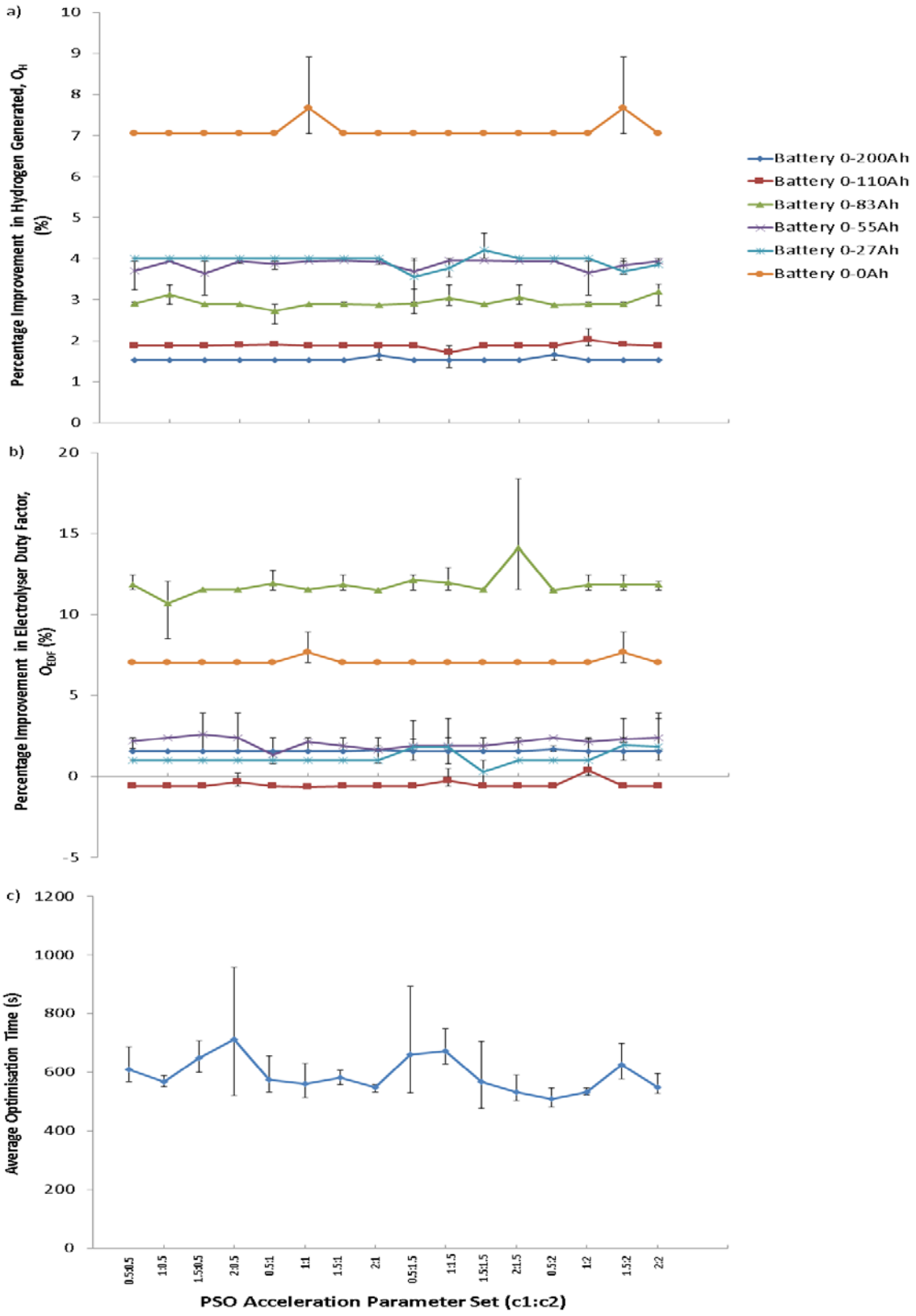

Figure 4.6 - The effects of battery scale and choice of PSO acceleration parameters (c1 and c2) on (a) total hydrogen output via electrolysis; (b) electrolyser duty factor; and (c) time to attain PSO solution over all values of c1 and c2 for Operational Objective Function-1.

Optimisation for maximum duty factor: Figure 4.7 presents data relating to Operational Objective Function-2 which uses a variety of c1 and c2 PSO acceleration parameters and constraints (C_B, C_{H2O}, T_E, C_H, C_{MH}) to maximise O_{EDF} whilst meeting a target O_H. Within the range O_H=1,468L to 13,044L, results show that as the target hydrogen generation increases, the use of PSO to optimise the PMS has less (relative) impact on improving electrolyser duty factor. Furthermore, there exist no clear combination of values for c1 and c2 which provide the best solution. This highlights the need to also consider the choice of acceleration parameters when using PSO to optimise hydrogen energy systems, something which has not been adequately tested in the published literature. The acceleration parameters also have a significant impact on the optimisation time under Operational Objective Function-2 as shown in Figure 4.7b. It is noted that PSO also results in two "negative improvements" for some combinations of c1/c2 at O_H=13,044L (at c1/c2=0.5/1 and 1.5/1). Examination of the raw data in these two cases reveals the PSO algorithm had met the stopping criteria (30 iterations without any change to G_{best}). By relaxing the stopping criteria, at the expense of optimisation time, this should be overcome, even though it appears the two stopping criteria used in this study suffices for all other cases tested.

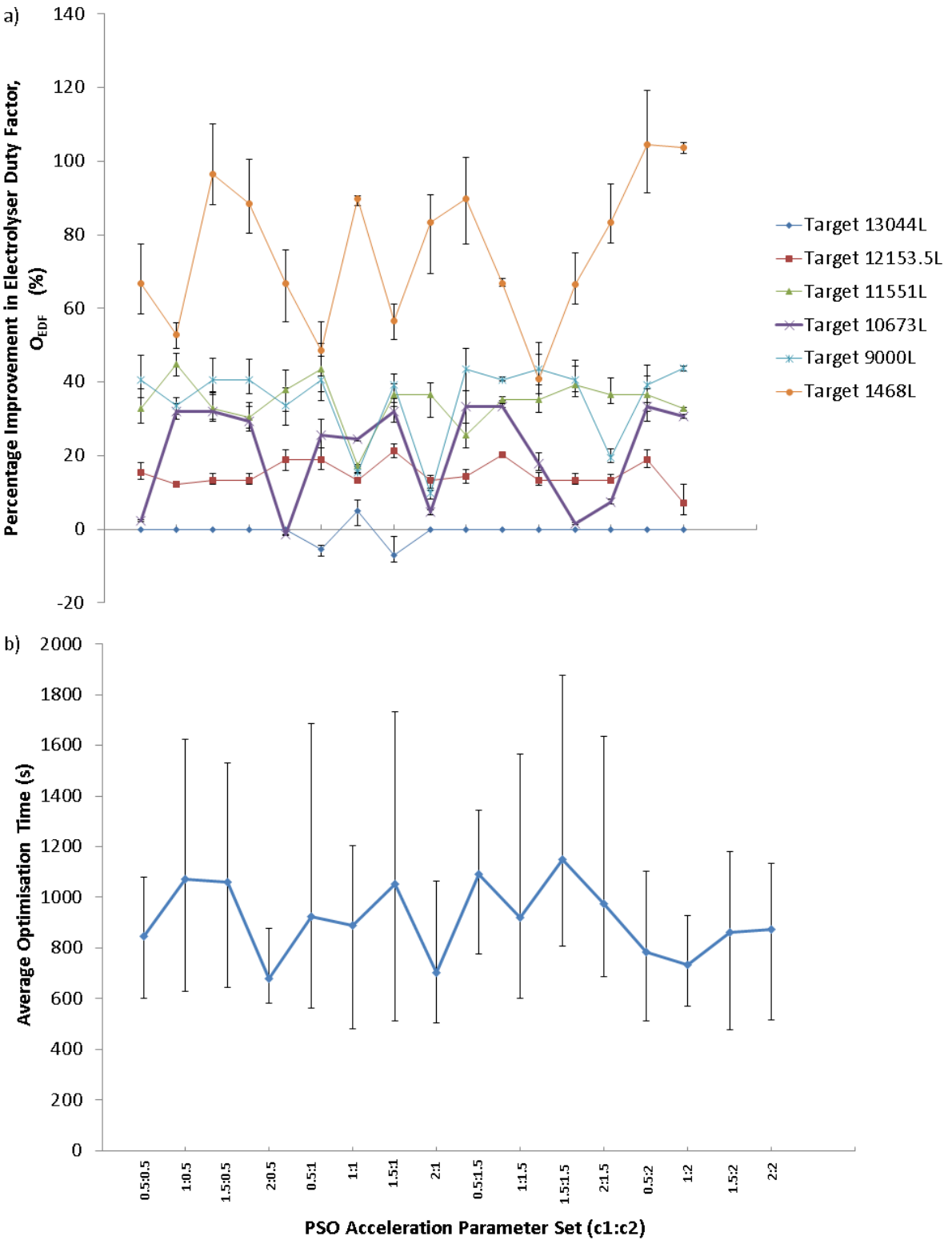

Figure 4.7 - The effects of size of (target) hydrogen production and choice of PSO acceleration parameters (c1 and c2) on (a) electrolyser duty factor and (b) time needed to arrive at PSO optimised solution for Operational Objective Function-2.

Optimisation for load demand: Operational Objective Function-3 uses different combinations of c1 and c2 to seek out the solution which minimises the Loss of Load time (T_{LOL}) within the constraints (C_B, C_{H2O}, T_E, C_H and C_{MH}). The incorporation of some battery storage allows for greater renewable energy penetration resulting in longer periods in which a PEM electrolyser can operate resulting in more hydrogen generated necessary for PEM fuel cell use. Figure 4.8a shows the starting Loss of Load for the entire stand-alone system when governed by a non-optimised PMS and compares this to a PSO optimised PMS in Figure 4.8b. Figure 4.8c also highlights the impact of maximum hydrogen storage (C_H) on the Loss of Load time. With higher hydrogen storage capacity, the PEM fuel cell has the potential to run for longer periods of time even when there is insufficient solar energy to replenish hydrogen reserves. This results in an increase in the hydrogen energy systems' ability to meet the external load and is evident across most battery capacities tested, particularly at lower scale. An example of the gains of using PSO, is the reduction (at C_B=0-27Ah, C_H=125L) of T_{LOL} from around 21,000 minutes over the season (132,480 minutes) to around 9,000 minutes. These gains mean the total time over which the system does not meet the seasonal load (at C_B=0-27Ah, C_H=125L) is more than halved from 15.8% to 6.8%.

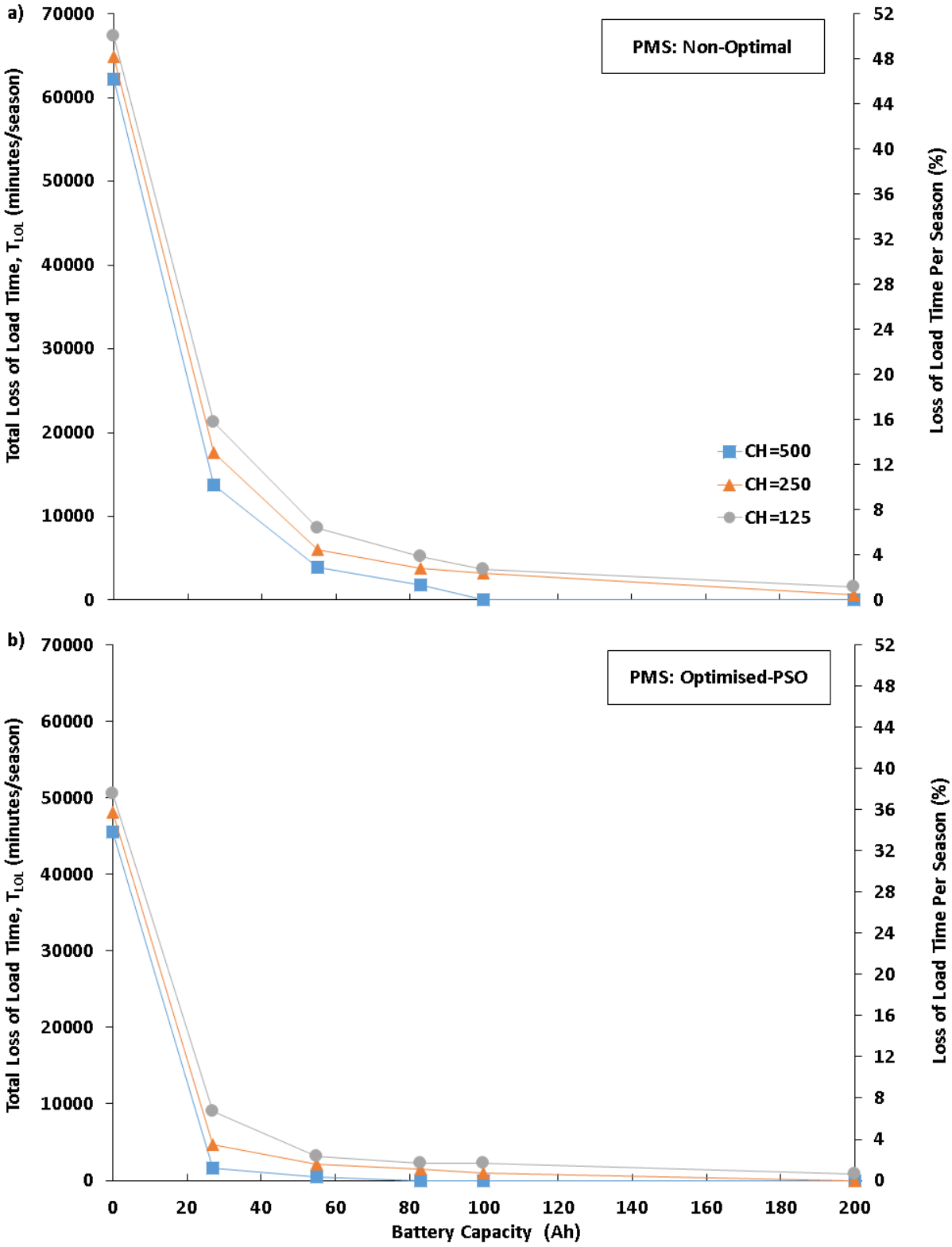

Figure 4.8 - The effects of size of hydrogen storage capacity and battery scale on Total Loss of Load given a (a) Non-optimised PMS, (b) PSO optimised PMS for Operational Objective Function-3.

Whilst reducing the Loss of Load is the primary outcome derived from Operational Objective Function-3, it also aims to maximise system component performance through the minimisation of PEM device start-stops and likely (conceptual) transients such as the number of start-stops of the PEM fuel cell whilst satisfying an external load (total kWh). The number of PEM fuel cell start-stops at a variety of battery and maximum hydrogen capacity intervals is also analysed at this condition (C_B=0-27Ah, C_H=125L), shown in Figure 4.9. Careful examination of the data shows in the case of the non-optimised PMS, battery-less (0Ah) operation results in about 205 start-stops of the fuel cell (Figure 4.9a) compared to an improvement to 173 start-stops when using PSO (Figure 4.9b). Therefore, using a PSO optimised PMS positively impacts the number of start-stops experienced by the PEM fuel cell through a 15.6% reduction. However, results also show that as battery capacity increases this effect of PSO diminishes. This is because as T_{LOL} approaches zero meaning all the load is met, the number of PEM fuel cell start-stops becomes more dependent on the external electric load profile, rather than the choice of parameters (C_B, C_{H2O}, T_E, C_H, C_{MH}) which govern the solution (X).

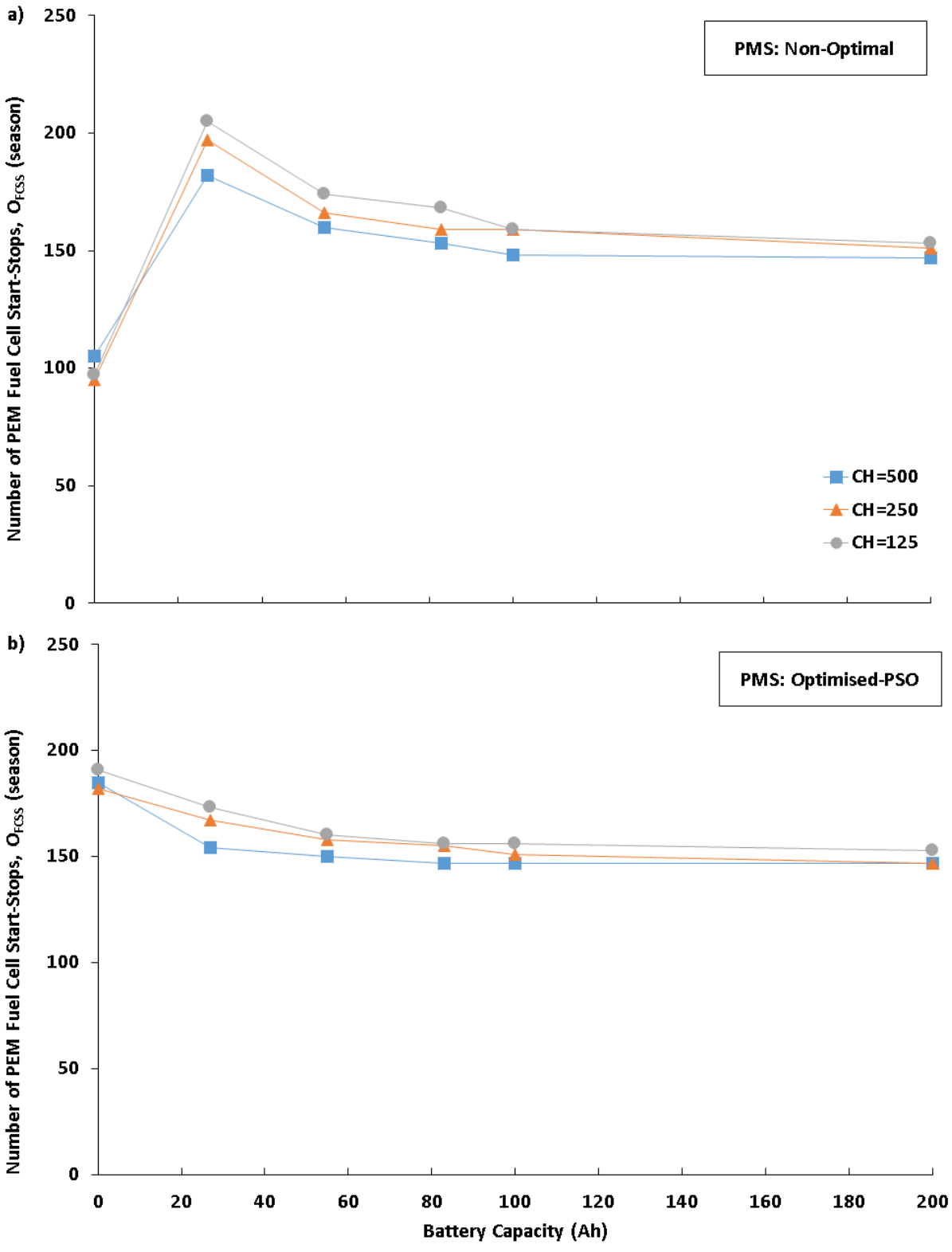

Figure 4.9 - The effects of size of hydrogen storage capacity and battery scale on the number of PEM fuel cell start-stops given a (a) Non-optimised PMS, (b) PSO optimised PMS for Operational Objective Function-3.

Figure 4.10 presents the PEM fuel cell duty factor at varying battery capacity and maximum hydrogen storage intervals. The number of PEM fuel cell start-stops and Loss of Load directly influence the duty factor of the fuel cell. Results indicate that allowing PSO to optimise the PMS generally allows the system to minimise Total Loss of Load but also maximises the PEM duty factor (Figure 4.10b) compared to a Power Management Strategy with pre-set control points (Figure 4.10a). Overall, Figure 4.10 also indicates that when battery scale is decreased, the use of PSO to optimise a PMS has more (relatively) greater impact resulting in a higher percentage increase in PEM duty factor. This highlights that implementing an optimisation to a Power Management Strategy further identifies the significance in smaller scale systems to best utilise available solar irradiance to meet an external load and limit the cyclic behaviour of PEM devices.

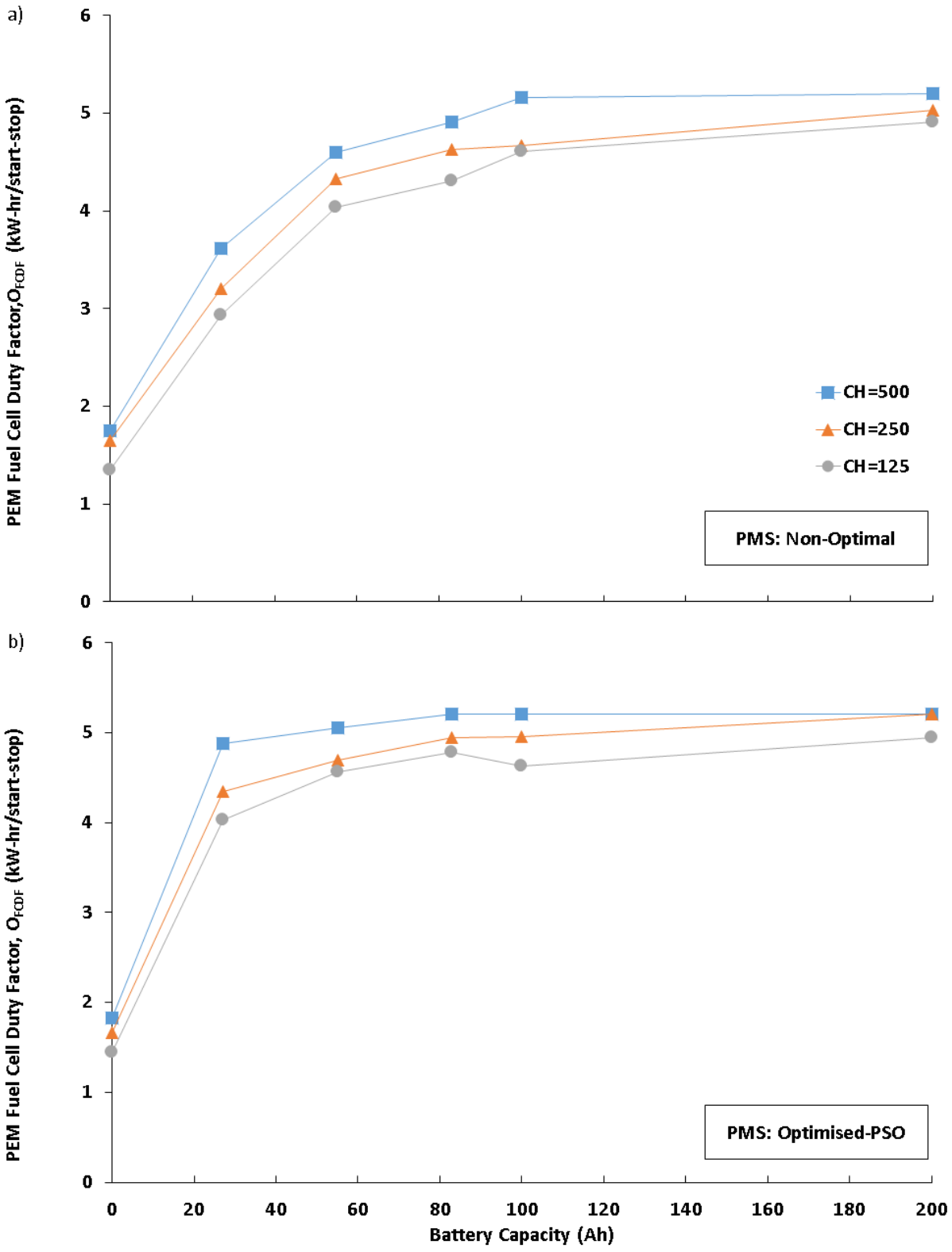

Figure 4.10 - The effects of size of hydrogen storage capacity and battery scale on the PEM fuel cell duty factor given a (a) Non-optimised PMS, (b) PSO optimised PMS for Operational Objective Function-3.

4.5 - Conclusions

The effects of using PSO to size some of the components and optimise the PMS for a stand-alone hydrogen system have been tested and analysed using three objectives. Simulations and the implementation of the PSO algorithm are done at one minute resolved solar irradiance data for an Australian winter period (August, June and July) and conducted using MATLAB/Simulink. The research conducted compares optimisation with PSO to that using a rule-based equivalent system in which control set points are predefined. The main outcomes may be summarised as:

- Using PSO to optimise the Power Management Strategy results in greater hydrogen yield from electrolysis and an improved PEM electrolyser duty factor. These improvements in electrolysis appear more pronounced as the systems scale (battery storage capacity, targeted hydrogen generation per season) is reduced.

- The likely performance gains to a PEM fuel cell, in terms of start-stops, also appears to improve with the use of PSO to size the system and optimise the Power Management Strategy.

- The use of PSO in the optimisation of stand-alone hydrogen energy systems, particularly at the scale investigated in this chapter, appears to yield significant reductions in Loss of Load time.

- To achieve the above, there needs to be a careful selection of the PSO acceleration parameters, c1 and c2, as well as the stopping criteria for the optimisation algorithm. All these factors can affect not only the solution attained (gains from using PSO), but also the time needed to arrive at the solution.

4.6 - Chapter References

[1] Doukas H, Patlitzianas KD, Kagiannas AG, Psarras J. Renewable energy sources and rationale use of energy development in the countries of GCC: Myth or reality? Renewable Energy. 2006;31:755-70.

[2] Brka A, Al-Abdeli YM, Kothapalli G. Influence of neural network training parameters on short-term wind forecasting. International Journal of Sustainable Energy. 2014:1-17.

[3] Jalilzadeh S, Rohani A, Kord H, Nemati M. Optimum design of a hybrid Photovoltaic/Fuel Cell energy system for stand-alone applications. 6th International Conference on Electrical Engineering/Electronics, Computer, Telecommunications and Information Technology, ECTI-CON Chonburi, Thailand 2009. p. 152-5.

[4] Beaudin M, Zareipour H, Schellenberglabe A, Rosehart W. Energy storage for mitigating the variability of renewable electricity sources: An updated review. Energy for Sustainable Development. 2010;14:302-14.

[5] Wu J, Yuan XZ, Martin JJ, Wang H, Zhang J, Shen J, Wu S, Merida W. A review of PEM fuel cell durability: degradation mechanisms and mitigation strategies. Journal of Power Sources. 2008;184:104-19.

[6] Dufo-López R, Bernal-Agustín JL, Contreras J. Optimization of control strategies for stand-alone renewable energy systems with hydrogen storage. Renewable Energy. 2007;32:1102-26.

[7] Zhou W, Lou C, Li Z, Lu L, Yang H. Current status of research on optimum sizing of stand-alone hybrid solar–wind power generation systems. Applied Energy. 2010;87:380-9.

[8] Luna-Rubio R, Trejo-Perea M, Vargas-Vázquez D, Ríos-Moreno GJ. Optimal sizing of renewable hybrids energy systems: A review of methodologies. Solar Energy. 2012;86:1077-88.

[9] Phuangpornpitak N, Prommee W, Tia S, Phuangpornpitak W. A study of particle swarm technique for renewable energy power systems. 2010 Proceedings of the International Conference on Energy and Sustainable Development: Issues and Strategies (ESD) 2010. p. 1-6.

[10] Nowdeh SA, Nasrollahnezhad MB, Khanabdal S. Optimal sizing of a stand-alone PV/FC/wind hybrid system using PSO modified method. International Journal of Electronics, Computer and Communications Technologies. 2013;3:12-9.

[11] Ghazvini M, Fard AAT, Firuzabad MF. A particle swarm optimization-based approach to achieve optimal design and operation strategy of standalone hybrid energy systems. Turkish Journal of Electrical Engineering and Computer Sciences. 2013;21:467-73.

[12] Nafeh AE-SA. Optimal economical sizing of a PV-wind hybrid energy system using genetic algorithms. International Journal of Green Energy. 2011;8:25-43.

[13] Hakimi SM, Moghaddas-Tafreshi SM. Optimal sizing of a stand-alone hybrid power system via particle swarm optimization for Kahnouj area in south-east of Iran. Renewable Energy. 2009;34:1855-62.

[14] Hakimi SM, Tafreshi SMM, Kashefi A. Unit sizing of a stand-alone hybrid power system using particle swarm optimization (PSO). 2007 IEEE International Conference on Automation and Logistics. China 2007. p. 3107-12.

[15] Rashidi H, Niazi S, Khorshidi J. Optimal sizing method of solar-hydrogen hybrid energy system for stand-alone application using fuzzy based particle swarm optimization algorithm. Australian Journal of Basic and Applied Sciences. 2012;6:249-56.

[16] Jahanbani F, Riahy GH. Optimum design of a hybrid renewable energy system. Renewable Energy - Trends and Applications. 2011. Available from, http://www.intechopen.com/books/renewable-energy-trends-and-applications/optimum-design-of-a-hybrid-renewable-energy-system

[17] Sinha AK, Bajpai P. Swarm intelligence based optimal sizing of a solar PV, fuel cell and battery hybrid system. 2012 International Conference on Power and Energy Systems. Hong Kong 2012. p. 467-73.

[18] Kornelakis A. Multiobjective Particle Swarm Optimization for the optimal design of photovoltaic grid-connected systems. Solar Energy. 2010;84:2022-33.

[19] Al-Alawi A, Islam SM. An integrated remote area power & water supply system using renewable energy in the middle east. Australasian Universities Power Engineering Conference. Christchurch, New Zealand 2003.

[20] Elbaset AA. Design, modelling and control strategy of PV/FC hybrid power system. Journal of Electrical Systems. 2011;7:270-86.

[21] Ipsakis D, Voutetakis S, Seferlis P, Stergiopoulos F, Elmasides C. Power management strategies for a stand-alone power system using renewable energy sources and hydrogen storage. International Journal of Hydrogen Energy. 2009;34:7081-95.

[22] Ghazvini M, Abbaspour-Tehrani-Fard A, Fotuhi-Firuzabad M, Othman MM. Optimizing size and operation of hybrid energy systems. 2013 IEEE 7th International Power Engineering and Optimization Conference (PEOCO) Malaysia 2013. p. 489-94.

[23] Ghazvini M, Fard AAT, Firuzabad MF. A particle swarm optimization-based approach to achieve optimal design and operation strategy of standalone hybrid energy systems. Turkish Journal of Electrical Engineering & Computer Sciences. 2013;21.

[24] Zhao YS, Zhan J, Zhang Y, Wang DP, Zou BG. The optimal capacity configuration of an independent Wind/PV hybrid power supply system based on improved PSO algorithm. 8th International Conference on Advances in Power System Control, Operation and Management (APSCOM 2009) 2009. p. 1-7.

[25] Clarke DP, Al-Abdeli YM, Kothapalli G. The impact of renewable energy intermittency on the operational characteristics of a stand-alone hydrogen generation system with on-site water production. International Journal of Hydrogen Energy. 2013;38:12253-65.

[26] Clarke DP, Al-Abdeli YM, Kothapalli G. The effects of including intricacies in the modelling of a small-scale solar-PV reverse osmosis desalination system. Desalination. 2013;311:127-36.

[27] Bureau of Meteorology (Australia). Solar exposure data for Geralton, Western Australia. Available from, http://reg.bom.gov.au/climate/reg/oneminsolar/index.shtml; 2012. [accessed 12 October,2012].

[28] Fahmy FH, Ahmed NM, Farghally HM. Optimization of renewable energy power system for small scale brackish reverse osmosis desalination unit and a tourism motel in Egypt. Smart Grid and Renewable Energy. 2012;3:43-50.

[29] Soric A, Cesaro R, Perez P, Guiol E, Moulin P. Eausmose project desalination by reverse osmosis and batteryless solar energy: design for a $1m^3$ per day delivery. Desalination. 2012;301:67-74.

[30] Avlonitis SA, Avlonitis DA, Panagiotidis T. Experimental study of the specific energy consumption for brackish water desalination by reverse osmosis. International Journal of Energy Research. 2012;36:36-45.

[31] Qiu TY, Davies PA. The scope to improve the efficiency of solar-powered reverse osmosis. Desalination and Water Treatment. 2011;35:14-32.

[32] Slama SB, Chaabene AB, Cherif A. Efficient design of a hybrid (PV-FC) water pumping system with serperate MPPT control algorithm. International Journal of Computer Science and Network Security. 2012;12:53-60.

[33] The National Health and Medical Research Council. Nutrient reference values for Australia and New Zealand including recomended dietary intakes. Available from, http://www.nhmrc.gov.au/_files_nhmrc/publications/attachments/n35.pdf; 2005. [accessed 25 May,2013].

[34] Khaligh A, Zhihao L. Battery, ultracapacitor, fuel cell, and hybrid energy storage systems for electric, hybrid electric, fuel cell, and plug-in hybrid electric vehicles: state of the art. IEEE Transactions on Vehicular Technology 2010;59:2806-14.

[35] Bajpai P, Dash V. Hybrid renewable energy systems for power generation in stand-alone applications: A review. Renewable and Sustainable Energy Reviews. 2012;16:2926-39.

[36] Kim T, Lee S, Park H. The potential of PEM fuel cell for a new drinking water source. Renewable & Sustainable Energy Reviews. 2011;15:3676-89.

[37] de Bruijn FA, Dam VAT, Janssen GJM. Review: durability and degradation issues of PEM fuel cell components. Fuel Cells. 2008;8:3-22.

[38] Thakur T, Goyal S, Garg S. Utilization of solar power through PEM fuel cells. 2008 Joint International Conference on Power System Technology (Powercon) and IEEE Power India Conference, Vols 1 and 2. India 2008. p. 827-32.

[39] Carter D, Ryan M, Wing J. The fuel cell industry review Available from, http://www.fuelcelltoday.com/media/1713685/fct_review_2012.pdf; 2012. [accessed 24 September,2013].

[40] Mehrpooya M, Daviran S. Dynamic modeling of a hybrid photovoltaic system with hydrogen/air PEM fuel cell. Iranica Journal of Energy and Environment. 2013;4:104-9.

[41] Carapellucci R, Giordano L. Modeling and optimization of an energy generation island based on renewable technologies and hydrogen storage systems. International Journal of Hydrogen Energy. 2012;37:2081-93.

[42] Ballard Power Systems Inc. Nexa Power Module User's Manual. Available from, http://my.fit.edu/~swood/Fuel%20Cell%20Manual.pdf 2003. [accessed 10 January,2013].

[43] Dong Y, Tang J, Xu B, Wang D. An application of swarm optimization to nonlinear programming. Computers and Mathematics with Applications. 2005;49:1655-68.

[44] Khare A, Rangnekar S. A review of particle swarm optimization and its applications in Solar Photovoltaic system. Applied Soft Computing. 2013;13:2997-3006.

[45] Fadaee M, Radzi MAM. Multi-objective optimization of a stand-alone hybrid renewable energy system by using evolutionary algorithms: A review. Renewable and Sustainable Energy Reviews. 2012;16:3364-9.

Chapter 5. Multi-Objective Optimisation of Renewably Powered Hybridised Energy Systems with Desalination

Daniel P. Clarke*, Yasir M. Al-Abdeli and Ganesh Kothapalli

This chapter was is currently under review as a full research paper in Energy. Whilst all efforts were made to retain the original features of this article, minor changes such as the layout, number formats, font size and style were implemented in order to maintain consistency in the formatting style of the thesis.

5.1 - Abstract

The optimisation, sizing and techno-economic assessment of stand-alone renewable energy systems affects not only the likelihood of deployment but also their reliability to supply electricity and potable water where needed. Very little work has been done earlier into the effects of integrating water desalination alongside meeting load demand. Moreover, the impact of intelligent techniques, in this context, against more established software tools has not been applied. In this chapter, Particle Swarm Optimisation (PSO) is compared to HOMER for the simultaneous optimisation of size and Power Management Strategy (PMS) in stand-alone hybrid energy systems. These systems incorporate significant relative water load met by reverse osmosis. Multi-objective functions in PSO minimise Total Net Present Cost (*NPC*) (includes capital, maintenance and replacement costs over a 25 year system lifetime) and lifetime CO_2 emissions whilst meeting these two loads. Results are analysed and compared for the conditions of dynamic (15 minute resolved) versus static water demand in addition to meeting varying electric loads. The PSO algorithm is implemented using MATLAB/Simulink and compared to a similar overall configuration developed in HOMER to meet the same loads (electric, water).

Results show using PSO achieves systems having lower *NPC* compared to HOMER, with the margin of improvement more pronounced in greater scale systems as water storage capacity and electrical load increase. Additionally, having a time-varying water profile negatively effects system performance by increasing *NPC* and CO_2 emissions compared to a static water profile.

5.2 - Introduction

With connection to the electrical grid very costly for remote locations, renewable energy is increasingly being integrated into stand-alone energy systems to reduce reliance on diesel power generation. Renewables (such as solar and wind) remain attractive as perpetual and secure long-term energy sources. As such, they are an excellent candidate for stand-alone power generation at reduced or negligible operational emissions [1]. However, renewable sources are highly stochastic and experience seasonal fluctuations [2]. Thus energy storage devices such as batteries and hydrogen are often used in stand-alone (hybrid) energy systems [3-6]. Energy storage is essential where there exists a mismatch between external electrical loads and the availability of renewables, and facilitates overall system operation by smoothing out load fluctuations [6] and improving operational characteristics [7].

Effective sizing of hybridised energy systems is necessary to achieve objectives such as meeting external load demand or reducing lifetime CO_2 footprint, whilst operating at the lowest energy cost ($/kWhr) [8, 9]. The sizing of such systems commonly relies on "simplistically" matching peak demand with the maximum rated capacity of system components [10, 11]. However, this approach has the likely outcome that systems are oversized which yields more costly solutions to meet a given electric load profile. More elaborate techniques attempt to optimise sizing through numerical methods, which can be iterative or probabilistic as well as based on genetic algorithms, fuzzy logic or neural networks [3, 8, 12-18]. Within this scope, Particle Swarm Optimisation (PSO) is an intelligent optimisation technique with many advantages such as fewer tuneable parameters and less dependence on the set of initial conditions, compared to some of the other intelligent techniques [19-21]. Additionally, the use of PSO has been shown to reduce environmental impact over a systems lifetime by reducing CO_2 emissions [22]. Software tools such as HOMER (Hybrid Optimisation Model *for* Electric Renewables) developed by the National Renewable Energy Laboratory, NREL-USA) have also been applied to allow techno-economic sizing of micro-power hybrid systems [23-25] and are freely available [26]. However, whilst such software tools are accompanied with excellent Graphical User Interfaces (GUI's), they are largely used as "black boxes" with some limited ability to parameterise. They are also not self-adaptive nor capable of accounting for device transients such as start-up time or control set points (e.g. storage capacity thresholds), both of which affects system performance.

In relation to the optimisation of hydrogen systems, published literature largely focusses on the use of pre-defined (static) Power Management Strategies (PMS) [8, 12, 27-29] even when other intelligent methods have been used [16]. This occurs despite system-level inputs (renewables) are highly intermittent and outputs (electric load demand) also fluctuate. An effective PMS is critical in hybridised systems as both the reliability of meeting external loads as well as system performance are affected by the PMS architecture and the control set-points within it [30-32]. Specifically, an optimised PMS can result in reduced payback time [22], improved system reliability at the smallest total infrastructure cost [33-39], and reductions to the cost of energy ($/kWhr) over the system lifetime [35, 40]. However, both the sizing of stand-alone energy systems and optimisation of their PMS typically needs to consider not only single objectives, such as minimising Net Present Cost (*NPC*), but multiple objectives which are economic, environmental or a combination of these three [41-43]. In this regard, multi-objective optimisation has targeted minimising the cost of energy by using different storage technologies [44], total hardware costs over the system's lifetime [29, 45] and operational emissions [46, 47], even though much of this research still encompasses diesel generation. Little research has been done to apply multi-objective optimisation to the PMS in renewably powered hybridised (hydrogen) energy systems designed to meet both electric load and desalinated water demand. Such elaborate optimisations are also beyond the scope of software tools such as HOMER because unlike PSO, such tools do not incorporate the dynamic characteristics of hardware components which is necessary to give system simulations the necessary realism as conditions fluctuate through the day.

Furthermore, few studies have attempted to compare the resulting performance gains when using PSO, in a multi-objective context to optimise both the Power Management Strategy (PMS) and component size, against widely adopted software optimisation tools such as HOMER. This type of research is worthwhile because for much lower levels of complexity (single objective function optimisations), the use of PSO compared to HOMER can decrease dependence on diesel generators by 10%, attain a lower *NPC* [39] and yield cost of energy improvements [48]. However, these earlier works have not accounted for the dynamic (time-resolved) operational characteristics of energy system components, have not considered systems which also sustain (small-scale) stand-alone desalination systems and have also overlooked the need to consider environmental impact (CO_2 emissions). This can be addressed through multi-objective optimisations like those covered by the present study.

This chapter extends our preliminary work whereby PSO was used to optimise Power Management Strategies with only single objectives [32]. In the present research, optimisation of both energy system (component) sizing and the PMS is done for multiple objective functions, and then compared to HOMER. The stand-alone energy system considered in the present study is completely powered by renewables and must meet two external loads: (i) power generation (kWhr) and (ii) desalinated water generation (litres). The two objective functions used to guide the optimisation are: (i) minimising total Net Present Cost (*NPC*, $) and (ii) CO_2 emissions (kg/kWhr over a lifetime). The present research also studies the effects of dynamic, versus static, water demand as well as varying the scale of electric load and water storage capacity. A secondary aim of this research is to also study the effects of Power Management optimisations on device cyclability. The PSO algorithm is implemented using MATLAB/Simulink (v.8.3) and the simulations are performed on a desktop PC having an Intel i3 processor. The reader is referred to our earlier work for details of the PSO methodology [32] which uses the optimised acceleration parameters c1=1.5 and c2=1. Many of the energy system components, featuring in the simulations, have already been experimentally resolved through our earlier works [7, 49]. Renewable data profiles for a specific coastal location (Geraldton, Western Australia) [50], having an abundant supply of salt water for Reverse Osmosis (RO), are utilised throughout.

5.3 - Methodology

Figure 5.1 presents the structure of the hybrid energy system which forms the focus of this study[20]. Table 5.1 lists typical component data used in the simulations (cost components) for PV panels[21], PEM fuel cell(s), PEM electrolyser(s), DC/DC converter(s), metal hydride canister(s) [51] as well as lead-acid batteries [52], reverse osmosis unit(s) [53] and water storage tank(s) [54] with their associated CO_2 emission rate (kg CO_2-eq/kWhr) [46, 55]. This data is specified per single unit, but the number of hardware units is derived through the optimisation[22].

[20] Refer to Appendix D for Chapter 5 system MATLAB/Simulink model.

[21] Refer to Appendix D for PV panel model.

[22] Refer to Appendix C for error analysis methods.

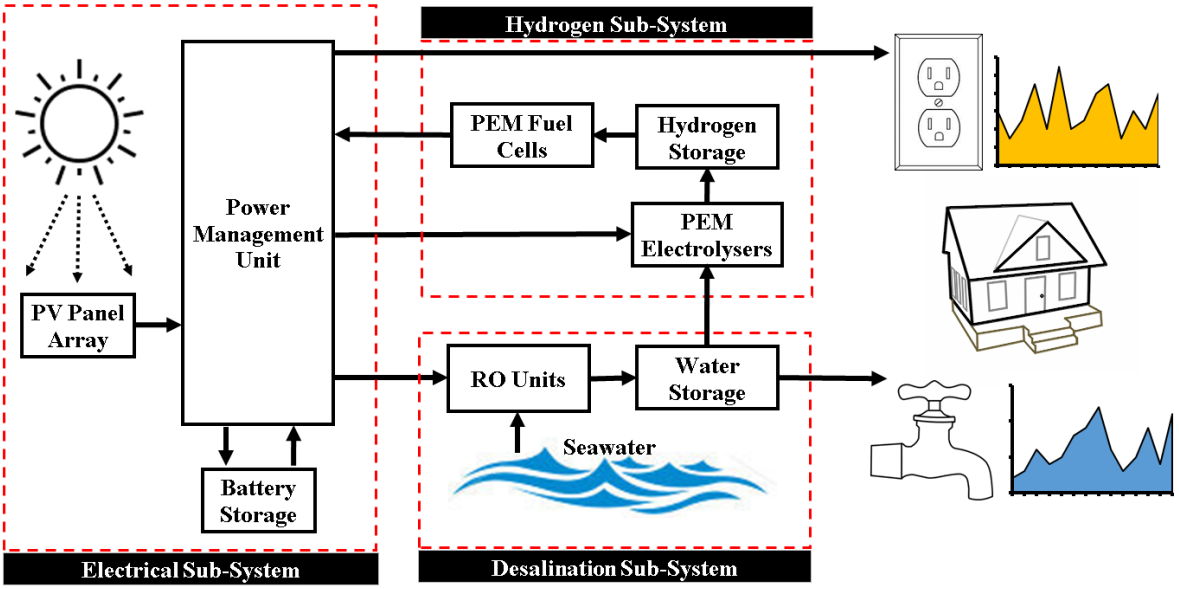

Figure 5.1 - Stand-alone hybrid energy system incorporating three distinct sub-systems: (i) electrical, (ii) hydrogen and (iii) desalination. The DC/DC converter is included within the PMU bundle.

Component Type	Component Model	Capital Cost (C_1)	Replacement Cost (R_1)	Operation & Maintenance ($O\&M_1$)	Lifetime (L)	Emissions ($kgCO_2/kWhr$) ($R_{i,CO2}$)
PV Panels	HS - PL135 (0.13kW, 0.8m_2), Heckert Solar - Germany	$7,000/kW	$6,000/kW	$20/year	20 Years	0.045
PEM Fuel Cell	Nexa 1200, Ballard Power Systems - Canada	$3,000/kW	$2,500/kW	$0.02/hr/kW	500 start-stops or 5,000 Hrs	0.02
PEM Electrolyser	NMH2 - 500 (0.025kW, 30SLH_2/hr), DBS - Italy	$2,000/kW	$1,500/kW	$20/year	5 Years	0.011
Metal Hydride	85G555B-NPT (500 SLH_2), Ovonic - Germany	$1,300/kg	$1,200/kg	$15/kg/year	20 Years	0.011
Lead-Acid Battery	SBV 12-55 (12V, 55Ah), Banner - Germany	$133/Bat	$113/Bat	$1.13/Bat/year	265kWhr	0.028
DC/DC Converter	Nexa DC1200, Heliocentris - Germany	$800/kW	$750/kW	$8/year	15 Years	0
Reverse Osmosis	Gunt RO CE530 (1.1kW,42L/hr), Germany	$4,500	$900	$900	5 Years	0.149
Water Storage	Various, 2kL-20kL	$730 - $2,852	$730 - $2,852	$0.05/kL	20 Years	0.149

Table 5.1 - Stand-alone hybridised energy system components. Cost components and emissions shown have been integrated into the simulations.

Electrical sub-system: This is responsible for converting solar energy to supply both the electrical load demand and other energy system components. Short-term energy storage (lead-acid batteries) are used for meeting daily demands while long-term storage (hydrogen) helps supplement battery capacity when seasonal or daily solar energy fluctuations mean short-term storage is insufficient to supply loads. Lead-acid batteries are used in the present research because of their lower capital costs compared to alternative technologies such as nickel-cadmium and Li-Ion [56]. Figure 5.2 shows the normalised daily variation of power and water demand as well as solar irradiance over a year. Although the values plotted show daily totals, this is derived using 15 minute resolved data which itself is used in the simulations. In these simulations, both external power and water demand is also scaled (up/down) to help analyse the effects of scalability. Cumulative power demand is scaled such that averaged daily demand over an entire year is at three levels (1.5, 2.5 and 3.5 kWhr/day). Although the annual water required is kept fixed at 146kL/yr, the simulation also consider the impact of assuming a uniformly distributed equivalent daily rate (400 litres/day over 365 days) versus a time-varying water profile as depicted in Figure 5.2. Furthermore, to satisfy this external water demand, the required power is approximately 3 to 6 times that of the external electric load.

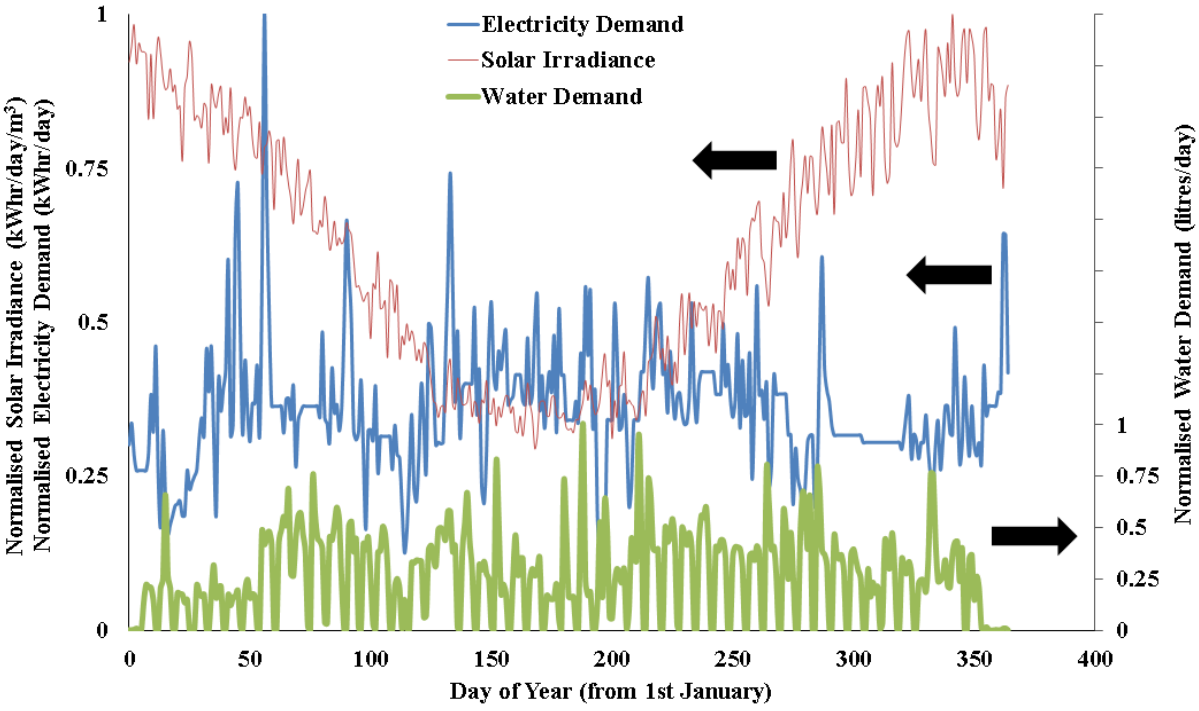

Figure 5.2 - Normalised daily variation of electricity demand, incident solar irradiance [45] and water demand over 365 days. The cumulative daily (normalised) profile of power and water, is scaled to yield 1.5, 2.5 or 3.5 kWhr/day over a year in addition to 400 litres/day, respectively.

Desalination sub-system: This incorporates RO units plus water storage tanks designated through their max storage capacity (H_2O_{max}) and is responsible for supplying potable (drinking) water as well as electrolysis, whereby water is deionised using non-power consuming static cartridges. The values for H_2O_{max} are either 2kL or 20kL in the simulations. Whilst many desalination techniques exist (multistage flash, vapour compression and electro dialysis [57]), RO is chosen because it is the most commonly integrated (non-thermal) desalination technique in renewable energy systems [15, 58-60]. Reverse Osmosis has lower energy consumption, low installation costs, minimal use of treatment chemicals and low maintenance compared to other desalination technologies [59-63]. To accurately model the AC powered Reverse Osmosis unit a series of tests were undertaken to resolve its power consumption characteristics for different levels of salinity, temperature and feed water pressure. Power characteristics were acquired with the help of an AC Power Data Logger (model: Clamp on Power HiTester 3169, make: Hioki-Japan). Figure 5.3 shows the experimental set-up used and some of the data acquired. Results showed that although RO performance is affected by feed water temperature, salinity and pump pressure, feed water

pressure has a more significant impact on the instantaneous power consumption and permeate (desalinated water) flow rate, compared to temperature. As feed water salinity and temperature decrease, both permeate flow rate and power increase. In the simulations undertaken, the supply of saline (sea) water is considered unlimited (Total Dissolved Salt, TDS = 2.69%), RO is operated at a pressure of 55bar with varying daily temperature taken into consideration. The simulations monitor the amount of desalinated water produced, stored and amounts withdrawn for consumption (drinking, electrolysis).

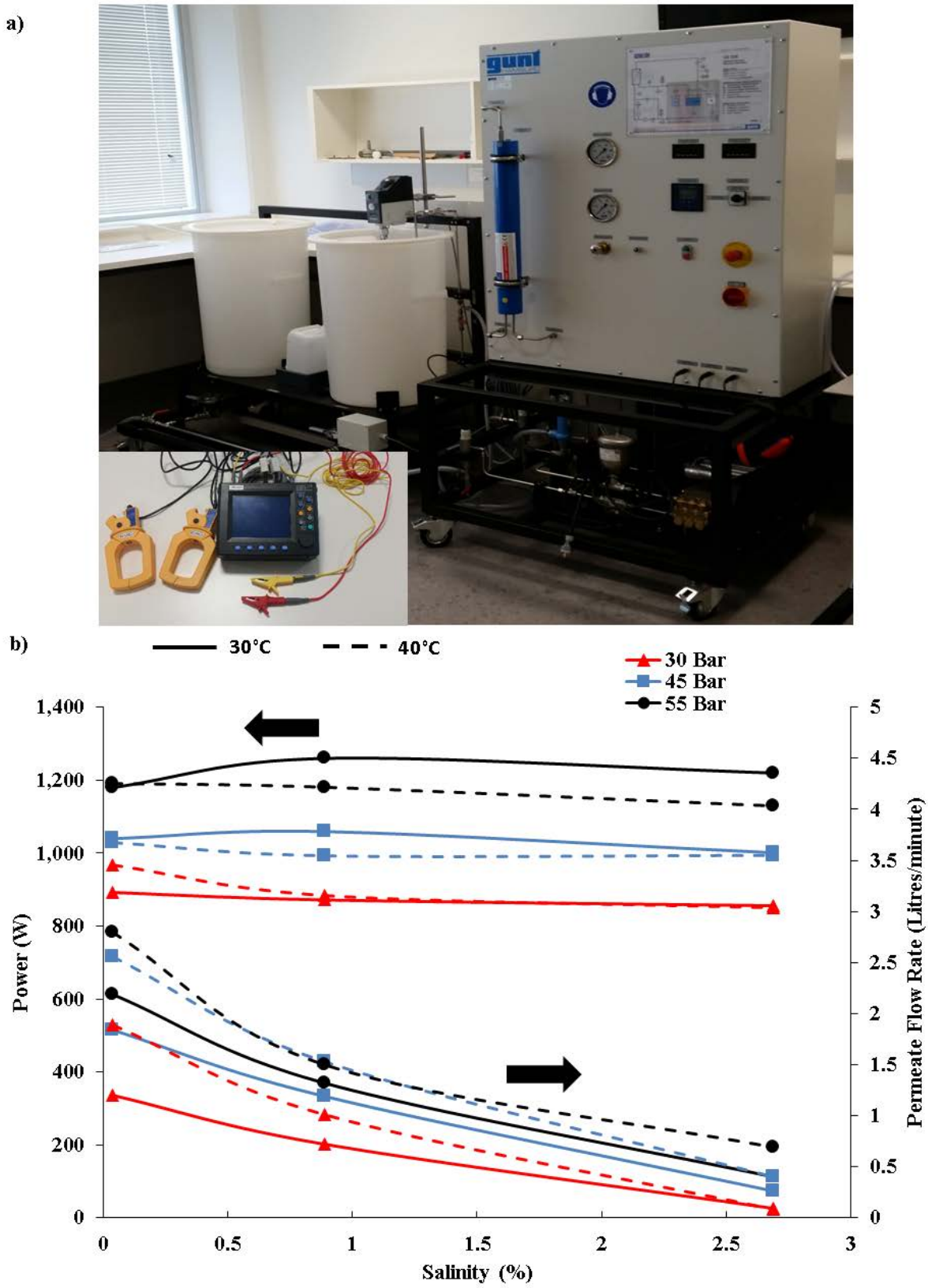

Figure 5.3 - a) Testing set-up of Reverse Osmosis unit (Gunt CE-350, 1.1kW, 42L/hr) and the power meter used to derive specific energy consumption (inset); b) device characteristics at varying feed water temperature and salinity as well as pumping pressure.

Hydrogen sub-system: This includes PEM electrolysers, PEM fuel cells and metal hydride storage (Table 5.1). Our earlier laboratory based testing showed the PEM electrolyser modelled has a start-up time of 5 minutes [7] which has also been integrated when simulating electrolyser operation. The PEM fuel cell supplies the external electric load during periods where solar irradiance is insufficient. Hydrogen storage is necessary to guarantee sufficient reserves of hydrogen fuel for use if solar irradiance is insufficient and achieved via hydride canisters each having a peak storage pressure of 10bar (to match the PEM electrolysers' output pressure). Further details on the operational characteristics of these devices is reported elsewhere [7, 32, 49].

Sizing methods: Two sizing techniques are used in this study so as to provide a comparison between adaptive techniques (Particle Swarm Optimisation) and a (deterministic) rule-based software tool (HOMER). Both optimisation techniques consider the left most bracketed term in Equation 5.1 comprising of the number of PV panels (N_{PV}), number of PEM fuel cell modules (N_{FC}), number of RO units (N_{RO}), number of PEM electrolysers (N_{Elect}), number of metal hydride canisters (N_H), quantity of Lead-Acid batteries (N_B) and maximum water storage capacity ($H2O_{max}$) to achieve an optimal solution subject to the objective function(s):

$$X = fn\left[N_{PV}, N_{FC}, N_{RO}, N_{Elect}, N_H, N_B, H_2O_{max}\right], \left[T_{Elect}, C_{H2O\ (PV)}, C_{Bmin}, C_{H2O\ (batt)}, C_{MH}\right] \quad \textit{Equ. 5.1}$$

Device capacities have already been presented in Table 5.1. The HOMER solution seeks an optimised system configuration (number of component units) for a given (software pre-set) PMS. Alternatively, an intelligent method such as PSO optimises the PMS as well as the scale of system by adaptively converging on the best control set points which regulate the operation of each component. While electrical demand takes priority over water generation, these set points allow the system to change this priority when reserves of desalinated water reach a lower threshold. In this case, under low electrical demand and high renewable energy availability, excess energy is diverted to water production rather than charging batteries or hydrogen canisters.

Decision Variable	Lower Bound	Upper Bound
N_{PV}	1	15
N_{FC}	0	3
N_{RO}	1	3
N_{Elect}	0	5
N_{H}	0	10
N_{B}	0	20
$H2O_{max}$ (L)	2,000	20,000
T_{Elect} (minutes)	15	60
$C_{H2O\ (PV)}$ (% of max)	0	1
C_{Bmin} (% of max)	0	1
$C_{H2O\ (batt)}$ (% of max)	0	1
C_{MH} (% of max)	0	1

Table 5.2 - Upper and lower bounds of the decision variables used by HOMER and those used to guide the Particle Swarm Optimisation of the PMS.

The second bracketed term of Equation 5.1 gives the five control set points (decision variables) that only PSO is able to integrate and adapt to find an optimal solution. Between the two optimisation methods (HOMER and PSO), it is this aspect of the PMS optimisation which differs between them. The starting PMS (successively optimised by PSO) is depicted in Figure 5.4 whereas HOMER looks at the available dispatchable power sources and assumes their operation in a manner which produces the required power most cheaply. Although the comparative analyses in this chapter are derived for this (starting) PMS, the aim is to demonstrate the benefits/challenges of using PSO versus HOMER. As such, any other PMS should also be possible to implement. Table 5.2 presents the different parameters used by the PSO optimisation algorithm and HOMER. The (starting) "initial conditions" during the first iteration of PSO assume water, battery and hydrogen storage State-of-Charge are at 100%. The value of (T_{Elect}) sets the duration of continuous solar-PV power needed before the electrolyser is operated to ensure the device is not unnecessarily cycled, bearing in mind its transient characteristics [7]. Prolonging (T_{Elect}) means less hydrogen produced over any time-step. Any energy not used to generate desalinated water is diverted to power the PEM

electrolyser(s). To govern whether RO is operated by solar-PV or battery storage, two control set points are defined as $C_{H2O\ (PV)}$ and $C_{H2O\ (batt)}$, respectively. The use of ($C_{H2O\ (PV)}$) defines the min percentage (of maximum desalinated water storage capacity) to ensure both electrolysis and potable water needs can be met over any time-step. If the water reserve falls below this threshold, desalination of potable water takes priority over hydrogen generation but if more solar-PV energy exists (after RO) then hydrogen is produced. When water storage and hydrogen capacity are at their maximum, surplus energy is used to charge batteries. Once the battery State-of-Charge reaches SOC=100%, any power not utilised to operate RO units or PEM electrolysers is then dumped and deemed an excess. The (C_{Bmin}) defines the minimum battery discharge capacity whilst ($C_{H2O\ (batt)}$) stipulates the minimum threshold water tank level (litres) before battery power is used for water generation. Due to the detrimental effects associated with PEM fuel cell technology [64, 65], effective battery utilisation through the use control set-points in the PMS is crucial in maximising PEM fuel cell performance by reducing the number of start-stop cycles. Lastly, (C_{MH}) determines the minimum metal hydride storage charge below which electrolysis is reactivated to top-up canisters. This decreases the number of start-stop cycles for the PEM electrolyser whenever the hydrogen reserve falls below 100%. If hydrogen capacity is above the minimum threshold and insufficient surplus power exists to generate water, this surplus is used to charge batteries.

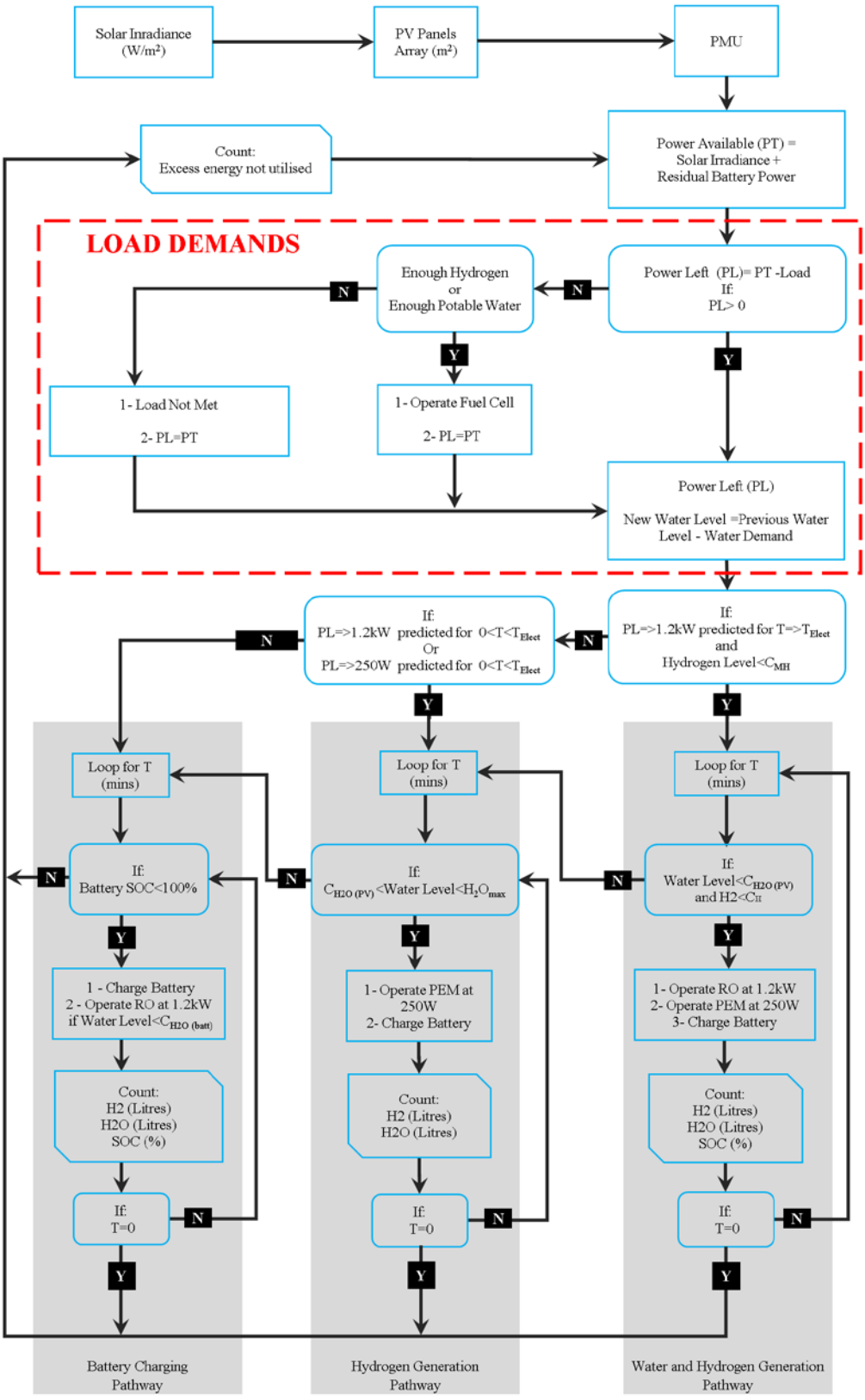

Figure 5.4 - Power Management Strategy (PMS) for the stand-alone hybrid energy system. The dashed box indicates the part of the PMS that enables the system to meet two load demands (electric and water).

Both HOMER and PSO consider a Load Following Control Method whereby battery charging is only allowed from renewables (e.g. solar) and not through other forms of power generation (e.g. fuel cell). HOMER deploys a PMS set by the software's in-built algorithms, whereby at each simulation time step (in this study,15 minutes) the software looks at all available dispatchable power sources and operates primary movers which meet the required amount of power and operating reserve most cheaply ($/kWhr). This "optimisation" is obviously subject to only a single objective function; cost of energy ($/kWhr). However, in a PSO optimised PMS, specific control set points within the PMS can be tuned such that device hardware transients and storage thresholds (battery, hydrogen and desalinated water) are also taken into consideration.

Objective Functions: The system includes two types of power demand: primary instantaneous loads and deferrable loads. A deferrable load can be met at any stage of the day, is not fixed to a specific time (hh:mm), and applied by HOMER when treating desalination. The optimisations done by PSO have been implemented to analyse the impact of two types of water demand: an instantaneous and dynamically changing demand (15 minute intervals) versus a single (static) value spread throughout the day. Both the deferrable and instantaneous water demand consider a cumulative requirement of 400 litres/day applied across 365 days, but with it fluctuating over every 15 minute time-step (dynamic) or fixed (static). An instantaneous water demand obviously needs to be met within the present time-step regardless of irradiance, whereas HOMERs' treatment of deferrable loads means it is met more conveniently over any period of the day when surplus renewables exist. The effects of these two approaches are analysed.

When deriving the optimal cost of energy ($/kWhr), the Net Present Cost (*NPC*) of the modelled energy system is the only objective function considered by HOMER. *NPC* takes into account the initial capital costs, component replacement costs as well as component operation and maintenance costs. Alternatively, multi-objective optimisation through PSO additionally considers minimising the associated CO_2 emissions over the system lifetime. The method of calculating the carbon emissions for the operation of any device (kg/kWhr) is based on Life Cycle Assessment (LCA). These CO_2 emissions are derived on a pro-rata basis using two inputs: the total CO_2 emissions (kg) over the entire lifetime of any single energy system component which are then proportioned per year (e.g., 120 kg for an electrolyser over 5 years which yields 24 kg/yr); and the maximum expected operational hours for any single

component until its replacement (e.g., 10950 kWhr for an electrolyser over 5 years). The resulting (kg/kWhr) is then used in conjunction with the actual usage (kWhr) for each device. Table 5.1 shows the values for these associated financial costs and emissions for each component in addition to their respective lifetimes. The operational objective function for total *NPC* is derived in Equation 5.3:

$$C_{ann,tot} = \sum_{i=component} C_i + R_i + O\&M_i - S_i \qquad \textit{Equ. 5.2}$$

$$NPC = \frac{C_{ann,tot} + C_{CO2}}{CRF(i_R, R_{proj})} \qquad \textit{Equ. 5.3}$$

$$CRF(i, R_{proj}) = \frac{i_R(1+i_R)^{R_{proj}}}{(1+i_R)^{R_{proj}}+1} \qquad \textit{Equ. 5.4}$$

The terms of Equation 5.2 - 5.4 denote the total annualised cost ($C_{ann,\,tot}$), the applicable interest rate (i_R), a project lifetime of 25 years (R_{proj}), the capacity recovery factor (*CRF*) and the annual cost of CO_2 emissions (C_{CO2}). The annualised cost is comprised of capital cost (C_i), replacement cost (R_i), salvage value (S_i), operational and maintenance cost ($O\&M_i$) for each component (i). The component (i) designates either a PV panel, Reverse Osmosis (RO) unit, PEM electrolyser, PEM fuel cell, metal hydride canister, converter or Lead-Acid battery. The gravimetric cost penalty for carbon emissions (C_{CO2}) associated with the systems is derived in Equation 5.5:

$$C_{CO2} = CP_{CO2}(E_i \times R_{i,CO2}) \qquad \textit{Equ. 5.5}$$

In this regard, (CP_{CO2}) is the monetary cost of CO_2 ($24.15/ton of CO_2), (E_i) is the annual system component power consumption/utilisation (kWhr) and ($R_{i,\,CO2}$) is the specific CO_2 emission rate (per kWhr) associated with each system component (Table 5.1). The specific CO_2 emissions rate is obtained using Life Cycle Assessment (LCA) which considers emissions over the component life including direct and indirect emissions. Direct emissions are associated with component construction, operation and decommissioning whereas indirect emissions are derived from manufacturing and transport of materials [61]. It is important that the emission rate (kg CO_2/kWhr installed) includes utilised energy and excess energy as this directly impacts the NPC and CO_2 emissions over the system lifetime [16]. Cost of energy (COE) is the average cost per kWh of useful electrical power (not including dumped surplus) produced by the system. To calculate the COE, the annualised cost of producing electricity

(the total annualised cost) is divided by the total electric energy produced and utilised to meet load. The COE is derived as follows:

$$COE = \frac{C_{ann,tot} + C_{CO2}}{E_{load,served} + W_{load,served}} \qquad \textit{Equ. 5.6}$$

Terms of Equation 5.6 denote cost of energy (*COE*) in ($/kWhr), total annualised system cost ($C_{ann,\,tot}$) in ($), electrical load served ($E_{load,\,served}$) in (kWhr/yr) and water load served ($W_{load,\,served}$) in (kWhr/yr).

Optimisation Constraints: In any plausible solution, a set of constraints (common to both PSO and HOMER) need to be satisfied:

i. **Unmet Load Constraint:** Over any time-step (15 minutes), the total power supplied by the stand-alone energy system must satisfy both load demands (direct electrical power and indirect power necessary for desalination) so as to achieve a certain supply reliability criterion. The reliability criteria affects component sizing/selection, energy cost ($/kWhr) and total emissions (CO_2 kg/year). Designing stand-alone systems for 100% power supply reliability can result in very high system costs because under such criteria even short duration peak demands must be met even if the likelihood for them to occur is rare. Therefore, a compromise is needed to allow high reliabilities for meeting power but at slightly lower constraints in relation to the occurrence of peaks (e.g. 98±0.25% reliability). In this manner, the majority of the load demand is met but with a smaller associated cost. This relation can be represented by Equation 5.7.

$$T_{LOL} \geq (1 - U_{Load})T_{annual} \qquad \textit{Equ. 5.7}$$

The terms of Equation 5.7 denote actual load served (T_{LOL}, kWhr/yr), total load demand to be served (T_{annual}, kWhr) and the maximum permissible unmet load (U_{Load}, %). In this study, optimisations consider a maximum U_{Load} of 2%, i.e. 98% of the load demand is met for any solution to satisfy the operational objective function(s). U_{Load} is defined as the difference between total load that must be satisfied (kWhr/yr) to achieve 100% (water and electricity) and actual load met (kWhr).

ii. **Design Variable Constraint:** To limit the solution space, any plausible solutions, must also fall within pre-designated limits to the variable (X) (Equation 5.1) as designated by Equation 5.8 and presented in Table 5.2:

$$X_{min} \leq X \leq X_{max} \qquad \textit{Equ. 5.8}$$

5.4 - Results and Discussion

Figure 5.5 shows the Net Present Cost ($) over the 25 year system lifetime for both optimisation techniques (HOMER and PSO). The *NPC* is derived for both daily static (Figure 5.5a) time-varying (Figure 5.5b) desalinated water profiles, both of which total 400 litres/day and are 15 minute resolved. Results indicate that PSO almost consistently achieves system sizing at much lower *NPC* compared to HOMER. This trend is maintained over different electrical loads (1.5, 2.5 and 3.5 kWhr/day/yr) and desalinated water storage capacity (which sets upper limits on the operational time for RO). Overall, the results show that *NPC* calculated using HOMER can sometimes be around double that derived from PSO which has the propensity to significantly affect the type/size of system configuration developed and techno-economic feasibility. This is also apparent in the Cost of Energy (*COE*) which is directly related to *NPC*, yielding greater cost ($/kWhr) with an increase in *NPC*. These cost savings based on PSO optimised systems however become even more apparent at greater water storage capacities or if varying water demand is assumed. The results also indicate that system sizing done assuming a constant (averaged) water demand, which has typically been followed in the published literature [12, 53], is likely to yield different outcomes compared to more realistic (dynamically) changing daily water requirements, even when the total (cumulative) annual demand remains the same (e.g. 400 litres/day over 365 days/yr). As such, the present research highlights that in relation to stand-alone desalination systems, modelling should incorporate the intricacies of daily demand if more accurate system sizing and techno-economic feasibility are desired. Another notable observation is the apparent immunity of PSO to whether static or dynamic water demand is used. This is attributed to the adaptive nature of PSO.

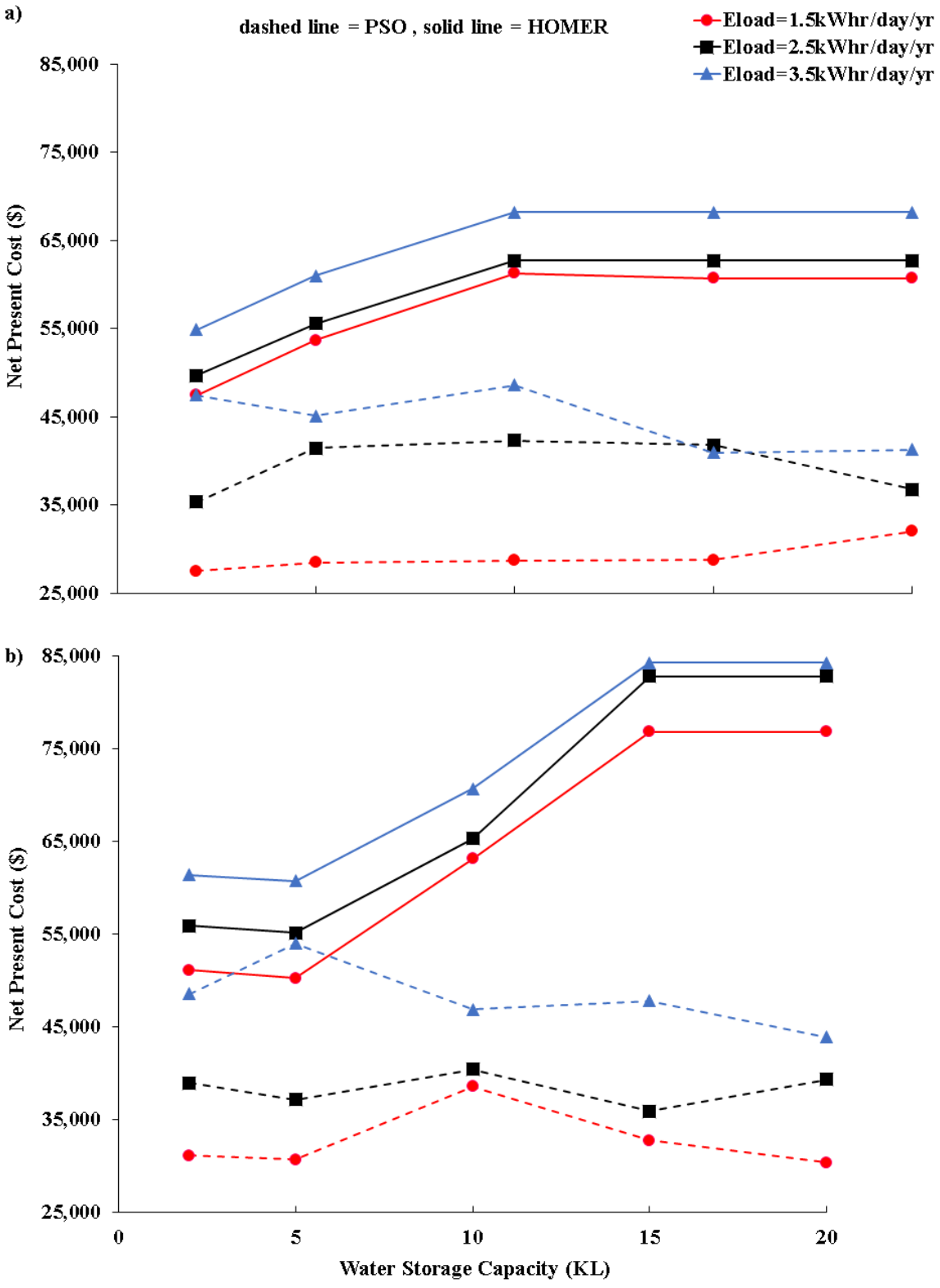

Figure 5.5 - Net Present Cost using two optimisation techniques (HOMER and PSO) at varying annually averaged electrical demand for; a) static; b) time-varying daily desalinated water demand.

Method	Water Load Profile	Electric Load (kWh/day)	RO Load (kWh/day)	Water Storage (L)	Optimised System Size (Average Components across range 2-20kL)					
					PV Panels	FC Units	Battery Units	Electrolyser Units	H2 Cannisters	RO Units
HOMER	Static	1.5	10	2 - 20	52	1	4	1	2	1
		2.5	10	2 - 20	52	1	7	1	2	1
		3.5	10	2 - 20	56	1	10	1	2	1
	Dynamic	1.5	10	2 - 20	52	1	15	1	2	1
		2.5	10	2 - 20	52	1	18	1	2	1
		3.5	10	2 - 20	52	1	20	1	2	1
PSO	Static	1.5	10	2 - 20	26	1	14	1	1	1
		2.5	10	2 - 20	35	1	19	1	2	1
		3.5	10	2 - 20	42	1	20	1	1	1
	Dynamic	1.5	10	2 - 20	29	1	17	1	1	1
		2.5	10	2 - 20	38	1	20	1	1	1
		3.5	10	2 - 20	48	1	19	1	1	1

Table 5.3 - The optimal number of system hardware components (HOMER and PSO) at varying annually averaged electrical demand for a static and time-varying desalinated water profiles.

In order to provide high reliability of meeting loads, energy storage is a critical component of stand-alone systems. In this regard, battery throughput (kWhr) is a performance measure and defined as the total amount of energy that cycles through the battery bank, whether in charging or discharge mode. Battery throughput can also be used to determine operational lifetime [68]. Figure 5.6 shows the annual battery throughput for systems optimised via HOMER and PSO, using static (Figure 5.6a) and time-varying (Figure 5.6b) desalinated water profiles. The data for varying electrical load demand and desalinated water storage capacity is also shown. Results show a higher battery throughput in a PSO optimised system across all water storage capacities and electric loads compared to HOMER. Whilst greater electric loads result in an expected increase battery throughput, the more surprising finding is that increased water storage capacity has no distinct effect on battery throughput when using PSO while a general decrease is seen with HOMER. With battery charging solely occurring from renewables (solar-PV), these battery throughput results also highlight PSO's ability to maintain comparable load reliability, but for a smaller solar-PV array size (kW). Table 5.3 provides the data to support these arguments whereby it is seen that for instances where PSO and HOMER have comparable battery numbers (e.g. dynamic load data for 1.5-3.5 kWhr/day), the number of PV panels selected by HOMER is significantly more at 52 panels against 29-48 via PSO. The significance of this variation becomes more apparent when based on data in Table 5.1, the capital cost of PV is around $7,000/kW which yields a unit cost of

around \$910/panel (at 0.13 kW/panel and panels of 0.8m^2). This demonstrates more effective energy management and sizing through PSO optimised systems. Furthermore, the results derived indicate that HOMER increases the solar-PV array size resulting in less battery throughput (with water storage capacity). Alternatively, for (12V, 55Ah) batteries the cost is \$113/battery. Hence, it is clearer why PSO optimised systems have lower *NPC*.

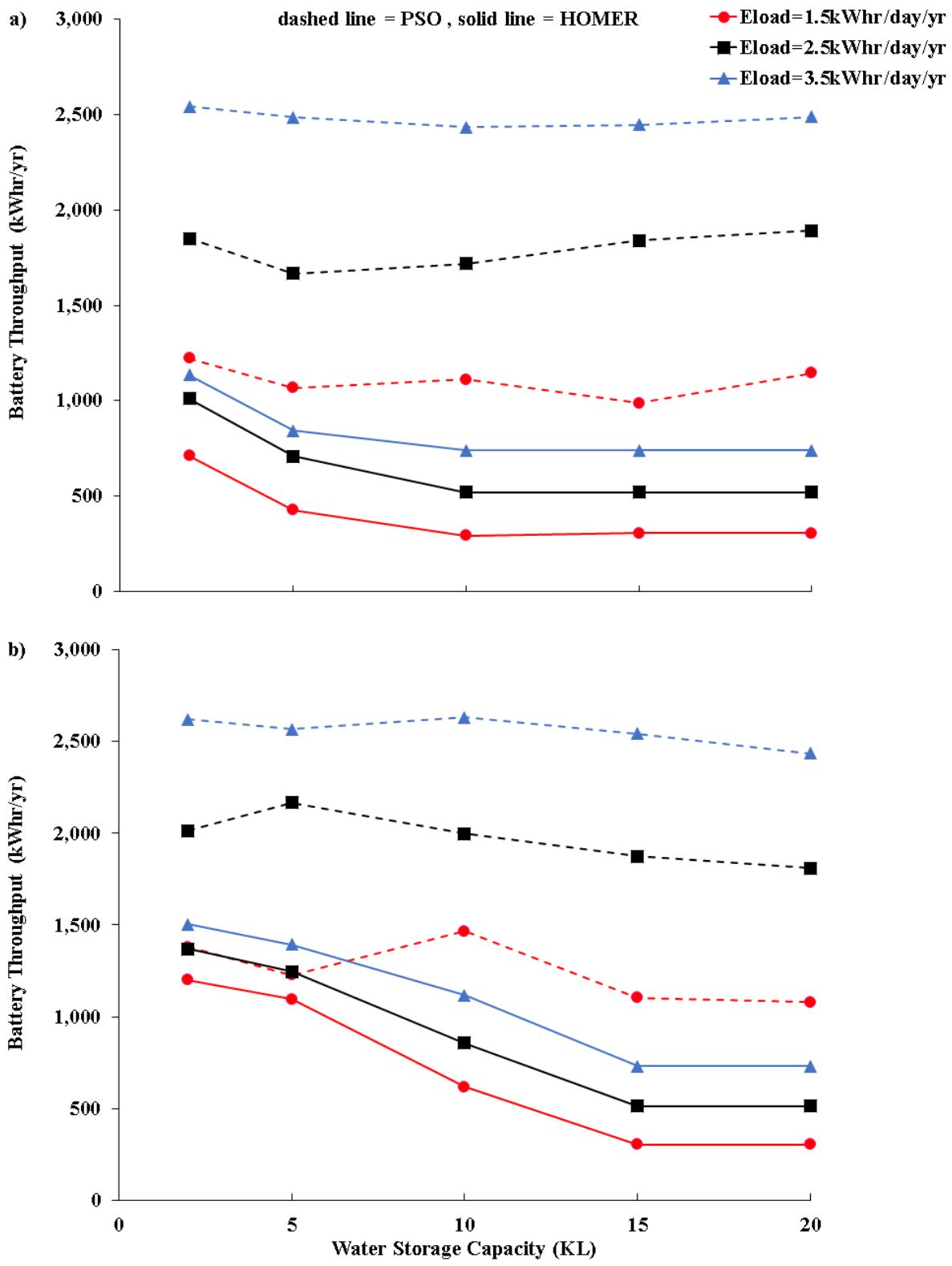

Figure 5.6 - Annual battery throughput using two optimisation techniques (HOMER and PSO) at varying annually averaged electrical demand for a) static; b) time-varying desalinated water profiles.

Detrimental effects are associated with cyclic operation of PEM fuel cells [64]. Attaining the same operational output, but over more start-stop cycles (i.e. a smaller duty factor), will indirectly affect the *NPC* in the long-term through more frequent replacements or service stoppages. The duty factor can be defined as kilowatt hours supplied (applicable for the PEM fuel cell) or litres of hydrogen generated (applicable for the PEM electrolyser) per total number of start-stop cycles of each device, respectively. Figures 5.7 and 5.8 show duty factors plotted for optimisations derived based on HOMER and PSO at varying electrical demand and water storage capacity (2kL and 20kL). Whilst, the same level of change is not always reflected in HOMER, the PSO optimised system does appear to have a significantly different duty factor, but which also changes proportionally with electric load. For fuel cells, the results show that PSO optimisations can yield duty factors which are 34% (Figure 5.7b) to 61% (Figure 5.7a) lower compared to duty factors from HOMER (at 3.5kWhr/day). In this regard, it is worth noting that such differences may be a factor of the varied system architectures selected by HOMER and PSO (Table 5.3) as well as the power served by the fuel cell. As for electrolysers, the results appear slightly more varied with duty factor with PSO likely to exceed those of HOMER (at 3.5kWhr/day, Figure 5.8a), but are generally lower. These results therefore highlight that a consequential effect of using PSO is to change the duty factors but which improve with scale. Finally, it is worth noting that although the total usage of the PEM fuel cell appears fairly low (kWhr values depicted in Figure 5.7), this value is a function of the daily usage assumed (1.5-3.5kWhr/day/yr), electric load profiles and availability of renewables. With greater electric loads and lower renewables penetration, total PEM fuel cell usage (kWhr) is expected to increase.

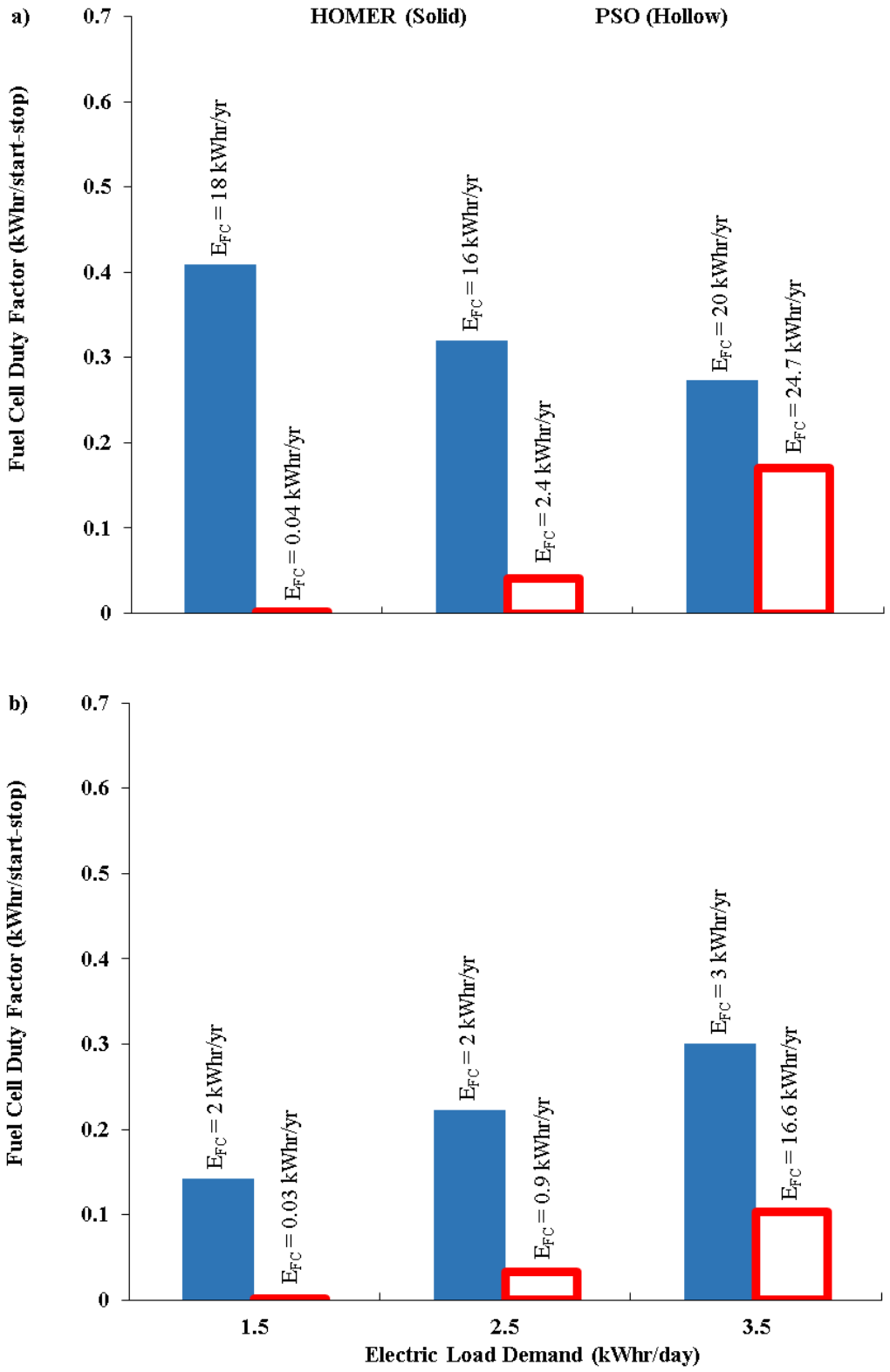

Figure 5.7 - Annual PEM fuel cell duty factor: a) 2kL water storage; b) 20kL water storage capacity. Results are at annually averaged electrical demand (1.5 to 3.5 kWhr/day) for a time-varying desalinated water profile using HOMER and PSO. Additionally, total annual power generated by the PEM fuel cell (kWhr/yr) are given for each case.

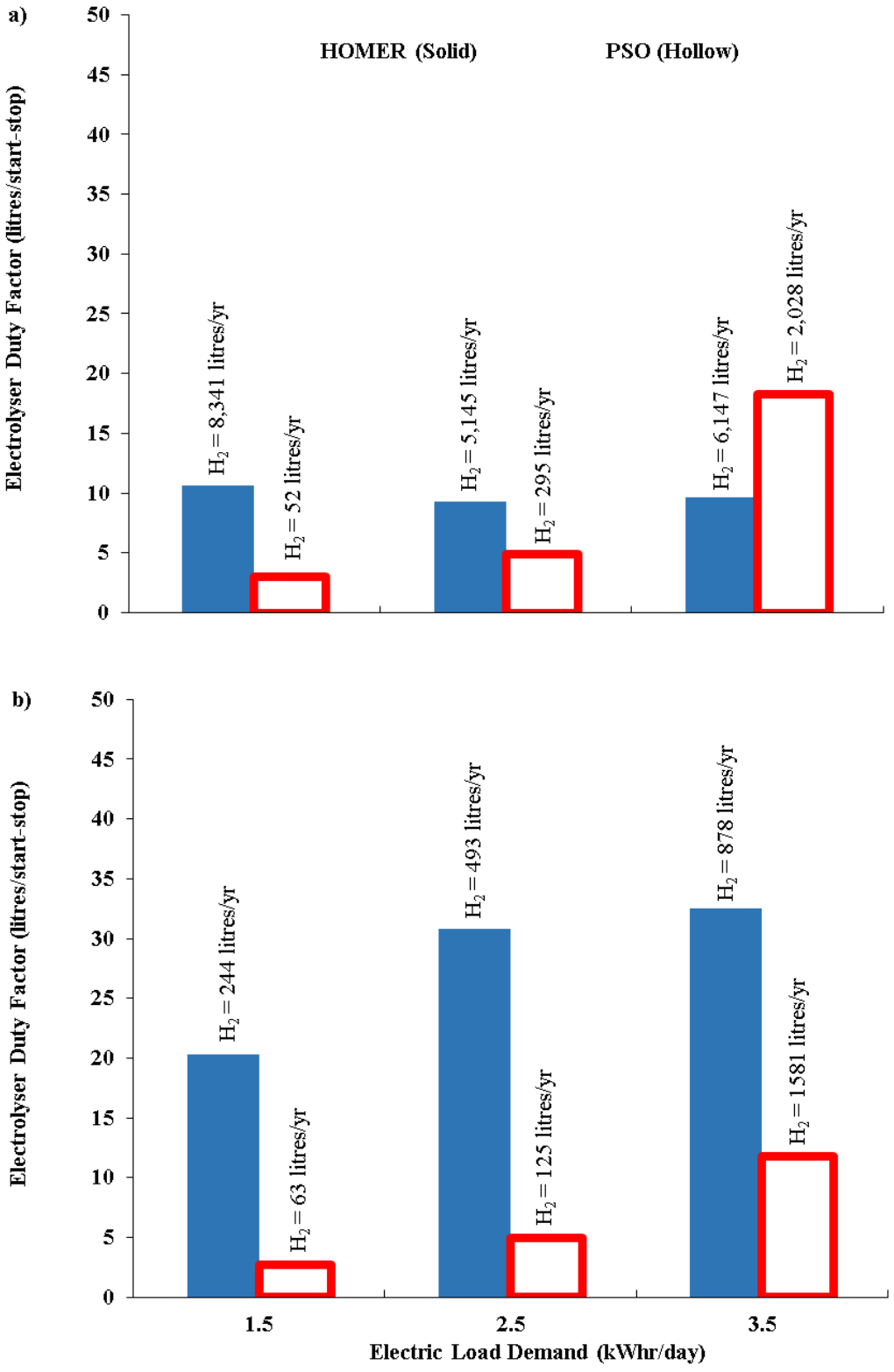

Figure 5.8 - Annual PEM electrolyser duty factor: a) 2kL water storage; b) 20kL water storage capacity. Results are at annually averaged electrical demand (1.5 to 3.5 kWhr/day) for a time-varying desalinated water profile using HOMER and PSO. Additionally, total annual hydrogen generated (litres/yr) are given for each case.

Table 5.4 shows CO_2 emissions (kg/yr) associated with HOMER and PSO optimised systems for time-varying water demand profiles at different electrical load demand and desalinated water storage capacities. Results highlight the anticipated greater amounts of CO_2 footprint with increased electric demand, since system components are involved with greater usage (kWhr/yr). In the PSO optimised system, the PMS assigns a lower $C_{H2O\ (PV)}$ threshold (% of maximum desalinated water storage capacity). The consequence is that the RO unit is in operation only when water reserves fall below this condition. However, the RO unit does not operate beyond the maximum desalinated water capacity (H_2O_{max}). With greater water storage capacity (H_2O_{max}), the value assigned by PSO to $C_{H2O\ (PV)}$ is adjusted such that RO does not have to operate as often. Although the lower and upper bounds for $C_{H2O\ (PV)}$ are given as 0 and 1, respectively (Table 5.2), for a water storage capacity of 20kL (electric load 1.5kWhr/day), the value of $C_{H2O\ (PV)}$ is 58 % which is equivalent to supplying 8,400 litres to the water load before RO is needed to operate (if initial water storage capacity is 100%). Alternatively, at 2kL (electric load 1.5kWhr/day), the value of $C_{H2O\ (PV)}$ is 14 % or supplying 1,720 litres to the water load before needing the RO to operate (if initial water storage capacity is 100%). The potential to supply more water volume (approximately 4.8 times) from the bigger tank before the RO is needed results in less CO_2 emissions associated with water desalination for a water storage capacity of 20kL compared to 2kL. Table 5.4 also identifies that RO and solar-PV contribute a higher portion of CO_2 emissions compared with any other system components. Whilst these arguments explain why the CO_2 emissions associated with maintaining adequate capacity in a 20kL tank appear generally lower than emissions for the 2kL desalinated water capacity, such an outcome may not always eventuate for other starting conditions. This particular outcome of the research may be an end result of the fact both tanks (2kL and 20kL) were assumed full at the first time instant in the simulations. Had both tanks been at partial capacity, more work (RO) might have been needed to bring the 20kL tank back to full capacity. Additionally, it appears that for the starting conditions considered, the adaptive PSO algorithm yielded $C_{H2O\ (PV)}$ values at 58% and 14% for the 20kL and 2kL desalinated water tanks, respectively. As such, for a specific single water volume draw-off from the tank (litres), it is expected the 2kL tank reaches its minimum allowed level ($C_{H2O\ (batt)}$) much earlier than the 20kL tank. In this case, the outcome would be the need to restart RO much earlier (or more frequently) with a 2kL tank. As such, this aspect of the comparison may require further research to see the effects if $C_{H2O\ (PV)}$ values selected had been the same.

Electric Load (kWhr/day)	Annualised CO_2 Emissions (kg/yr)	HOMER		PSO	
		Water Storage Capacity (kL)		Water Storage Capacity (kL)	
		2	20	2	20
1.5	PEM Fuel Cell	0.36	0.04	0.00	0.00
	PEM Electrolyser	3.06	0.09	0.01	0.02
	Lead-acid Batteries	30.04	7.59	30.12	20.82
	PV Panels	409.77	774.00	342.16	334.89
	RO unit	531.53	524.89	468.51	421.10
Total CO_2 Emissions (kg/yr)		975	1,307	841	777
2.5	PEM Fuel Cell	0.32	0.04	0.05	0.02
	PEM Electrolyser	1.88	0.18	0.04	0.02
	Lead-acid Batteries	34.33	12.85	49.03	46.26
	PV Panels	455.31	819.54	455.61	452.73
	RO unit	531.65	526.32	479.28	453.47
Total CO_2 Emissions (kg/yr)		1,023	1,359	984	953
3.5	PEM Fuel Cell	0.40	0.06	0.49	0.33
	PEM Electrolyser	2.26	0.32	0.23	0.18
	Lead-acid Batteries	37.63	18.28	66.14	66.32
	PV Panels	500.81	819.54	574.05	521.25
	RO unit	531.65	522.92	469.94	473.79
Total CO_2 Emissions (kg/yr)		1,073	1,361	1,111	1,062

Table 5.4 - The breakdown of CO_2 emissions for each hardware component using HOMER and PSO. Results are for a dynamic desalinated water profile.

Data in Table 5.3 has already indicated that PSO optimised systems over the range 2-20kL (dynamic water profiles) show on average fewer solar-PV panels due to greater reliance on battery throughput compared to HOMER (Figure 5.6). Whilst battery CO_2 emissions are less in HOMER optimised systems (Table 5.4), in the majority of the cases studied, the PSO optimised system appears to have lower CO_2 emissions associated with other system components. This results in PSO achieving mostly lower total system CO_2 emissions compared to HOMER across different electrical load and water storage capacities. However, these effects become relatively more pronounced as electrical load is decreased or for greater water storage capacity which is interesting. This highlights the adaptive nature of PSO by effectively sizing and optimising the PMS achieving lower solar-PV array resulting in much lower *NPC* and CO_2 emissions compared to HOMER. It also highlights the need for more research into the effects of optimising and sizing stand-alone energy systems when desalination via RO is integrated.

5.5 - Conclusions

PSO and HOMER have been compared when simultaneously sizing and optimising the control set-points in the PMS of a stand-alone hybrid energy system. Whilst the HOMER optimisations have used only *NPC*, the custom developed PSO model uses multi-objectives which include both Net Present Cost and CO_2 emissions. Simulations and the implementation of the PSO algorithm is done at fifteen minute resolution for an assumed system lifetime of 25 years. The research conducted compares optimisations with PSO to a system developed to meet an equivalent load in HOMER over different scales of electrical load demand and desalinated water storage capacity (static water profiles compared to time-varying for equal annual totals). Whilst few works have undertaken comparisons between intelligent techniques (such as PSO) and commonly used software tools in stand-alone system optimisations (e.g. HOMER), the present work also applies both techniques to energy systems incorporating desalination.

Under the conditions and hardware characteristics tested, the main outcomes may be summarised as:

- Using PSO to optimise the sizing and the Power Management Strategy results in lower Net Present Cost compared to HOMER. These improvements (up to half at 3.5kWhr/day) in *NPC* appear more pronounced as the systems scale (water storage capacity, electrical load demand) is increased;
- In order to provide accurate system sizing and techno-economic analyses, modelling of stand-alone hybrid energy systems should incorporate intricacies in load demands (electric and water);
- A smaller solar-PV array is needed in PSO optimised systems through reliance on greater battery throughput which results in more effective energy management and sizing compared to HOMER;
- Using PSO improves the cost performance of stand-alone hybrid energy systems, particularly at the scale investigated in this chapter and generally appears to yield significant decreases in NPC and CO_2 emissions compared to HOMER.

While each of these outcomes impacts the cost effective design and operation of stand-alone hybrid energy systems, there is still more opportunity to further our understanding of the

factors affecting the optimisation of stand-alone (hybrid) energy systems that integrate on-site desalination. Factors to investigate include the integration of different energy storage technologies into these systems, using combinations of different prime movers (diesel generator sets and/or wind turbines) and testing the optimisation for sensitivity to different starting conditions for water capacity, metal hydride level or battery State-of-Charge.

5.6 - Chapter References

[1] Doukas H, Patlitzianas KD, Kagiannas AG, Psarras J. Renewable energy sources and rationale use of energy development in the countries of GCC: Myth or reality? Renewable Energy. 2006;31:755-70.

[2] Brka A, Al-Abdeli YM, Kothapalli G. Influence of neural network training parameters on short-term wind forecasting. International Journal of Sustainable Energy. 2014;10.1080/14786451.2013.873437:1-17.

[3] Bielmann M, Vogt UF, Zimmermann M, Zuttel A. Seasonal energy storage system based on hydrogen for self sufficient living. Journal of Power Sources. 2011;196:4054-60.

[4] Glavin ME, Hurley WG. Optimisation of a photovoltaic battery ultracapacitor hybrid energy storage system. Solar Energy. 2012;86:3009-20.

[5] Gray EM, Webb CJ, Andrews J, Shabani B, Tsai PJ, Chan SLI. Hydrogen storage for off-grid power supply. International Journal of Hydrogen Energy. 2011;36:654-63.

[6] Hadjipaschalis I, Poullikkas A, Efthimiou V. Overview of current and future energy storage technologies for electric power applications. Renewable and Sustainable Energy Reviews. 2009;13:1513-22.

[7] Clarke DP, Al-Abdeli YM, Kothapalli G. The impact of renewable energy intermittency on the operational characteristics of a stand-alone hydrogen generation system with on-site water production. International Journal of Hydrogen Energy. 2013;38:12253-65.

[8] Luna-Rubio R, Trejo-Perea M, Vargas-Vázquez D, Ríos-Moreno GJ. Optimal sizing of renewable hybrids energy systems: A review of methodologies. Solar Energy. 2012;86:1077-88.

[9] Rohani G, Nour M. Techno-economical analysis of stand-alone hybrid renewable power system for Ras Musherib in United Arab Emirates. Energy. 2014;64:828-41.

[10] Nelson DB, Nehrir MH, Wang C. Unit sizing and cost analysis of stand-alone hybrid wind/PV/fuel cell power generation systems. Renewable Energy. 2006;31:1641-56.

[11] Nelson DB, Nehrir MH, Wang C. Unit sizing of stand-alone hybrid wind/PV/fuel cell power generation systems. Power Engineering Society General Meeting, 2005 IEEE 2005. p. 2116-22 Vol. 3.

[12] Al-Alawi A, Islam SM. An integrated remote area power & water supply system using renewable energy in the middle east. Australasian universities power engineering. Christchurch, New Zealand 2003.

[13] Pedrazzi S, Zini G, Tartarini P. Complete modeling and software implementation of a virtual solar hydrogen hybrid system. Energy Conversion and Management. 2010;51:122-9.

[14] Zhou W, Lou C, Li Z, Lu L, Yang H. Current status of research on optimum sizing of stand-alone hybrid solar–wind power generation systems. Applied Energy. 2010;87:380-9.

[15] Fahmy FH, Ahmed NM, Farghally HM. Optimization of renewable energy power system for small scale brackish reverse osmosis desalination unit and a tourism motel in Egypt. Smart Grid and Renewable Energy. 2012;3:43-50.

[16] Brka A, Al-Abdeli YM, Kothapalli G. The interplay between renewables penetration, costing and emissions in the sizing of stand-alone hydrogen systems. International Journal of Hydrogen Energy. 2015;40:125-35.

[17] Erdinc O, Uzunoglu M. Optimum design of hybrid renewable energy systems: Overview of different approaches. Renewable and Sustainable Energy Reviews. 2012;16:1412-25.

[18] Rajkumar RK, Ramachandaramurthy VK, Yong BL, Chia DB. Techno-economical optimization of hybrid pv/wind/battery system using Neuro-Fuzzy. Energy. 2011;36:5148-53.

[19] Phuangpornpitak N, Prommee W, Tia S, Phuangpornpitak W. A study of particle swarm technique for renewable energy power systems. 2010 Proceedings of the International Conference on Energy and Sustainable Development: Issues and Strategies (ESD) 2010. p. 1-6.

[20] Lee KY, Jong-Bae P. Application of particle swarm optimization to economic dispatch problem: Advantages and disadvantages. Power Systems Conference and Exposition, 2006 PSCE '06 2006 IEEE PES 2006. p. 188-92.

[21] Del Valle Y, Venayagamoorthy GK, Mohagheghi S, Hernandez JC, Harley RG. Particle swarm optimization: Basic concepts, variants and applications in power systems. IEEE Transactions on Evolutionary Computation. 2008;12:171-95.

[22] Kornelakis A. Multiobjective Particle Swarm Optimization for the optimal design of photovoltaic grid-connected systems. Solar Energy. 2010;84:2022-33.

[23] Rohani A, Mazlumi K, Kord H. Modeling of a hybrid power system for economic analysis and environmental impact in HOMER. Electrical Engineering (ICEE), 2010 18th Iranian Conference on 2010. p. 819-23.

[24] Lau KY, Tan CW, Yatim AHM. Photovoltaic systems for Malaysian islands: Effects of interest rates, diesel prices and load sizes. Energy. 2015;83:204-16.

[25] Basir Khan MR, Jidin R, Pasupuleti J, Shaaya SA. Optimal combination of solar, wind, micro-hydro and diesel systems based on actual seasonal load profiles for a resort island in the South China Sea. Energy. 2015;82:80-97.

[26] National Renewable Energy Laboratory (NREL). The hybrid optimisation model for electric renewables (HOMER). Available from, www.nrel.gov/homer; 2014. [accessed 2 Febuary 2014].

[27] Elbaset AA. Design, modelling and control strategy of PV/FC hybrid power system. Journal of Electrical Systems. 2011;7:270-86.

[28] Slama SB, Chaabene AB, Cherif A. Efficient design of a hybrid (PV-FC) water pumping system with serperate MPPT control algorithm. International Journal of Computer Science and Network Security. 2012;12:53-60.

[29] Farahat S, Yazdanpanah Jahromi MA, Barakati M. Modeling and sizing optimization of stand-alone hybrid renewable energy systems. International Conference on Mechanical, Nanotechnology and Cryogenics Engineering (ICMNC'2012). Kuala Lumpur, Malaysia 2012. p. 212-7.

[30] Ulleberg Ø. The importance of control strategies in PV–hydrogen systems. Solar Energy. 2004;76:323-9.

[31] Ipsakis D, Voutetakis S, Seferlis P, Stergiopoulos F, Elmasides C. Power management strategies for a stand-alone power system using renewable energy sources and hydrogen storage. International Journal of Hydrogen Energy. 2009;34:7081-95.

[32] Clarke DP, Al-Abdeli YM, Kothapalli G. The impact of using Particle Swarm Optimisation on the operational characteristics of a stand-alone hydrogen system with on-site water production. International Journal of Hydrogen Energy. 2014;39:15307-19.

[33] Rouhani A, Kord H, Mehrabi M. A comprehensive method for optimum sizing of hybrid energy systems using intelligence evolutionary algorithms. Indian Journal of Science and Technology. 2013;6:4702-12.

[34] Naveen Ram G, Devi Shree J, Kiruthiga A. Cost optimization of stand alone hybrid power generation system using PSO. International Journal of Advanced Reseach in Electrical, Electronics and Intrumentation Engineering. 2013;2:4048-57.

[35] Sinha AK, Bajpai P. Swarm intelligence based optimal sizing of a solar PV, fuel cell and battery hybrid system. 2012 International Conference on Power and Energy Systems. Hong Kong 2012. p. 467-73.

[36] Nowdeh SA, Nasrollahnezhad MB, Khanabdal S. Optimal sizing of a stand-alone PV/FC/wind hybrid system using PSO modified method. International Journal of Electronics, Computer and Communications Technologies. 2013;3:12-9.

[37] Rashidi H, Niazi S, Khorshidi J. Optimal sizing method of solar-hydrogen hybrid energy system for stand-alone application using fuzzy based particle swarm optimization algorithm. Australian Journal of Basic and Applied Sciences. 2012;6:249-56.

[38] Hakimi SM, Moghaddas-Tafreshi SM. Optimal sizing of a stand-alone hybrid power system via particle swarm optimization for Kahnouj area in south-east of Iran. Renewable Energy. 2009;34:1855-62.

[39] Ghazvini M, Abbaspour-Tehrani-Fard A, Fotuhi-Firuzabad M, Othman MM. Optimizing size and operation of hybrid energy systems. 2013 IEEE 7th International Power Engineering and Optimization Conference (PEOCO) Malaysia 2013. p. 489-94.

[40] Wu W, Christiana VI, Chen S-A, Hwang J-J. Design and techno-economic optimization of a stand-alone PV (photovoltaic)/FC (fuel cell)/battery hybrid power system connected to a wastewater-to-hydrogen processor. Energy. 2015.

[41] Mahor A, Prasad V, Rangnekar S. Economic dispatch using particle swarm optimization: A review. Renewable & Sustainable Energy Reviews. 2009;13:2134-41.

[42] Stoppato A, Cavazzini G, Ardizzon G, Rossetti A. A PSO (particle swarm optimization)-based model for the optimal management of a small PV(Photovoltaic)-pump hydro energy storage in a rural dry area. Energy. 2014;76:168-74.

[43] Perera ATD, Attalage RA, Perera KKCK, Dassanayake VPC. Designing standalone hybrid energy systems minimizing initial investment, life cycle cost and pollutant emission. Energy. 2013;54:220-30.

[44] Avril S, Arnaud G, Florentin A, Vinard M. Multi-objective optimization of batteries and hydrogen storage technologies for remote photovoltaic systems. Energy. 2010;35:5300-8.

[45] Lingfeng W, Singh C. Multicriteria design of hybrid power generation systems based on a modified particle swarm optimization algorithm. IEEE Transactions on Energy Conversion. 2009;24:163-72.

[46] Katsigiannis YA, Georgilakis PS, Karapidakis ES. Multiobjective genetic algorithm solution to the optimum economic and environmental performance problem of small autonomous hybrid power systems with renewables. Renewable Power Generation, IET. 2010;4:404-19.

[47] Bernal-Agustín JL, Dufo-López R, Rivas-Ascaso DM. Design of isolated hybrid systems minimizing costs and pollutant emissions. Renewable Energy. 2006;31:2227-44.

[48] Das P. Economic of distributed generation using particle swarm optimization: A case study. International Journal of Science, Engineering and Technology Research (IJSETR). 2012;1:191-9.

[49] Clarke DP, Al-Abdeli YM, Kothapalli G. The effects of including intricacies in the modelling of a small-scale solar-PV reverse osmosis desalination system. Desalination. 2013;311:127-36.

[50] Bureau of Meteorology (Australia). Solar exposure data for Geralton, Western Australia. Available from, http://reg.bom.gov.au/climate/reg/oneminsolar/index.shtml; 2012. [accessed 10 October,2012].

[51] Khan MJ, Iqbal MT. Pre-feasibility study of stand-alone hybrid energy systems for applications in Newfoundland. Renewable Energy. 2005;30:835-54.

[52] Bazyar R. Optimal design and energy management of stand-alone wind/PV/diesel/battery using bacterial foraging algorithm. 8th International Energy Conference. Iran 2011. p. 1-14.

[53] Banat F, Qiblawey H, Al-Nasser Q. Economic evaluation of a small RO unit powered by PV installed in the village of Hartha, Jordan. Desalination and Water Treatment. 2009;3:169-74.

[54] Marsden Jacob Associates. The cost-effectiveness of rainwater tanks in urban Australia. Available from, http://archive.nwc.gov.au/__data/assets/pdf_file/0014/10751/cost-effectiveness-rainwater-tanks-body-waterlines-0407.pdf; 2007. [accessed 22 June,2014].

[55] Beery M, Hortop A, Wozny G, Knops F, Repke J-U. Carbon footprint of seawater reverse osmosis desalination pre-treatment: Initial results from a new computational tool. Desalination and Water Treatment. 2011;31:164-71.

[56] Poullikkas A. A comparative overview of large-scale battery systems for electricity storage. Renewable and Sustainable Energy Reviews. 2013;27:778-88.

[57] Mahmoud M. Solar electric powered reverse osmosis water desalination system for the rural village, Al Maleh: design and simulation. International Journal of Sustainable Energy. 2003;23:51-62.

[58] Soric A, Cesaro R, Perez P, Guiol E, Moulin P. Eausmose project desalination by reverse osmosis and batteryless solar energy: design for a $1m^3$ per day delivery. Desalination. 2012;301:67-74.

[59] Avlonitis SA, Avlonitis DA, Panagiotidis T. Experimental study of the specific energy consumption for brackish water desalination by reverse osmosis. International Journal of Energy Research. 2012;36:36-45.

[60] Qiu TY, Davies PA. The scope to improve the efficiency of solar-powered reverse osmosis. Desalination and Water Treatment. 2011;35:14-32.

[61] Gude VG. Energy consumption and recovery in reverse osmosis. Desalination and Water Treatment. 2011;36:239-60.

[62] Gude VG, Nirmalakhandan N, Deng S. Renewable and sustainable approaches for desalination. Renewable and Sustainable Energy Reviews. 2010;14:2641-54.

[63] Helal AM, Al-Malek SA, Al-Katheeri ES. Economic feasibility of alternative designs of a PV-RO desalination unit for remote areas in the United Arab Emirates. Desalination. 2008;221:1-16.

[64] de Bruijn FA, Dam VAT, Janssen GJM. Review: durability and degradation issues of PEM fuel cell components. Fuel Cells. 2008;8:3-22.

[65] Wu J, Yuan XZ, Martin JJ, Wang H, Zhang J, Shen J, et al. A review of PEM fuel cell durability: degradation mechanisms and mitigation strategies. Journal of Power Sources. 2008;184:104-19.

[66] Clean Energy Regulator. Guide to Carbon Price Liability under the Clean Energy Act 2011. Available from, https://www.cleanenergyregulator.gov.au/Carbon-Pricing-Mechanism/Fact-sheets-FAQs-and guidelines/Guidelines/Documents/Guide%20to%20Carbon%20Price%20Liability.pdf; 2012. [accessed 4 April,2015].

[67] Nieuwlaar E. Life cycle assessment and energy systems. In: Cleveland CJ, editor. Encyclopedia of Energy. New York: Elsevier; 2004. p. 647-54. Available from, http://www.sciencedirect.com/science/article/pii/B012176480X002333

[68] Wenzl H, Baring-Gould I, Kaiser R, Liaw BY, Lundsager P, Manwell J, et al. Life prediction of batteries for selecting the technically most suitable and cost effective battery. Journal of Power Sources. 2005;144:373-84.

Chapter 6. General Discussion

For many small off-grid communities in Australia, access to potable water is limited as is the availability of electricity from renewable energy sources. Solar or wind provide an opportunity to utilise small-scale renewably powered energy systems to help supply power and to operate desalination systems. However, many factors in stand-alone energy systems directly impact upon operational characteristics that affect performance as well as the ability to meet load demands, including renewables and load (electricity, water) prediction, system optimisation and energy system component selection. For this reason, the thesis addressed 4 key research questions pertaining to the factors influencing stand-alone renewable energy system performance.

Research Question 1 (RQ 1): *How is the overall performance of solar-PV energy systems affected when accounting for dynamic device transients?*

The first step in this research was to establish time-resolved characteristics for system components, with Reverse Osmosis and the PEM electrolyser being major challenges. With water being a critical aspect of the system, as it contributes to drinking requirements and water for electrolysis, characteristics for time-varying versus nominal power profiles are compared for a renewably powered Reverse Osmosis (RO) unit. From the analysis in Chapter 2, simulations identified that using a (dynamic) RO power profile significantly decreases annual total desalinated water yield by approximately 76% for a $1m^2$ solar-PV array compared to nominal I-V characteristics. These effects became less pronounced for solar-PV/RO systems with higher PV conversion capacity (e.g., per metre square of panels) as the decrease in total desalinated water yield is only about 4%. With the dynamic RO unit as the only source of water, this deficiency in total desalinated water output, negatively impacted upon system performance in terms of both meeting water demand and hydrogen generation.

Combined with RO device characteristics, the start-up transient of the PEM electrolyser must be accounted for in system models and simulations. Chapter 3 experimentally derived the start-up transient of the PEM electrolyser to be approximately 275 seconds before useful hydrogen is generated. For a stand-alone renewable power system utilising hydrogen as an energy source, the transient puts a constraint on the ability to utilise the electrolyser every time it is started and the amounts of hydrogen that can be produced. As such, a Power Management Strategy (PMS) was needed to ensure that only when available power levels

were sufficient to maintain the PEM electrolyser for greater than the start-up transient, will the device be activated. Failure to stipulate the activation time of the PEM electrolyser results in unnecessarily cycling the device thus causing energy expenditure without hydrogen generation where the system would be better served by charging batteries or powering the RO unit. Overall, time-resolved power characteristics of system components, particularly Reverse Osmosis (RO) units and PEM electrolysers, are important and should be incorporated when analysing system performance rather than merely using power derived from nominal (time-averaged) I-V specifications. This provided accurate system simulations based on real conditions thus allowing correct sizing of stand-alone systems to successfully satisfy load demands.

Research Question 2 (RQ 2): *Can the incorporation of (intelligent/adaptive) predictive software tools significantly improve the performance of these energy systems, compared to non-predictive (simplistic) energy balancing techniques?*

Within stand-alone solar-PV energy systems, the prediction of solar irradiance was crucial for deploying effective resource management through Power Management Strategies aimed at satisfying system objectives. Due to the highly stochastic nature of solar irradiance, to estimate the power generated by the PV-array (the energy input into the entire system), the magnitudes and time-series for solar energy data should be based on irradiance measurements. However, because those deploying new stand-alone energy systems in remote locations might not always have access to measured solar irradiance, predictions are needed to correctly size these systems.

Chapter 3 analysed an intelligent method (Neural Network) for solar irradiance prediction by comparing it to a simplistic alternative (ASHRAE clear sky model). The comparison was analysed in terms of the prediction methods impact on the hydrogen energy systems operational characteristics. Whilst, the ASHRAE clear sky model has the merit of being a mathematical model with (some) empirically refined constants used to predict solar irradiance, it has the distinct disadvantage of not being able to predict the generally stochastic nature of solar irradiance. Whereas Neural Network (NN) requires very large amounts of (historical) training data to successfully predict the fluctuations (minute resolved) in solar irradiance. It was found that, through the use of particular historical meteorological data (i.e. rainfall), predictions can become more accurate. However, the choice of meteorological data

to be used is important as rainfall increases accuracy of prediction in winter but has no effect in summer (where rainfall is limited), for non-tropical parts of Western Australia.

The use of intelligent predictive techniques to account for the power needed to run a hydrogen generation system results in more subtle inaccuracies in relation to some characteristics such as electrolyser operational time compared to simplistic alternatives. However, the impact becomes more pronounced on device-level operational characteristics for the PEM electrolyser. Based on a system using measured solar irradiance, a Neural Network allows for a higher prediction accuracy of the number of start/stops and the duty factor of a PEM electrolyser compared to ASHRAE. The ASHRAE model's inability to accurately follow the stochastic nature of the solar irradiance results in a higher duty factor while having fewer start-stops compared to Neural Network. While ASHRAE affects system performance positively, when benchmarked against a system using measured solar irradiance, Neural Network was superior in predicting system performance. The solar irradiance prediction techniques also have varying influence depending on season. The ability to predict accurate levels of solar irradiance becomes important in winter (where irradiance were both low and fluctuating) and less in summer (where irradiance were both higher and more stable). This indicates when establishing techno-economic analysis targeted at stand-alone hydrogen generation systems, intelligent predictive techniques such as Neural Network should be used.

Research Question 3 (RQ 3): *Can the use of (intelligent/adaptive) optimisation software tools improve system performance when meeting single and multi-objective functions compared to a more widely adopted technique?*

To ascertain the impact that intelligent optimisation has on system performance, it is compared to rule-based alternatives for various system objectives. Based on factors influencing system performance such as device transients, scalability and prediction of available solar irradiance, the implementation of optimisation techniques is essential for providing effective sizing and operation of hybridised energy systems. For the purpose of implementing intelligent optimisation techniques into stand-alone solar-PV energy systems, Particle Swarm Optimisation (PSO) was selected as it can be easily implemented into system simulations with fewer tuneable parameters. However, it was found that acceleration parameters associated with PSO need to be determined for each scenario so that results obtained are consistently optimised. Chapter 4 provides an analysis pertaining to multiple single-objective functions which include optimising a system's Power Management Strategy

to maximise device duty factors and hydrogen yield as well as reliably meeting the external electric load.

In regard to hydrogen generation, the research undertaken indicates that using PSO, to optimise the control set-points in the PMS, allows the system to generate more hydrogen compared to a rule-based optimised Power Management Strategy. Increases of up to 7% in hydrogen yield and a 12% increase in the PEM electrolyser duty factor are achieved with PSO compared to simplistic techniques. Using intelligent techniques allows the optimised Power Management Strategy to deliver more hydrogen for fewer electrolyser start-stop cycles. For the scale of system investigated in Chapter 4, using PSO to optimise a PMS has a greater impact on PEM electrolyser duty factor (up to 80% for a lower quantity target of hydrogen) when meeting a specified seasonal hydrogen generation target.

Furthermore, in order to meet an electric load demand, solar-PV systems must have an additional source of energy to supply demand in periods of insufficient solar irradiance. With this in mind, the incorporation of some battery and hydrogen storage allows for greater renewable energy penetration and thus longer periods in which a PEM electrolyser can operate to generate more hydrogen for PEM fuel cell use. With higher hydrogen storage capacity, the PEM fuel cell was able to run for longer periods even when there was insufficient solar energy to replenish hydrogen reserves. The improvements in the system's ability to meet an external electric load demand, when using PSO, mean the total time over which the system does not meet the seasonal load was more than halved from 15.8% to 6.8% (Chapter 4). While a load demand is generally considered to be a power profile, communities at remote locations often also need desalinated water for consumption, hence multi-objective functions are necessary.

Chapter 5 further extended the analysis of using PSO through simultaneously optimising size and the Power Management Strategy. Optimisations are based on techno-economic and environmental objective functions while meeting external electric and water demand profiles. PSO outputs are then compared to those for a well-known optimisation program (HOMER). Additionally, the type of water demand (static vs time-varying) is analysed to ascertain the impact on system performance. Results showed that PSO almost consistently achieves lower system sizing at much lower Net Present Cost (NPC) compared to HOMER over different electrical loads (1.5, 2.5 and 3.5 kWhr/day/yr) and desalinated water storage capacities. These positive improvements in NPC show the superiority of using intelligent optimisation

techniques compared to simplistic alternatives. The disadvantage occurred in an increase of 13% in CO_2 emissions using PSO, even though a 50% decrease in NPC is evident compared to HOMER. Also, having a time-varying water demand profile negatively affects system performance, resulting in increases in NPC, CO_2 emissions and PEM device operational characteristics compared to a static profile. However, PSO was less susceptible to type of water demand probably because of its adaptive nature. This highlights the adaptive nature of PSO by achieving a much lower NPC compared to HOMER but a balance, between the economic and environmental aspects of sizing stand-alone hybrid energy systems, was necessary when implementing multi-objective functions.

Research Question 4 (RQ 4): *How does scalability affect energy systems incorporating desalination, solar-PV and hydrogen fuel cells/storage?*

In the context of this thesis, the effect of scalability analyses on, the impact of increasing energy storage (e.g. batteries and water storage capacity), size of the solar-PV array as well as scale of external load demands (electric and water) on system performance is very important. The role of desalinated water storage becomes essential with stand-alone solar-PV energy systems which have to generate water on-site. Chapter 2 showed that increasing the solar-PV size positively impacts upon system performance by allowing greater operational periods for the RO unit as well as maintaining battery State-of-Charge at 100% for longer. Storing excess renewable energy (via batteries) has a greater impact on the performance of smaller systems compared to larger ones by allowing devices such as RO and PEM electrolysers to run for extended periods thus resulting in higher duty factors, as evident in Chapters 2 to 4. Through having greater battery and water storage capacity, better renewable energy penetration is attained resulting in an increase in reliability, water and hydrogen yield. Any excess energy beyond hydrogen generation or charging of batteries is diverted to water production which acts as a useful dump load for supplying the PEM electrolyser and external water demands.

The work presented in Chapter 5 enabled the analysis of increasing load demand and its effect on system performance in relation to Net Present Cost (NPC) and carbon emissions at varying water storage capacities. Simulations revealed, negative improvements in carbon emissions and NPC occur with greater system size when greater electric load was increased. For a PSO optimised system, NPC and CO_2 emissions rise by approximately 77% and 57%, respectively as electric load is increased, for a water storage capacity of 2kL. However, for greater water storage capacity (20kL) the NPC and CO_2 emissions only increase by 45% and

59%, respectively. Having larger water storage capacity allows energy otherwise utilised for RO to be diverted to hydrogen generation and charging of batteries thus maximising the system's ability to meet load demands. Increasing energy storage capacity (i.e. batteries and indirectly water storage) has a positive influence on the system's performance. However, optimisation is necessary so that external load demands are met at minimum cost.

Overall, this research has analysed many factors influencing stand-alone solar-PV energy systems for both power generation and the provision of desalinated water the incorporation of a Reverse Osmosis unit. Such systems have received little attention within current literature, with the provision of suitable water for drinking and hydrogen generation through water electrolysis, these systems are becoming more important in remote communities. The results of this research show that modelling of stand-alone solar-PV energy systems should account for the intricacies of daily demand profiles as well as dynamic device characteristics if more accurate system sizing and techno-economic feasibility are desired. While the system investigated was limited to only solar-PV providing the input power, the methodologies developed in this thesis can be easily adapted to systems incorporating multiple renewable energy sources (i.e. solar and wind).

Chapter 7. Conclusion and Future work

7.1 - Findings

This thesis has largely focused on the methodologies that affect stand-alone solar-PV systems incorporating desalination. Through a combination of mathematical models and experiments, a full system was developed in MATLAB/Simulink to address the research questions derived in Chapter 1. The solar radiation data incorporated in this work are specific to a non-tropical Western Australian location and the assumed cost factors of system components are consistent with present literature values. The developed models are used to evaluate factors influencing stand-alone solar-PV systems including the incorporation of dynamic device transients, minute resolved system simulations as well as applying predictive and optimisation techniques for various system objectives.

This thesis evaluates three solar-PV systems through simulated models with each succeeding system being an extension of the previous architecture. These are:

1. A stand-alone solar-PV desalination system (Figure 1.3a), responsible for providing potable water via renewables through the use of a Reverse Osmosis device;
2. Through the addition of a PEM electrolyser to the architecture of Figure 1.3a, a stand-alone solar hydrogen generation subsystem is formed responsible for producing hydrogen and potable water from on-site desalination; and
3. Finally, integrating a fuel cell into the architecture of 1.3b, a full stand-alone solar-PV hydrogen energy system is created (Figure 1.3c) responsible for generating power and desalinated water.

For many small off-grid communities in Australia, access to potable water are limited as are the availability of power generated from renewable energy sources. For this reason, the stand-alone solar-PV energy system explored in this thesis are beneficial for remote communities as it is able to generate power as well as potable water making these communities more self-reliant. Solar photovoltaics are a suitable choice for many remote areas in Australia as solar irradiance is plentiful. As a result, the current dependence on diesel power generation in such communities would be alleviated reducing carbon emissions and thus having a more positive environmental impact. However, in a stand-alone solar-PV hydrogen energy system incorporating Reverse Osmosis, having not enough potable water means the amount of

hydrogen that can be generated as well as the time in which the fuel cell can be operated is reduced. This shows maintaining the subsystems as shown in Figure 1.3 (i.e. water production, hydrogen and power generation) is critical for system operation as each subsystem makes use of the other.

As the stand-alone energy system is dependent on the devices deployed, establishing dynamic (time-resolved) characteristics for the system components are important with battery, Reverse Osmosis and the PEM electrolyser being the major challenge. With water being a critical aspect of the system, characteristics for time-varying versus nominal power profile are compared for a renewably powered Reverse Osmosis (RO) unit. According to the research conducted, using nominal I-V curves results in an overestimation of desalinated water production with minute resolved simulations able to capture dynamic behaviour better than hourly resolution. Furthermore, seasonal variations in water generation occurs with less water produced in winter (lower solar irradiance) compared to summer and this highlights the importance of energy storage.

Secondly, with the inclusion of a PEM electrolyser having a start-up transient, the effect of solar energy prediction and battery capacity on the operational characteristics of a solar-PV powered hydrogen generation system was explored. The simulations conducted utilised two specific methods of irradiance prediction (ASHRAE clear sky model and Neural Networks) which were benchmarked against measured irradiance data for Geraldton (Western Australia). The research identified that using a simplistic solar prediction technique (ASHRAE clear sky) produces larger relative errors in energy availability than Neural Networks when compared to measured irradiance data. Additionally, Neural Networks were able to predict fluctuations better than ASHRAE model across two seasons (Australian summer and winter). Using a Neural Network, particularly to predict solar irradiance input, yielded more accurate operational characteristics and hydrogen yield compared to ASHRAE.

The thesis also explored the validity of applying Particle Swarm Optimisation (PSO) to size analyses and optimisation of stand-alone solar-PV hydrogen energy systems. Allowing PSO to adjust the system's Power Management Strategy (PMS) results in improvements in system operational characteristics compared to using simplistic rule-based design methods. Additionally, PSO is compared to HOMER for the simultaneous optimisation of system size and PMS. Both Total Net Present Cost (NPC) and carbon emissions were considered whilst meeting two external loads (electricity and desalinated water generation). Using PSO with

stand-alone hybrid energy systems achieved systems having a significantly lower NPC compared to HOMER but at a cost of a small increase in associated CO_2 emissions, with the margin of improvement more pronounced when water storage capacity and electrical load are increased. Additionally, having a time-varying water profile negatively affects system performance by increasing NPC and CO_2 emissions compared to a static profile.

Lastly, the research on the effect of scalability focussed on the impact, of increasing energy storage (e.g. batteries and water storage capacity), size of the solar-PV array and the type and scale of external load demand (electric and water), on system performance. Increasing the solar-PV size positively impacts upon system performance by allowing greater periods when an electrolyser and RO unit can operate and maintaining battery State-of-Charge at 100% for longer. Storing excess renewable energy (via batteries) has greater impact on the performance of smaller systems compared to larger ones with increasing electric load demand. Through having greater battery or water storage capacity, better renewable energy penetration was attained resulting in increased reliability, water and hydrogen yield. Any excess energy, beyond hydrogen generation or charging of batteries, is diverted to water production thus acting as a useful dump load for supplying the PEM electrolyser and external water demands. While increasing the scale of components has a positive impact on system operational characteristics, it has a detrimental effect on the techno-economic viability when sizing stand-alone energy systems.

7.2 - Future Work

While each of the aspects analysed in this thesis has contributed to knowledge aiding the design of accurate, reliable, cost effective stand-alone solar-PV energy systems, there is still more room for further development of this research to further improve such systems. For example:

- With device-level characteristics playing a major role in the performance of stand-alone energy systems, future work should incorporate the dynamic transients of different types of devices. Based on a library of dynamic models of possible system components, a tool can be developed for sizing a stand-alone energy system that is most cost effective and suitable to the desired application.
- Within stand-alone renewable energy systems, energy storage remains a critical component for ensuring that high system reliability. Further work is warranted into

the integration of energy storage with particular focus on limiting amounts of excess energy whilst at low systems costs. Additionally, storage device characteristics are of importance which relates to start-up as well as charging and discharging characteristics. A potential storage mechanism, that could be further modelled, is the Superconducting Magnetic Energy Storage unit (SMES).

- A complete life cycle assessment to determine the most cost effective system configuration of stand-alone solar energy systems, incorporating reverse osmosis for the provision of energy and water. This would extend to comparing different types of configurations to achieve the same objective.
- Seasonal variation in load demands and renewable energy availability means systems must be correctly sized to ensure system reliability. The ability to predict solar irradiance and load demand (i.e. water and power) presents the opportunity to analyse an adaptive Power Management Strategy (PMS) compared to a static PMS.
- Lastly, the construction of a laboratory-scale, stand-alone solar-PV energy system would be of considerable interest, to validate simulation results for a variety of scenarios. This would offer a means of testing the integration of intelligent techniques into a pilot system and adaptive system control.

At the request of the author,

Appendix A and B are not included in this version of the thesis.

Appendix C - Error Analysis

In regards to this thesis, all experimental work there is a possibility of experimental error. Experimental measurements always have uncertainties that are referred to as errors. As a result, the value of any experimentally measured value will deviate from its true (nominal) value. It is of the utmost importance to be able to estimate how big the difference between these two values to determine the validity of such experiments.

Experimental errors can be classified either as Systematic Errors or Random Errors. Systematic errors are errors associated with measurement instruments or techniques that produce consistent errors, e.g. an improperly calibrated Total Dissolved Salts (TDS) meter. Table 8.1 shows the uncertainties in data acquisition devices used in this thesis. Errors in reading a measurement may also produce systematic errors. Avoiding these systematic errors depends on the skill of the observer to detect and prevent or correct them by being consistent.

Data Acquisition Unit	**Accuracy**
Hioki Power Data Logger	±2%
CompactRIO	±0.5%
Hydrogen Generator Monitor	±5%
CyberScan CON 10 Cond/TDS meter	±1%

Table 8.1 – Accuracies of experimental measurement equipment.

Random errors are from unknown or unpredictable events in during an experiment. Random errors are just as likely to produce a result that is too large as they are likely to produce one that is too low. These errors are sometimes beyond the control of the observer with likely causes being fluctuations in temperature, piston position of the Reverse Osmosis unit or estimates of measurement readings by the observer. To minimise the effect of random errors, multiple trails or measurements and averaging the results are taken so that the random fluctuations become statistically insignificant.

This thesis uses three methods of accounting for errors. These are:

1) **Average (Mean) Value**: The experimental measurements or system simulations in this thesis are repeated several times, and it is unlikely that identical results will be obtained for all trials. For a set of measurements the true value is most probably given by the average or mean value. The average or mean value <x> of a set of n measurements is

$$<x> = \frac{x_1 + x_2 + ... + x_n}{n} = \frac{1}{n}\sum_{i=1}^{n} x_i \qquad \text{Equ. C1}$$

As all experiments were conducted multiple times, the errors are reduced by taking the mean value.

2) **Difference:** The error is defined as the difference between your measured value and the "nominal" value.

$$\text{Error} = (\text{Measured Value}) - (\text{Accepted Value}) \qquad \text{Equ. C2}$$

This type of error analysis suited the comparisons of the number of start-stop cycles of PEM devices.

3) **Percentage Error:** The percent error (relative error) is of much greater significance than the actual difference between the observed value and the accepted value. The percent error of an experimental value is

$$\text{Percent error} = \left(\frac{\text{Error}}{\text{accepted value}}\right) \times 100\% \qquad \text{Equ. C3}$$

If the percent error is >0, the measurement is greater than the accepted value. If it is <0, then the measurement is less than the accepted value. This error analysis can be seen in Figure 3.6.

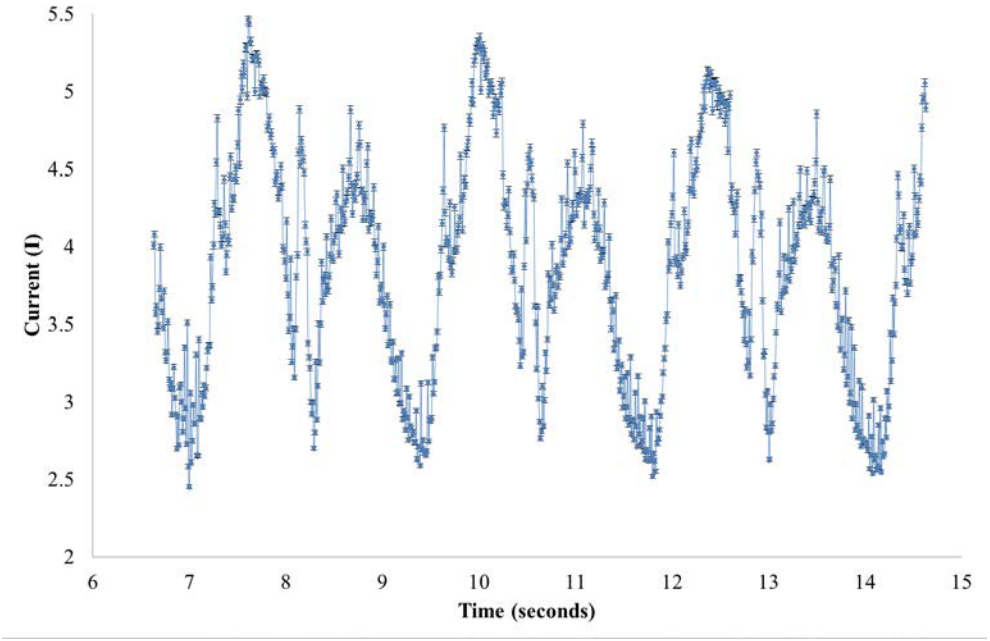

Figure 8.1 – Reverse Osmosis current profile. Sampled at 10ms.

For example, when reading real-time voltages and current to determine device transients to incorporate into a MATLAB/Simulink model, the digital values are continuously fluctuating in steady state. Based the error analyse using averaged values and the uncertainties of measurement devices, Figure 8.1 shows the Reverse Osmosis unit current profile of Chapter 2 with errors. Due to determining the dynamic transients of system devices, the data is sampled as low as possible to capture all fluctuations in the profile. As a result, applying error bars would make plots congested and not easily read so plots throughout thesis depict the average value of experiments.

Appendix D - System Modelling

The technical details for system components used for the modelling of a stand-alone solar hydrogen system in this thesis are given below. However, for full details, manuals and the MATLAB/Simulink system coding for the system covered in each chapter of this thesis, please refer to attached CD.

D-1 - Solar-PV modules

Parameter	Value
P_{MAX}	$130W_P$
T_{REF}(reference temperature)	25°C
T_{CELL}(normal operating cell temperature)	48.2°C
I_{SC}(short circuit current)	8.33A
I_R(reverse current feed)	15A
I_{MP}(current at max load)	7.85A
U_{OC}(open circuit voltage)	21.56V
U_{MP}(voltage at max load)	17.2V
μ_{Isc}(Temperature coefficient I_{SC})	$0.05\%K^{-1}$
μ_{Uoc}(Temperature coefficient U_{OC})	$-0.34\%K^{-1}$
μ_{pupp}(performance coefficient)	$-0.45\%K^{-1}$
Ŋ(efficiency)	13.61%
Efficiency	13.61%

Table 8.2 - Solar module technical specifications.

D-2 - Power Management Unit

Parameter	Value
Modes	3
Mode 1	Automatic without PC
Mode 2	Automatic with PC(user can monitor and change parameters)
Mode 3	HG30 (manual hydrogen generator mode)
Data Communication	Ethernet/Serial
Solar Battery Generator	MS300-S01
$N_{BatBank}$(supported battery bank)	2
I_{CHARGE}(max charging current)	30A
V_{OUT}(output voltages)	2x 12VDC/1x 230VAC
Programmable Logic Controller	Beckhoff BC9000
Measurements	3x 50A Shunts
I_{PV}(photovoltaic module current)	Varying
$I_{BatCHARGE}$(battery charge current)	Varying
L_{LOADS}(parasitic loads fuel cell)	Varying

Table 8.3 - Power Management Unit (PMU) technical specifications.

D-3 - Battery

Parameter	Value
Battery	2x Banner Standby Bull
V_{BAT}(battery voltage)	12VDC
C_{BAT}(battery capacity)	55Ah (@C=20hrs.)
Type	Lead Acid AGM(Absorbed Glass Mats)

Table 8.4 - Battery technical specifications.

D-4 - Reverse Osmosis Unit

Parameter	Value
I_{RO}(operating current)	4A/3A
V_{RO}(operating voltage)	12VDC/24VDC
Q_{FEED}(feed water flow rate)	56L/hr.
Q_W(rate of water production)	5.6L/hr.(@13.8VDC)
P_{BR}(pump pressure)	800 psi
Pump type	Rotary/Reciprocating

Table 8.5 - Katadyn Reverse Osmosis unit technical specifications.

Parameter	Value
I_{RO}(operating current)	5.2A
V_{RO}(operating voltage)	230V/50Hz
Q_{FEED}(feed water flow rate)	425L/hr.
Q_W(rate of water production)	108L/hr(maximum)
P_{BR}(pump pressure)	120 bar
Pump type	Piston

Table 8.6 - Gunt Reverse Osmosis unit technical specifications.

D-5 - Hydrogen Generator

Parameter	Value
Hydrogen input	Max 17 bar
Hydrogen out	0-17 bar
Solenoid valve control signal	12V
Pressure Relief Valve	25 bar
Stop valve	Manual
Type	Metal Hydride Storage
Storage capacity	Max 3x 760 SL
Discharge rate	3x 5.5 SL/min
Filling pressure	10-17 bar

Table 8.7 - PEM electrolyser and Metal Hydride storage technical specifications.

D-6 - Fuel Cell

Parameter	Value
Rated Output	1200W
Operating Voltage	22-50V
Rated Voltage	26V
Power consumption during start	60W
Hydrogen flow meter	±1.5% of final value

Table 8.8 - PEM Fuel Cell technical specifications.

Appendix E - Neural Networks

An Artificial Neural Network[23] (ANN) is a computer model that takes inspiration from the way biological systems, such as the brain, process information. It is composed of a large number of interconnected elements, called neurons, working to solve specific problems. However, in order for ANNs to solve problems they need a set of training data that it uses to learn relationships between inputs and outputs. An ANN must be trained and configured for a specific application, such as pattern recognition or data classification, through a learning process.

ANNs have many advantages over traditional (e.g. statistical analysis) methods of modelling. These advantages include but not limited to:

1. Adaptive: An ability to learn how to do tasks based on the data given for training.
2. Self-Organisation: An ANN can create its own organisation or representation of the information it receives during learning time.
3. Real Time Operation: ANN computations can be carried out in parallel.

While ANNs have numerous applications, in regard to this thesis an ANN was used for the prediction of solar irradiance. As solar irradiance like many environmental conditions (e.g. temperature, rainfall, wind speed etc.) are time-series, feedforward Neural Networks are the most widely used to forecast this data due to its straightforwardness as found through the literature review conducted in Chapter 3. However, while feedforward networks are worthwhile for static time-series data, inaccuracy occurs in more complex stochastic data such as solar irradiance. This complexity arises due to season, location, cloud cover etc. In this regard, recurrent networks are networks with one or more cycles that apply to time series data and that use outputs of network units at time t as input to other units at time t+1 are more

[23] Further Neural Network theory can be obtained from:

[1] White H. Artificial Neural Networks: Approximation and Learning Theory: Blackwell Publishers, Inc.; 1992.

[2] Reed RD, Marks RJ. Neural Smithing: Supervised Learning in Feedforward Artificial Neural Networks: MIT Press; 1998.

[3] Vidyasagar M. A Theory of Learning and Generalization: Springer-Verlag New York, Inc.; 2002.

suitable. However, the main disadvantage of such a network lies in their difficulty to train as large amounts of historical data must be used.

As meteorological datasets (i.e. solar irradiance, rainfall etc.) are season dependant, a NARX (Nonlinear autoregressive with external input) network, as shown in Figure 8-2, was utilised because it is able to predict one time series given past values of the same time series.

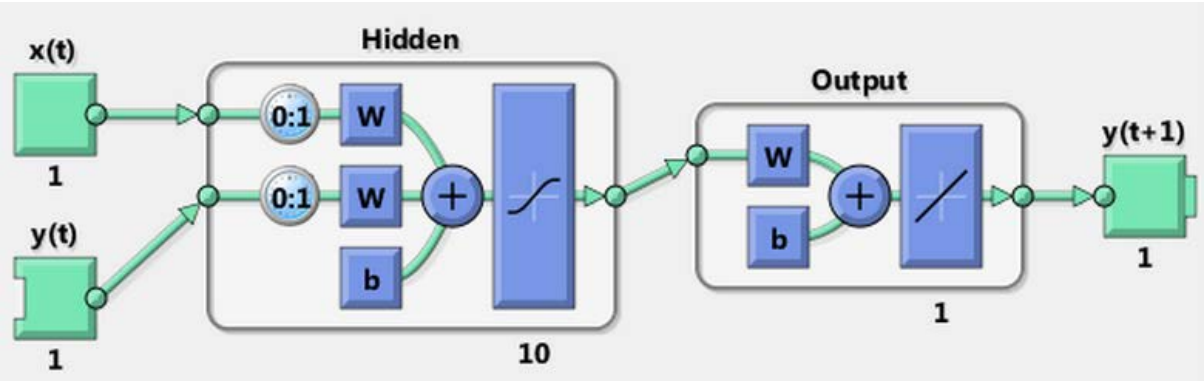

Figure 8.2 - NARX (Non-linear autoregressive with external input) network.

A Nonlinear AutoRegressive network with eXogenous inputs (NARX) is a type of recurrent dynamic network which is commonly used in time-series modelling and uses a feedback process to self-iterate. The defining equation for the NARX model is given below in Equation 2, whereby the output signal *y*(*t*) is regressed on previous (historical) values of the output signal and previous values of an independent (exogenous) input signal u(t):

$$y(t) = f(y(t-1), y(t-2), \ldots, y(t-n_y), u(t-1), u(t-2), \ldots, u(t-n_u)) \qquad \text{Equ. E1}$$

Appendix F - Particle Swarm Optimisation

In particle swarm optimization, simple software agents, called *particles*, move in the search space of an optimization problem. The position of a particle represents a candidate solution to

the optimization problem at hand. Each particle searches for better positions in the search space by changing its velocity according to rules originally inspired by behavioural models of bird flocking.

The PSO algorithm starts by generating random positions for the particles, within an initialization region. Velocities are usually initialized within a region but they can also be initialized to zero or to small random values to prevent particles from leaving the search space during the first iterations. During the main loop of the algorithm, the velocities and positions of the particles are iteratively updated until a stopping criterion is met.

$$V_t^{k+1} = K(V_i^k \times w + c_1 \times R_1 \times \left(P_{best}(i) - X_i^k\right) + c_2 \times R_2 \times \left(G_{best} - X_i^k\right)) \quad \text{Equ. F1}$$

Where V_t^k is the possible dimension for i particles with position (X_i^k) and velocity (V_i^k), the individual best position of particle I (P_{best}), the global best position (G_{best}), inertia weight (w) which controls how much of the particles previous velocity (speed which particle moves in the search space) is retained, iteration number (k) for a total of n iterations, non-negative acceleration factors (C_1 and C_2), random numbers (R_1 and R_2) in the range of [0, 1] and a constriction factor (K) which controls the velocity magnitude. The cognitive acceleration constant (c1) controlling how much the particle heads towards its personal best position. The social acceleration constant (c2) which controls the tendency that the particle heads towards the global best position. The acceleration parameters of the PSO algorithm are selected based on a "grid search" method whereby each parameter (c1 and c2) are changed in intervals of 0.5 to a maximum of 2.

The optimisation technique used within this research is Particle Swarm Optimisation (PSO). PSO is not available in MATLAB tools, thus the PSO algorithm had to be developed and adapted to optimise the stand-alone renewable energy system. The PSO algorithm is based upon previous MATLAB PSO coding[24] and modified for maximum performance for the stand-alone energy systems explored in this thesis. For the PSO algorithm coding as well as values for the system configuration, please refer to the attached CD.

[24] Ebbesen, S., Kiwitz, P. and Guzzella, L. "A Generic Particle Swarm Optimization Matlab Function", 2012 American Control Conference, Proceedings of the, June 27-29, Montreal, Canada, pp. 1514-1524

Appendix G - Datasets

This thesis utilised the following datasets for simulations:

1. Solar Irradiance;
2. Wind Speed;
3. Rainfall;
4. Electric load demand profile; and
5. Water load demand (consumption) profile

Due to the resolution of the data used (i.e. 1 minute) over an entire year/s, please refer to attached CD for the full datasets.